Direct Measurement of the Gluon Polarisation in the Nucleon Using the All-p_{T} Method at the COMPASS Experiment at CERN

Marcin Stolarski

LIP Lisboa

D.Sc. thesis

Lisbon, December 2016

Abstract

Almost 30 years ago the EMC experiment discovered that the quark helicity contribution to the nucleon spin is small. Afterwards this result was confirmed by several other experiments. It came as a surprise, as it contradicts the expectation from simple models which otherwise were quite successful in describing the nucleon properties. A possible solution for this "spin puzzle" is that gluons are polarised. Therefore, gluon polarisation measurements are of great importance and motivated the flagship measurement of the COMPASS proposal.

In this monograph details about the direct measurement of the gluon polarisation in the nucleon, extracted from the data of the COMPASS experiment at CERN are presented. A novel method, the so-called all-p_{T} method, was developed by the author who was also responsible for the corresponding analysis in COMPASS.

The proposed method allows simultaneous extraction of the gluon polarisation and spin-dependent asymmetry A_1, resulting in a considerable reduction of statistical and systematic uncertainties by a factor of 1.6 and 1.8, respectively, comparing to the previously used method. The analysed data cover the kinematic region of $Q^2 > 1$ GeV^2, which allows the use of perturbative QCD. The obtained result of the gluon polarisation at LO pQCD is Δg/g$= 0.113 \pm 0.038 \pm 0.036$ for average nucleon momentum fraction carried by the gluon about 0.10 and average hard scale of 3 GeV^2. The obtained results suggest that the gluon polarisation in the nucleon is positive. This observation is in line with recent NLO QCD fits, which include RHIC pp data.

Contents

Chapter 1

Introduction

One of the early ideas to describe the atom internal structure were given by W. Prout already in 1815 in an anonymously published paper [1]. The author has shown that, within experimental uncertainties, the atomic weights of various compounds are multiples of the hydrogen atom weight. This observation lead him to the hypothesis that the hydrogen atom is the only truly fundamental object, which he called protyle. Later on, once more precise measurements got available this hypothesis was disproved (existence of isotopes).

Almost a century later E. Rutherford in 1911 discovered the existence of atomic nuclei [2] – the discovery which started the modern understanding of the atom structure. In experiments made in 1917 (and reported in 1919) he also managed to observe the hydrogen nucleus as a product of bombarding ordinary nitrogen-14 with alpha particles. Influenced by the earlier hypothesis of W. Prout, E. Rutherford assumed that the hydrogen nucleus is present in all other nuclei and called it proton. With the later discovery of the neutron by J. Chadwick, [3], the modern structure of the atom was fully established. At that time both protons and neutrons were considered as fundamental objects. However, with the increasing energy of scattering experiments many new particle types were produced. The emerging particle "ZOO" in late 50's and beginning of 60's put a question mark on which are the really fundamental objects of matter.

The model of the internal nucleon structure by M. Gell-Mann [4] and G. Zweig [5] from 1964 predicted that a nucleon is composed of 3 quarks. These are point-like fermions with spin 1/2 and fractional electric charge ($\pm 1/3, \pm 2/3$). At the time of the model introduction only 3 types quarks were needed, up, down and strange. The proton and neutron were built exclusively from up and down quarks, uud and ddu respectively. As the nucleon itself is a fermion with a spin 1/2, it was not too difficult to explain how the spin of the proton is built out of three 1/2 fermions. Moreover, such a simple model quite accurately predicted the anomalous magnetic moment of the nucleon, a quantity directly related to the quark orientation inside the nucleon, see *e.g.* [6]. The only problem of this model was the fact that the predicted particles with fractional electric charge were not found in any experiment. Citing the Nobel prize winner J.I. Friedman [7], "To many physicists this was not surprising. Fractional charges were considered to be a really strange and unacceptable concept, and the general point of view in 1966 was that quarks were most likely just mathematical representations – useful but not real".

Even when the first evidences of point-like objects in the nucleon were reported by SLAC [8,9], the existence of quarks was not fully recognised by the whole particle physics community until the 4th quark predicted by the theory [10], the charm quark, was discovered in 1974 in the observation of the J/Ψ meson in e^+e^- annihilation [11, 12].

With the onset of the Parton Model by R. Feynman [13], and later of the Quark Parton Model [14], in addition to the three aforementioned quarks now called the valence quarks, also sea quark and antiquark pairs were considered, as well as electrically neutral partons with spin 1 (bosons), later called gluons. Experimental evidence of the gluons existence was obtained in 1979 in DESY [15]. However, even with these complications it was assumed that only quarks carry the spin of the proton.

In the same year of the J/Ψ discovery, an experiment at SLAC for the first time scattered a polarised beam on a polarised target. From the obtained results one could conclude that, within the large statistical uncertainties, indeed as expected quarks could explain the spin of the nucleon [16, 17]. As in addition the (closely related) anomalous magnetic moments of baryons were well described by the simplest Quark Parton Model, for the next almost 15 years the study of the internal spin structure of the nucleon was not considered a top priority.

For the vast majority of the community the EMC experiment, in which polarised muons were interacting with a polarised target was supposed to just confirm the earlier SLAC measurements and the expectation from the Ellis-Jaffe sum rule [19]. Needless to say, the EMC result [20] came as a true surprise, the fraction of the proton spin carried by quarks, $\Delta\Sigma$, was measured to be $\Delta\Sigma = 0.12 \pm 0.10 \pm 0.14$, instead of 1. Even if relativistic corrections were later considered, see *e.g.* [21], the expected value of $\Delta\Sigma \approx 0.6$ was far away from the actual measurement. The importance of this discovery was clearly recognised by the physics community, the two EMC papers having in total 3406 citations as on 15 March 2016. The EMC experiment had a significant Polish contribution by

B. Badełek, J. Ciborowski, J. Gajewski, J.P. Nassalski, E. Rondio, L. Ropelewski and A. Sandacz. The EMC discovery started the so called "spin crisis". For the next two decades it shaped the way the field of spin measurements evolved. The next generation of experiments performed at CERN (SMC) [22], DESY (HERMES) [23] and at JLAB [24–26] confirmed the EMC observation that the quarks can explain only a small fraction of the nucleon spin.

In a more general case the spin of the nucleon can be carried by the helicity of quarks, $\Delta\Sigma$, the helicity of gluons $\Delta\mathrm{G}$, as well as by the orbital angular momenta of quarks and gluons L_{q} and L_{g}, respectively. In the so-called Jaffe-Manohar scheme this can be written as

$$\frac{1}{2} = \frac{1}{2}\Delta\Sigma + \Delta\mathrm{G} + L_{\mathrm{q}} + L_{\mathrm{g}}. \tag{1.1}$$

Observe that this definition is not gauge invariant. It holds only in the so-called light-cone gauge. However, this decomposition still plays an important role, as many of the experimental results concerning lepton-nucleon scattering are interpreted in the light-cone gauge. The proper gauge invariant definition of the nucleon spin is given by the Ji sum rule [27].

At the end of the 90's there were several reasons why the community decided to go after a measurement of $\Delta\mathrm{G}$. From early unpolarised deep inelastic scattering measurements it was known that quarks carry only about 50% of the proton momentum (in the infinite momentum frame) [6]. The rest was postulated and later proved to be carried by gluons. Thus, gluons were a natural candidate to solve yet another "crisis". Moreover, due to the so-called axial anomaly [28, 29], in case the gluon polarisation is large ($\Delta\mathrm{G} \approx 2$–$3$), quarks could still carry a large fraction of the nucleon spin as predicted by simple models. Observe however that such a large gluons polarisation would have to be compensated by quark and gluon orbital momenta. This fact is hard to reconcile with the simple QPM, where three quarks in the nucleon are supposed to be in the lowest orbital momentum state. There was also one additional argument in favour of $\Delta\mathrm{G}$ measurements, namely, at that time there was no physical observable known which could be linked with the orbital momenta of quarks and/or gluons in the nucleon.

Therefore, it was only natural that experiments like HERMES and SMC put the gluon polarisation measurement in their agenda. Several experiments were planned, where the gluon polarisation in the nucleon was considered as a flagship measurement in COMPASS at CERN, STAR and PHENIX at RHIC.

Since then almost 30 years have passed but the "spin puzzle" persists. Originally the COMPASS golden channel of analysis was the observation of the decay products of the

D^0 meson, $D^0 \to K\pi$. In the COMPASS kinematics the observation of a D^0 meson is a signature of the so-called photon-gluon fusion process, which is sensitive to the gluon polarization in the nucleon. In the COMPASS proposal this channel was discussed in detail using Monte-Carlo techniques. However, when the measurement was performed it turned out that the background was vastly underestimated, and some of the crucial efficiencies related to the spectrometer were overestimated. As a result the precision of the gluon polarisation measurement was worse by a factor of about four compared to the proposal expectations. This strongly motivated the search for more efficient methods of gluon polarisation estimation. One of such new analysis methods was developed by the author and it is described in this monograph.

The method is successful as it leads to the best estimate of the gluon polarisation in the nucleon from all direct measurements performed so far. At the same time the method is rather complex, and so far poorly documented[1], which is unfortunate as the idea and the method itself can be used in other experiments. Taking this into account the author decided to include more details concerning the method and its application in the data analysis than a reader would expect in this type of monograph.

The organisation of the monograph is the following. In the next chapter the formalism describing deep inelastic scattering is given, as well as ideas concerning direct and indirect methods of ΔG extraction. The results concerning the gluon helicity in the nucleon obtained in previous measurements are presented in Chapter 3. Chapter 5 describes the proposed method of $\Delta G/G$ extraction which is based on analysis of data with a hadron observed in the final state. In Chapter 4 the COMPASS spectrometer is described. The details concerning data selection are described in Chapter 6, while Monte Carlo models, parametrised by Neural Network, which are needed to relate experimental observables with the gluon polarisation are described in Chapter 7. In Chapter 8 the details concerning the study of systematic uncertainties are presented. In Chapter 9 the obtained results of the gluon polarisation in the nucleon are given, including a comparison with previous measurements as well as with the extraction from global QCD fits. The summary and outlook is presented in Chapter 10. Throughout the monograph natural units are assumed in which $\hbar = c = 1$. Observe that some figures are not intellectual property of the author, therefore it may happen that the aforementioned convention is not fulfilled.

It should be stressed that in recent years large activities were started in order to understand the three-dimensional picture of the nucleon by studying Transverse Momentum

[1]Soon there will be a COMPASS paper published [30], of which I am the corresponding author. The complexity of the analysis was one of the reasons why it was done by a team of post-docs, but as a result there is no Ph.D. thesis on the subject.

Dependent Parton Distribution functions and the Generalised Parton Distribution functions. Presently, these functions can be linked in a model dependent way to the orbital momenta of quarks and gluons. These very important steps forward in understanding the multidimensional structure of the nucleon are beyond the scope of this monograph. For a recent review of the spin physics of the nucleon see *e.g.* [31].

Chapter 2

Deep inelastic scattering

The inelastic scattering process is a lepton nucleon scattering ($\mathrm{lN} \to \mathrm{l}'X$) interaction where a gauge boson (γ or Z^0) is exchanged and the parent nucleon is destroyed. In case the wavelength of the exchanged gauge boson allows to probe the internal structure of the nucleon, we talk about Deep Inelastic Scattering (DIS). In such a case DIS is an elastic scattering of the lepton on a parton from the nucleon. A more precise definition of DIS will be given once the relevant kinematic variables are defined, later in this section. Here, it is worth mentioning that the COMPASS experiment has a centre of mass energy of about 17 GeV, much lower than the mass of the Z^0 boson, and therefore Z^0 mediated DIS can be safely neglected. Another simplification used is that only one photon is exchanged between the lepton and the target nucleon. It is the so-called "one photon approximation". This approximation is justified by the small value of the electromagnetic constant $\alpha \approx 1/137$ and the fact that the COMPASS target is built mainly of low atomic number elements. The schematic Feynman diagram of the DIS process is presented in Fig. 2.1.

2.1 DIS kinematics

As already mentioned DIS is in fact an elastic scattering of a lepton on a parton inside the nucleon. It turns out that for fixed beam energy only two variables are needed to define the DIS kinematics. Let us define the following four-vectors of incoming (k) and scattered lepton (k') and target nucleon (p)

$$k = (E, \vec{k}) = (E, 0, 0, |\vec{k}|), \tag{2.1}$$

$$k' = (E', \vec{k'}) = (E, |\vec{k'}| \sin\theta \cos\phi, |\vec{k'}| \sin\theta \sin\phi, |\vec{k}| \cos\theta), \tag{2.2}$$

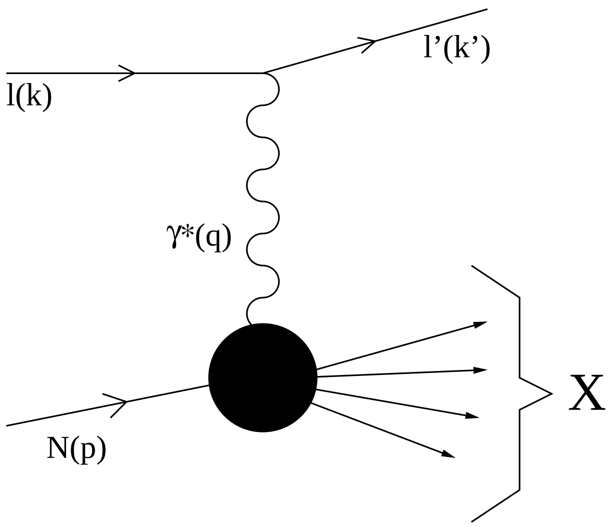

Figure 2.1: Feynman diagram of DIS.

$$p = (E_N, \vec{p}) = (M, 0, 0, 0). \tag{2.3}$$

Here E and $\vec{k}$ are the energy and three-momentum of the incoming lepton, respectively, while E' and $\vec{k'}$ have the same respective meaning but for the scattered lepton. COMPASS is a fixed target experiment, therefore the four-vector of the incoming nucleon p, is defined as a proton at rest, *i.e.* the energy $E_{\rm N}$ is only related with the nucleon mass (M) and the proton three-momentum $\vec{p}$ is zero. The angles θ, and ϕ are defined in Fig. 2.2. In this figure there are also two other angles (φ and ζ), which will be defined later in the text.

A definition of the DIS kinematics by just using k, k' and p is possible, but inconvenient due to their frame dependence. It is more natural to use the following Lorentz invariants,

$$Q^2 = -q^2 = (k - k')^2 \approx 4EE' \sin\theta/2, \tag{2.4}$$

$$\nu = \frac{pq}{M} = E - E', \tag{2.5}$$

$$y = \frac{pq}{pk} = \frac{\nu}{E}, \tag{2.6}$$

$$x_{\rm Bj} = \frac{-q^2}{2pq} = \frac{Q^2}{2M\nu}, \tag{2.7}$$

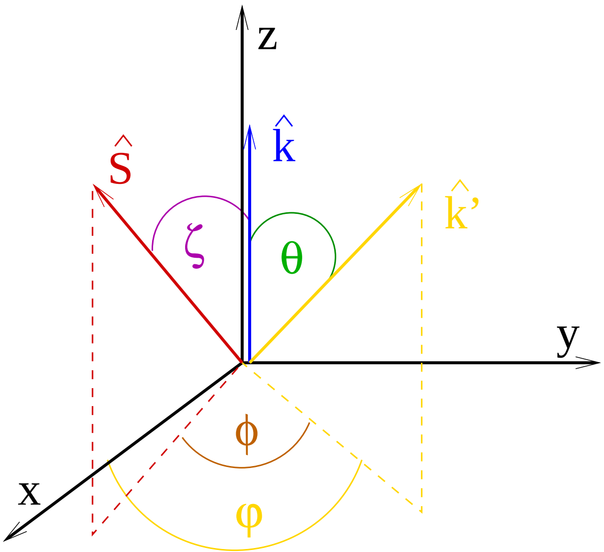

Figure 2.2: Definition of angles used to describe DIS.

$$W^2 = (p+q)^2 = M^2 + 2M\nu - Q^2 = M^2 + Q^2\left(\frac{1}{x_{\mathrm{Bj}}} - 1\right). \tag{2.8}$$

Here, the negative four-momentum transfer Q^2 is related to the virtual photon wavelength. The invariant ν is the energy of the virtual photon in the laboratory system. The dimensionless variable y is in the range $y \in (0,1)$ and in the laboratory frame is the fraction of the beam energy carried by the virtual photon. This variable is quite important in spin measurements as the spin transfer from the muon to the virtual photon is strongly correlated with the value of y. The second dimensionless variable is the so-called Bjorken x, which also spans the range $x_{\mathrm{Bj}} \in (0,1)$. It has an interesting interpretation given by Feynman [13]. Namely, in the so-called proton infinite momentum frame, where all transverse momenta can be neglected, the Bjorken x corresponds to the fraction of the nucleon momentum carried by the interacting parton. The variable W is the mass of the produced hadronic system. At low values of W the interaction of a virtual photon with the nucleon can produce an excited nucleon state. Such interactions are not part of DIS and must be rejected. Observe that out of the five invariants presented in Eqs. (2.4)–(2.8) only two are independent.

As a common practise the DIS region is defined as $Q^2 > 1$ GeV^2, so that the photon wavelength is sufficiently small in order to probe the internal structure of the proton, and the value of the strong coupling constant α_S is small enough that perturbative Quantum Chromodynamics is applicable. In addition $W^2 > 5$ GeV^2 is required to avoid the aforementioned nucleon excitation region.

2.2 DIS cross section and structure functions

The DIS process double differential cross section, $\mathrm{d}^2\sigma$, can be defined in elements of $\mathrm{d}E'$ and solid angle of the scattered muon emission $\mathrm{d}\Omega$ as

$$\frac{\mathrm{d}^2\sigma}{\mathrm{d}E'\mathrm{d}\Omega} = \frac{\alpha}{Q^2} L_{\mu\nu} W^{\mu\nu}. \tag{2.9}$$

Here $L_{\mu\nu}$ and $W^{\mu\nu}$ correspond to two four-rank tensors. The first one, $L_{\mu\nu}$, describes the emission of a virtual photon from the lepton while the second tensor, $W^{\mu\nu}$, describes the internal structure of the hadron. In the description of DIS one assumes that the cross section factorises, namely that the photon emission and its interaction with the hadron are independent processes. Thus in Eq. 2.9 the product of the two aforementioned tensors appears. The tensor $L_{\mu\nu}$ can be calculated using the formalism of Quantum Electro Dynamics (QED). Contrary to the previous case, $W^{\mu\nu}$ cannot be calculated within the QCD formalism. The input must come from experimental data. However, QCD is able to predict the Q^2 evolution of $W^{\mu\nu}$ in case the latter is known at a certain reference scale Q_0^2.

These tensors can be decomposed into symmetric and antisymmetric parts. The symmetric part is related to unpolarised lepton-nucleon scattering, while the antisymmetric part depends on the helicity of the interacting particles. It should be noted that in order to measure spin effects in DIS both the beam and the target must be polarised. For a spin-1/2 target, both tensors can be parametrised by a combination of two structure functions: the symmetric tensor by means of the F_1 and F_2 structure functions, while for the antisymmetric tensor the g_1 and g_2 spin-dependent structure functions appear. In the case of a spin-1 target, in addition to the four aforementioned functions other four functions called b_{1-4} [32] are also present. However, these functions are expected to be small for the deuteron case [32, 33], and hence, are usually neglected in the analyses and also in the formalism.

The spin-dependent part of the cross-section can be decomposed as a linear combination of longitudinal and transverse terms. For the longitudinal term ($\sigma_{||}$) the proton is polarised parallel or antiparallel to the incoming lepton direction, *i.e.* the angle ζ defined in Fig. 2.2 is 0 or π. For the transverse term ($\sigma_{\perp}$) the polarisation of the target is perpendicular to the incoming lepton direction, ζ being $\pi/2$.

$$\Delta\sigma = \cos\zeta\sigma_{||} + \sin\zeta\cos\phi\sigma_{\perp}. \tag{2.10}$$

From the experimental point of view the absolute measurement of $\Delta\sigma$ is difficult. It is more convenient to measure asymmetries, $\Delta\sigma/\sigma$, where part of the possible experimental uncertainties cancel. In order to measure the gluon polarisation Δg, it is sufficient to study only the case of the longitudinal polarisation of the target. The gluon polarisation measurement relies on the counting rate asymmetry measurement,

$$A_{||} \equiv A_{\mathrm{LL}} = \frac{N_{\uparrow\downarrow} - N_{\uparrow\uparrow}}{N_{\uparrow\downarrow} + N_{\uparrow\uparrow}}. \tag{2.11}$$

Here, the subscript "LL" denotes the longitudinal polarisation of both beam lepton and target nucleon, while the arrows indicate the relative polarisations of beam and target.

As will be discussed later in Chapter 4, the COMPASS beam has negative polarisation, while the target nucleons are polarised with either $\zeta = 0$ or $\zeta = \pi$. It is easier to understand the connection between the measured asymmetry and the structure functions if one re-writes the formalism of the lepton-nucleon scattering as a photon-nucleon one. The latter formalism relies on Compton amplitudes, which depend upon the helicity of the photon and nucleon. In the case of spin-1/2 target there are four Compton amplitudes, while in the case of spin-1 target there are eight of them, see [32]. Note that all these amplitudes can be related to the structure functions described earlier in the text,

$$\sigma_2^{\mathrm{T}} = (+1, +1, +1, +1) \sim F_1 - g_1 + (\kappa - 1)g_2, \tag{2.12}$$

$$\sigma_1^{\mathrm{T}} = (+1, 0, +1, 0) \sim F_1, \tag{2.13}$$

$$\sigma_0^{\mathrm{T}} = (+1, -1, +1, -1) \sim F_1 + g_1 - (\kappa - 1)g_2, \tag{2.14}$$

$$\sigma_1^{\mathrm{TL}} = (+1, 0; 0, +1) \approx \sigma_0^{TL} = (+1, -1, 0, 0) \sim \sqrt{\kappa - 1}(g_1 + g_2), \tag{2.15}$$

$$\sigma_0^{\mathrm{TT}}(+1, -1; -1, +1) \sim 0, \tag{2.16}$$

$$\sigma_1^{\mathrm{L}}(0, +1; 0 + 1) \approx \sigma_0^{L}(0, 0; 0, 0) \sim -F_1 + \frac{\kappa}{2x_{\mathrm{Bj}}}F_2, \tag{2.17}$$

where $\sigma_i^{\gamma^*_{\mathrm{pol}}}(s_{\gamma^*}, S_{\mathrm{N}}; s'_{\gamma^*}, s'_{\mathrm{N}})$ denotes the absorption cross section, where i is the third component of the total angular momentum of the γ^*N system; the superscript γ^*_{pol} denotes the virtual photon polarisation (transverse (T) or longitudinal (L)). In case γ^*_{pol} is the same for s_{γ^*} and s'_{γ^*} only one letter is used, and two are used otherwise; $(s_{\gamma^*}, S_{\mathrm{N}})$ and $(s'_{\gamma^*}, s'_{\mathrm{N}})$ are the third components of the spin vector of the photon and of the nucleon before and after the interaction, respectively; κ is a kinematic factor, $\kappa = 1 + 4x_{\mathrm{Bj}}M^2/Q^2 = 1 + \gamma^2$. Due to rather high values of ν in the COMPASS kinematics the factor κ is close to one, or equivalently γ^2 is close to zero. Observe that for simplicity b_{1-4} were omitted in Eqs. (2.12)–(2.17).

Using the above formalism one can define the spin-dependent asymmetries A_1 and A_2

$$A_1 = \frac{3}{2}\frac{\sigma_0^{\mathrm{T}} - \sigma_2^{\mathrm{T}}}{\sigma_0^{\mathrm{T}} + \sigma_1^{\mathrm{T}} + \sigma_2^{\mathrm{T}}}, \tag{2.18}$$

$$A_2 = \frac{3}{2}\frac{\sigma_0^{\mathrm{TL}} + \sigma_1^{\mathrm{TL}}}{\sigma_0^{\mathrm{T}} + \sigma_1^{\mathrm{T}} + \sigma_2^{\mathrm{T}}}. \tag{2.19}$$

It is worth mentioning that the earlier omitted contribution from b_{1-4} anyway cancels in the A_1 and A_2 definitions. Combining Eq. (2.18) and Eq. (2.19) with Eqs. (2.12)–(2.17) one can rewrite A_1 and A_2 as a function of the spin-dependent g_1, g_2 and the spin independent F_1 structure function, namely

$$A_1 = \frac{g_1 - \gamma^2 g_2}{F_1}, \tag{2.20}$$

$$A_2 = \gamma\frac{g_1 + g_2}{F_1}. \tag{2.21}$$

The relation with the experimentally measured asymmetry $A_{||}$ is the following

$$A_{||} = D(A_1 + \eta A_2). \tag{2.22}$$

Here, the depolarisation factor $D \in (0, 1)$ describes the spin transfer from the incoming lepton to the virtual photon, more details about this are given in Section 6.2. The factor $\eta \approx \gamma(1-y)/(1-y/2)$ is small in the COMPASS case. Moreover, the measurements show that the A_2 asymmetry is small [34–37], especially with deuteron target. Therefore, the term ηA_2 can be safely neglected in the COMPASS case. In the COMPASS kinematic region the following approximations hold

$$A_{||} \approx DA_1; \qquad\qquad g_1 \approx A_1 F_1 \approx A_1\frac{F_2}{2x(1+R)}. \tag{2.23}$$

Here, the formula on the right-hand side comes directly from Eq. (2.20), where the γ^2 factor is neglected. The variable R is defined as the ratio of photo absorption cross section for longitudinally and transversely polarised photons, $\sigma^{\mathrm{L}}/\sigma^{\mathrm{T}}$.

2.3 Structure functions and gluons

In the previous section the DIS formalism was discussed and the connection between structure functions, which describe the internal structure of the nucleon and physical observables was established. Here, more details concerning the interpretation of the structure functions and their connection with the gluon distribution and gluon polarisation in the nucleon is given.

In the simplest naive Quark Parton Model the structure functions can be expressed by the quark distribution functions, $\mathrm{q}(x_{\mathrm{Bj}})$,

$$F_1(x_{\mathrm{Bj}}) = \frac{1}{2}\sum_{\mathrm{q}} e_{\mathrm{q}}^2 \mathrm{q}(x_{\mathrm{Bj}}) \equiv \frac{1}{2}\sum_{\mathrm{q}} e_{\mathrm{q}}^2 (\mathrm{q}^+(x_{\mathrm{Bj}}) + \mathrm{q}^-(x_{\mathrm{Bj}})), \tag{2.24}$$

$$g_1(x_{\mathrm{Bj}}) = \frac{1}{2}\sum_{\mathrm{q}} e_{\mathrm{q}}^2 \Delta\mathrm{q}(x_{\mathrm{Bj}}) \equiv \frac{1}{2}\sum_{\mathrm{q}} e_{\mathrm{q}}^2 (\mathrm{q}^+(x_{\mathrm{Bj}}) - \mathrm{q}^-(x_{\mathrm{Bj}})). \tag{2.25}$$

The sum is over active flavours, however in the COMPASS kinematics it is usually enough to consider only the lightest quarks u, d, s and their corresponding anti-quarks. The electric charge of quark flavours q is denoted by e_{q}. The superscripts '+' or '−' refer to the 3rd component of the quark spin vector being parallel or antiparallel to that of the parent nucleon. The most important information from the point of view of the gluon distribution function or gluon polarisation in the nucleon is that gluons are not present in the definition of structure functions. This steams from the simple fact that the gluon has zero electric charge, and thus do not couple directly to photons. This fact makes the gluon polarisation measurements quite difficult. It is also the reason why almost 20 years after the first ideas of gluon polarisation measurements were proposed the gluon polarisation in the nucleon is still not accurately known.

It is worth mentioning that in this model $R = 0$, *i.e.* only transverse photons can interact with the nucleon. Therefore, $F_2 = 2x_{\mathrm{Bj}}F_1$, which is called Callan–Gross relation [38]. There is no physical interpretation for the g_2 structure function in the QPM, but it is predicted to be zero.

In the naive QPM the structure functions depend only upon x_{Bj}, this is the so-called Bjorken scaling. This is indeed observed in the data in the moderate range $x_{\mathrm{Bj}} \approx 0.1$ where, as a matter of fact the first experiments exploring the internal structure of the nucleon were lucky to perform measurements. However, as Q^2 increases the virtual photon wavelength decreases, thus becoming sensitive to more details of the internal nucleon structure. The object which at a certain Q^2 may be identified as a quark, if measured at higher Q^2 could be identified as a quark which emitted a gluon. Therefore, in the

QCD improved parton model a scaling violation is observed. The structure function g_1 is defined as

$$\begin{aligned} g_1(x_{\mathrm{Bj}}, Q^2) = \frac{1}{2} \sum_{\mathrm{q}} e_{\mathrm{q}}^2 \int_x^1 \frac{\mathrm{d}u}{u} \Delta \mathrm{q}(u, Q^2) C_{\mathrm{q}}(x/u, \alpha_S(Q^2)) \\ + \frac{\langle e_{\mathrm{q}}^2 \rangle}{2} n_f \int_x^1 \frac{\mathrm{d}u}{u} \Delta \mathrm{g}(u, Q^2) C_{\mathrm{g}}(x/u, \alpha_S(Q^2)), \end{aligned} \tag{2.26}$$

where C_{q} and C_{g} are the so-called coefficient functions. These functions can be approximated by series in powers of α_S. For example in LO the first term $C_{\mathrm{q}} = \delta(1-x)$, and $C_{\mathrm{g}} = 0$. In NLO in addition to the LO terms corrections proportional to $\alpha_S(Q^2)/(2\pi)$ appear. For simplicity a generic x has been used. As will be explained later in the text, beyond LO approximation one can define different x variables for different types of processes. However, note that on the left-hand side of Eqs. (2.26) the x_{Bj} is used and not just x. The (polarised) gluon distribution function is indicated by $(\Delta)\mathrm{g}(x, Q^2)$. The gluon contribution to the nucleon spin, $\Delta\mathrm{G}$, is the first moment of $\Delta\mathrm{g}(x, Q^2)$, *i.e.* $\int_0^1 \Delta\mathrm{g}(x, Q^2)\mathrm{d}x$.

One of the consequences of C_{q} and C_{g} values at LO is that one retrieves back the simple formula in Eq. (2.25) for the g_1 structure function, except for explicit (x_{Bj}, Q^2) dependencies instead of just x_{Bj}. This means that in LO, even in the QCD improved parton model, gluons do not contribute directly to the g_1 structure function. However, they do contribute in NLO approximation.

One of the aspects of the QCD improved parton model is that the Q^2 dependence of the parton distribution functions can be predicted for any Q^2 value in case it is known at some other reference Q_0^2 value. The so-called PDF evolution is governed by the DGLAP evolution equations [39–41]

$$\begin{aligned} \frac{\mathrm{d}}{\mathrm{d}\log(Q^2)} \begin{pmatrix} \Delta \mathrm{q}^{\mathrm{S}} \\ \Delta \mathrm{g} \end{pmatrix} (x, Q^2) = \frac{\alpha_S(Q^2)}{2\pi} \int_x^1 \frac{\mathrm{d}u}{u} \\ \begin{pmatrix} \Delta P_{\mathrm{qq}} & \Delta P_{\mathrm{qg}} \\ \Delta 2 n_f P_{\mathrm{gq}} & \Delta P_{\mathrm{gg}} \end{pmatrix} (x/u, \alpha_S(Q^2)) \begin{pmatrix} \Delta \mathrm{q}^{\mathrm{S}} \\ \Delta \mathrm{g} \end{pmatrix} (x, Q_0^2). \end{aligned} \tag{2.27}$$

Assuming that only the three lightest quark flavours are active, *i.e.* u, d, s, and for simplicity skipping (x, Q^2) dependence, here $\Delta\mathrm{q}^{\mathrm{S}} = \Delta\mathrm{u} + \Delta\mathrm{d} + \Delta\mathrm{s}$, where for each flavour the sum of quarks and antiquarks is considered. The first moment of $\Delta\mathrm{q}^{\mathrm{S}}$ is equal to $\Delta\Sigma$. The splitting functions P_{ij} can be calculated as a series in α_S. The evolution of the non-singlet distributions $\eta_3 = \Delta\mathrm{u} - \Delta\mathrm{d}$ and $\eta_8 = \Delta\mathrm{u} + \Delta\mathrm{d} - 2\Delta\mathrm{s}$ is also governed by the

DGLAP equations. However, these non-singlet evolutions are decoupled from the gluon one.

The most common approach to the unpolarised gluon PDF measurement is to study the scaling violation of the F_2 structure function. The world data on the cross-section measurement are presented in Fig. 2.3, [42]. The scaling violation is clearly seen as an increase of the cross section at low x_{Bj} with increasing Q^2. The studies are performed by means of the so-called QCD fit. In the simplest scenario the quark and gluon distributions are parametrised at the reference scale, Q_0^2. By means of the DGLAP equations these distributions can be evolved to the Q^2 value of each experimental point used in the analysis. Using *e.g.* a χ^2 estimator one can define how well given input densities describe the data and by χ^2 minimisation one obtains optimal parton densities at the reference scale. In Fig. 2.4 the actual results of the PDFs obtained in the HERAPDF2.0 QCD fit are presented [42]. The gluon PDF is reasonably well constrained.

Exactly the same idea can be used in order to constrain the gluon polarisation in the nucleon. Namely, the scaling violation of the g_1 structure function needs to be studied. The COMPASS NLO QCD fit to the world data on the g_1 of proton, deuteron and neutron is presented in Section 3.1. Here, one should mention that the gluon polarisation is not well constrained by such a fit. The main reason being that so far only polarised DIS was measured in the fixed target experiments, which forms just a corner of the phase space presented in Fig. 2.3. Therefore, more direct methods for the extraction of the gluon polarisation in the nucleon have to be found.

2.4 Direct Δg/g measurements

As mentioned in the previous section the gluons do not contribute to the DIS cross-section at LO pQCD, therefore higher-order processes have to be studied. The two diagrams contributing at NLO to the cross section are presented in Fig. 2.5 together with leading process (LP) photo absorption. In the first NLO diagram, denoted as b) in Fig. 2.5, the gluon emission in the Compton process (QCDC) is accounted for. This process does not carry any information about the gluon polarisation and can be treated together with LP as a background. The second NLO diagram, denoted as c) in Fig. 2.5, is the photon-gluon fusion (PGF) process, where the virtual photon interacts with a quark or antiquark from g $\rightarrow$ q$\bar{\mathrm{q}}$. This process is sensitive to the gluon polarisation in the nucleon and is considered as the signal process. Observe that the direct measurement of Δg/g will be performed at a certain x_{g} range, where x_{g} is the nucleon momentum fraction carried by the gluon in a PGF process. The available range of x_{g} is limited by the experimental

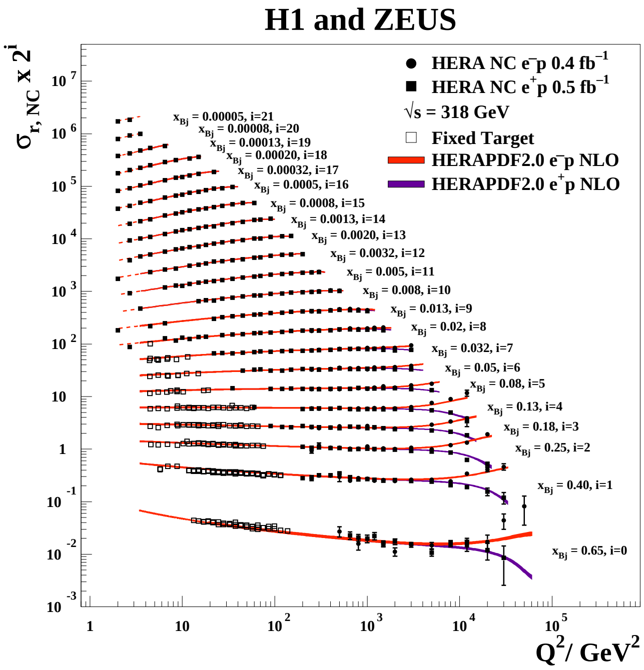

Figure 2.3: Cross-section measurement results of lepton proton scattering. The fitted lines correspond to the HERAPDF2.0 fit. Reprinted figure from [42] under Creative Common 4.0 license.

conditions and thus the extraction of ΔG, *i.e.* the 1st moment of $\Delta g(x_g)$ would require considerable extrapolations. One can also define x_C as the nucleon momentum fraction carried by the struck quark in the QCDC process. Note that for each PGF and QCDC event type one can also calculate x_{Bj}, where $x_{Bj} < x_g, x_C$. However, only for the LP the x_{Bj} can be interpreted as the nucleon momentum fraction carried by the struck quark. For simplicity reasons sometimes these different types of x are not distinguished, see *e.g.* Eqs. (2.26).

The optimal process for the direct gluon polarisation measurement seems to be the measurement of the spin-dependent asymmetries from open charm events. Since heavy charm quarks are not present in the nucleon in the first approximation they do not contribute to LP or QCDC processes. Therefore, in a LO approximation the open charm production is a pure PGF process. Such events were studied in COMPASS, and the analysis of the gluon polarisation at LO and NLO was performed. The details are presented in Subsection 3.2.1. Unfortunately, due to the COMPASS moderate centre-of-mass energy and high charm quark mass the gluon polarisation measurement from open charm has a

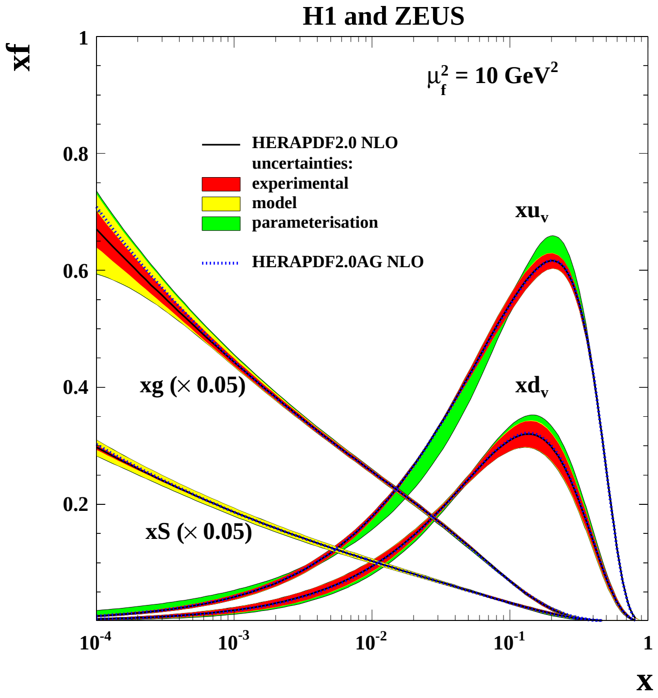

Figure 2.4: The PDFs extracted in HERAPDF2.0. Reprinted figure from [42] under Creative Common 4.0 license.

limited statistical precision.

What is left from the point of view of DIS are studies of the PGF process in the case when a gluon fluctuates into a pair of light quarks. In such case there is a considerable background related to LP and QCDC processes, which has to be accounted for and subtracted. One should stress that PGF and QCDC kinematics are defined on the parton level, see *e.g.* [43]. However, in the experiment only final state hadrons are detected. Therefore, a model is needed to interpret the “raw” results of such measurement. In fact typically only 6% of the events, according to the LEPTO [44] model are coming from PGF, the remaining being about 12% from QCDC and the rest from LP. What makes such an analysis possible is the fact that hadrons produced in PGF and QCDC have larger transverse momenta than in LP. Namely, in the case of LP the transverse momentum of the hadron is related to the intrinsic k_{T} of the quark in the nucleon as well as to the $p_{\perp}$ obtained in the fragmentation process. Both k_{T} and $p_{\perp}$ are rather small, resulting in a small value of hadron transverse momentum (p_{T}) measured with respect to the virtual photon direction. The situation is different for PGF and QCDC processes where significant p_{T} can be generated in the hard process itself.

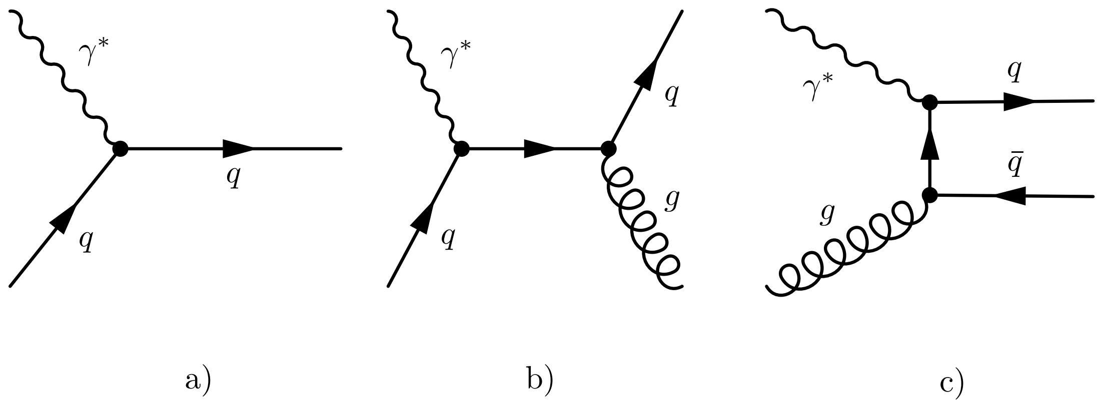

Figure 2.5: Feynman diagrams for a) the leading-order process (LP), b) Compton gluon radiation (QCDC), and c) photon–gluon fusion (PGF).

Therefore, the idea of a Δg/g measurement from PGF with light quarks in the final state is to study the spin asymmetries (A_1 or A_{LL}) of hadrons produced with large p_{T}, where the contribution of higher-order processes (PGF and QCDC) is enhanced with respect to LP. Results of such measurements are presented in Section 3.2. In fact the same idea as presented here for the DIS case can be also used to study low Q^2 data, where p_{T}^2 becomes a hard scale and allows for perturbative treatment. Results of such studies are also presented in Section 3.2.

The aim of this monograph is to present a novel method of Δg/g extraction using PGF events with light quarks produced in the final state. Instead of using only the high-p_{T} region the proposed method uses hadrons in the whole p_{T} spectrum to be able to simultaneously extract A_1^{LP} asymmetries as well as Δg/g. Such a treatment reduces the systematic uncertainties related to the Δg/g extraction as well as improves the statistical uncertainties as compared to the method used previously. The details of the proposed method are presented in Section 5.2.

Chapter 3

Previous ΔG measurements

In this section an overview of previous ΔG and Δg/g measurements is presented. First is discussed the most model-independent way of ΔG extraction from the scaling violation of the spin-dependent structure function g_1. Next, the direct methods of Δg/g extraction from analyses of asymmetries in the production of high transverse momentum hadrons (pairs) and open charm events are presented. Results of SMC, HERMES and COMPASS experiments are described in this section. Finally, in the last part, the results of STAR, PHENIX and COMPASS experiments on double longitudinal spin asymmetries A_{LL} are discussed.

3.1 Scaling violation of g_1

As mentioned in Section 2.3, the polarised gluon distribution $\Delta g(x_{\mathrm{g}})$ can be obtained from the scaling violation of the $g_1(x_{\mathrm{Bj}}, Q^2)$ spin-dependent structure function.

The scaling violation is an ideal tool for studying Δg. On one side, the g_1 is well understood in the theory. On the other side, its measurement involves only the reconstruction of incoming and scattered leptons (*i.e.* inclusive measurement), thus it is relatively easy to perform. Therefore, the measurement of the scaling violation of g_1 is considered to be the most model-independent way of measuring the gluon helicity contribution to the nucleon spin. However, so far the g_1 measurements in the perturbative region exist only in a limited range of x_{Bj} and Q^2. The reason is that all world-wide measurements were performed in fixed-target experiments as no polarised ep collider ever existed. This may change if the planned EIC accelerator is built [45].

There are quite some NLO pQCD fits of the g_1 structure function available, see *e.g.* [46–49]. In the recent COMPASS fit the world-wide data set of the g_1 structure function for p, n and d were used in the fit [20, 22, 24, 26, 47–54]. The example of the data coverage on the deuteron g_1 structure function is presented in Fig. 3.1. The kinematic coverage on the proton data is very similar to the deuteron case. Note the much smaller kinematic coverage of the existing data in the polarised case comparing to unpolarised case presented in Fig. 2.3.

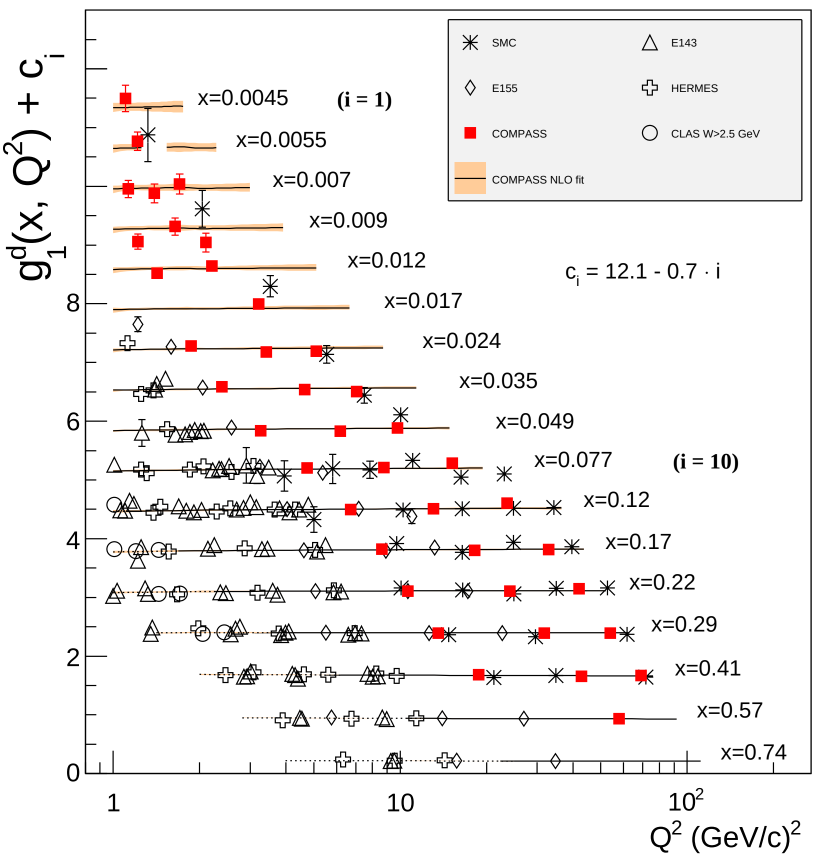

Figure 3.1: World $g_1^{\rm d}$ data used in the COMPASS NLO fit. See text for details. Reprinted figure from [50] under Creative Common 4.0 license.

In Fig. 3.2 the polarised quark and gluon distributions are presented. In the top row the results from $x\Delta q^{\rm S}$ and $x\Delta g$ are shown in the left and right panel respectively. In the bottom row quark combinations of $x\Delta u$, $x\Delta d$ and $x\Delta s$ are presented from left to right respectively. The distributions are shown at $Q^2 = 3$ GeV^2, figure comes from [50]. Note that for simplicity the x variable is used, without distinction between $x_{\rm Bj}$ or $x_{\rm g}$. The two

Δg solutions shown correspond to two different assumptions concerning the functional form of Δq^S (with/without zero crossing). It should be noted that both solutions give comparable χ^2 in the fit. The dark blue band marks the statistical uncertainty defined as $\chi^2_{\text{min}} + 1$. The light blue band defines systematic uncertainties. For example, it turns out that by just changing the reference scale Q_0^2 at which Δg and Δq^S are parametrised one is able to obtain almost any solution within the marked region.

In summary the scaling violation of the spin-dependent g_1 structure function gives the most model-independent access to Δg and its first moment ΔG. Unfortunately, the limited kinematics coverage of the present experimental data results in imprecise values of Δg obtained from the QCD fits of g_1. The future EIC machine would largely improve the available kinematic coverage in x_{Bj} and Q^2, and thus significantly improve the precision of Δg obtained with this method.

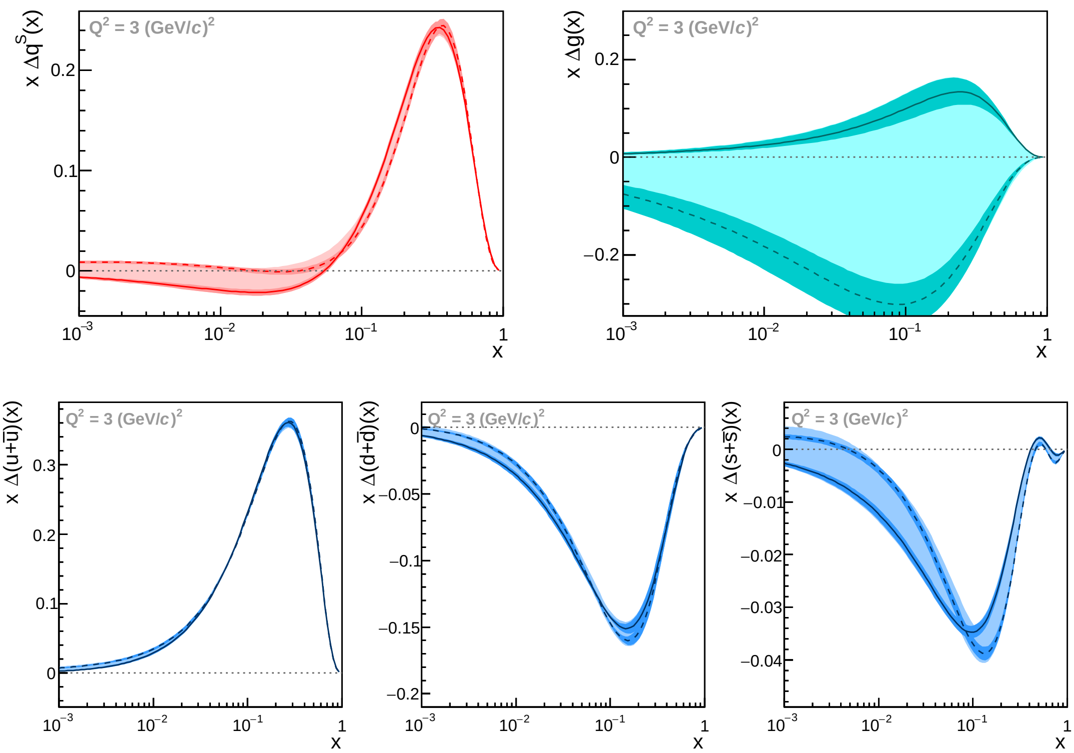

Figure 3.2: The results of the COMPASS NLO pQCD fit to the world g_1 data. Top row: Extracted distribution of $\Delta q^S(x)$ and $\Delta g(x)$, on left and right panel respectively. Bottom row, from left to right: Extracted values of $x\Delta u$, $x\Delta d$ and $x\Delta s$, respectively. No distinction is made between x_{Bj} and x_g. See text for details. Reprinted figure from [50] under Creative Common 4.0 license.

3.2 Direct measurements of $\Delta g/g$

As the most model-independent way of accessing the gluon polarisation gives currently rather imprecise results, other methods were developed in order to study Δg. The direct extraction methods concentrated on studying the photon-gluon-fusion process (PGF), which in the lowest order (in α_S) is sensitive to the gluon polarisation in the nucleon. In this section several such attempts are presented. They are ordered not according to the date of publication but rather in the degree of model dependence of the corresponding $\Delta g/g$ result.

3.2.1 COMPASS open charm analyses

The cleanest way to access the PGF process in the COMPASS kinematic domain is the observation of open charm mesons. The charm quarks, due to their large mass ($m_c \approx 1.5$ GeV^2) are not present in the nucleon. Therefore, when the D^0 meson is detected it is very likely that it was created in a PGF process. To be more precise, in LO pQCD there is no other process except PGF which contributes to the open charm production. Unfortunately, the COMPASS centre-of-mass energy is only about 17 GeV. At such low energy the cross-section for open charm meson production is rather low. Therefore, the $\Delta g/g$ results from the analysis of open charm events in COMPASS have limited statistical precision.

The analysis of open charm events is presented in [55], while a detailed description of the experimental part can be found in a Ph.D. thesis [56] and more theoretical details are presented in the D.Sc. thesis [57]. The resulting value of $\Delta g/g$ obtained in the LO analysis of COMPASS data is

$$\frac{\Delta g}{g}^{\mathrm{LO}} = -0.06 \pm 0.21_{\mathrm{stat.}} \pm 0.08_{\mathrm{syst.}} \tag{3.1}$$

at hard scale $\langle \mu^2 \rangle = 13$ GeV^2, and $\langle x_g \rangle = 0.11$.

In the same works, the NLO analysis for direct $\Delta g/g$ extraction is performed. So far it is the only analysis in the world which managed to extract directly $\Delta g/g$ in NLO. In NLO approximation the charm mesons are produced not only in the PGF process, but also in processes which probe the quark polarisation. This contribution from non-PGF processes has to be calculated and subtracted, see aforementioned [55] and [57]. The obtained result from the COMPASS NLO analysis is:

$$\frac{\Delta g}{g}^{\mathrm{NLO}} = -0.13 \pm 0.15_{\mathrm{stat.}} \pm 0.15_{\mathrm{syst.}} \tag{3.2}$$

at average hard scale $\langle \mu^2 \rangle = 13$ and $\langle x_g \rangle = 0.20$.

Here, it is also worth noticing the large difference between the estimated $\langle x_g \rangle$ values probed in the two approximations. It was verified that the larger $\langle x_g \rangle$ value for NLO comes from the kinematic constraints for additional gluon emissions. These constraints can only be simulated properly in Monte Carlo programs where the COMPASS spectrometer acceptance is well described. It was indeed verified that without acceptance simulation the average x_g values in LO and NLO are very similar. This fact may also explain the observation made in [58], that $\langle x_g \rangle$ between LO and NLO approximation is similar [1].

3.2.2 SMC high-p_T hadron pairs analysis

The main idea of accessing the gluon polarisation from hadrons (pairs) produced with high-p_T is that in leading order the photon absorption process is suppressed, while higher-order processes like PGF and QCDC are enhanced, see *e.g.* [59]. The first successful experiment which tried this kind of approach was SMC. This experiment was a predecessor of COMPASS, located in the same experimental hall and using positive muon beam at 190 GeV, *i.e.* 30 GeV higher beam energy than COMPASS.

The fractions of the processes contributing to the collected event sample cannot be estimated from data, instead models like the LEPTO generator with LUND string fragmentation have to be used [44]. Observe that contrary to the open charm case presented before, in the LO analysis of high-p_T pairs there is a physics background which has to be subtracted.

In order to keep the physics background description under control the analysis was performed in the DIS region $Q^2 > 1$ GeV^2. The two hadrons with the highest transverse momentum with respect to the virtual photon direction were selected with $p_{T,1}, p_{T,2} > 0.7$ GeV and $p^2_{T,1} + p^2_{T,2} > 2.5$ GeV^2. The details of the analysis can be found in [60]. In this study artificial Neural Network (NN) was used for the first time to optimise the signal (PGF) selection, *cf.* [61]. The obtained result was

$$\frac{\Delta g}{g} = -0.20 \pm 0.28_{\text{stat.}} \pm 0.10_{\text{syst.}} \tag{3.3}$$

at $\langle \mu^2 \rangle = 3$ GeV^2 and $\langle x_g \rangle = 0.07$. The statistical uncertainty of the obtained results was quite large. Thus, the measurement was inconclusive.

[1] For the work presented in [58], the authors did not have access to detailed COMPASS spectrometer simulation program.

3.2.3 COMPASS analysis of high-p_{T} hadron pairs with $Q^2 > 1$ GeV^2

The COMPASS analysis of high-p_{T} hadron pairs is based on a similar principle to the aforementioned analysis of SMC. However, there were noteworthy improvements performed. First of all, the background treatment was improved. This fact allowed to be less restrictive with p_{T} cuts, which were kept as $p_{\mathrm{T},1} > 0.7$ GeV, $p_{\mathrm{T},2} > 0.4$ GeV and $p^2_{\mathrm{T},1} + p^2_{\mathrm{T},2} > 1.0$ GeV^2, resulting in a large increase in figure of merit (FOM). Secondly, a more advanced method of NN usage allowed for an estimation of the signal and background process fractions on an event-by-event basis. This further improved the FOM. In addition the extraction of Δg/g was for the first time performed in three x_{g} bins.

The described analysis is a predecessor of the analysis presented in this thesis, therefore it will be described in more details in Chapter 5. The most detailed description can be found in the Ph.D. theses [62,63], and D.Sc. thesis [57]. The final result of Δg/g, published in [64], is:

$$\frac{\Delta \mathrm{g}}{\mathrm{g}} = 0.125 \pm 0.060_{\mathrm{stat.}} \pm 0.065_{\mathrm{syst.}} \tag{3.4}$$

at average hard scale $\langle \mu^2 \rangle = 3$ GeV^2, and $\langle x_{\mathrm{g}} \rangle = 0.09$.

3.2.4 COMPASS high-p_{T} hadron pairs analysis with $Q^2 < 1$ GeV^2

COMPASS collected about 10 times more data in the range of $Q^2 < 1$ GeV^2 than for $Q^2 > 1$ GeV^2. Therefore, using these data in the Δg/g analysis should bring a significant increase in precision. The low Q^2 region, $Q^2 < 1$ GeV^2, is non-perturbative. However, for the high-p_{T} hadron pair production there is a hard scale, given by the hadron p_{T} itself. Thus, in order to ensure factorisation it was decided to keep the p_{T} cuts rather high, $p^2_{\mathrm{T},1} + p^2_{\mathrm{T},2} > 2.5$ GeV^2. In this analysis the background description is much more complex than in the DIS region. According to the PYTHIA generator [69], which was used to interpret these data, the region of interest is dominated by resolved photon processes and some of them are background while others are sensitive to the gluon polarisation. In addition there are also the so-called low p_{T} processes, which cannot be interpreted in pQCD. In spite of all these difficulties it should be noted that the average fraction of PGF process in the sample is large, about 30%, so these data are indeed sensitive to Δg/g. Also, it is worth mentioning that the fraction of QCDC process predicted by PYTHIA amounts to only about 12% of the total cross-section. This value will be further discussed in Subsection 3.3.2.

The details of the analysis can be found in the Ph.D. thesis of [65], which also contains the most up-to-date results of this type of analysis:

$$\frac{\Delta g}{g} = 0.016 \pm 0.058_{\text{stat.}} \pm 0.055_{\text{syst.}} \tag{3.5}$$

at scale $\langle \mu^2 \rangle = 3$ GeV^2 and $\langle x_g \rangle$=0.09. Only the COMPASS data from the period 2002–2004 were analysed in this work. The results which are actually published, *cf*. [66], contain only the analysis of 2002–2003 data, and the value of Δg/g is:

$$\frac{\Delta g}{g} = 0.024 \pm 0.089_{\text{stat.}} \pm 0.057_{\text{syst.}} \tag{3.6}$$

at $\langle \mu^2 \rangle = 3$ GeV^2 and $\langle x_g \rangle = 0.095$.

3.2.5 HERMES high-p_T analysis, all Q^2 domain

The HERMES fixed-target experiment at the HERA accelerator at DESY used polarised electron or positron beams with momentum 27.6 GeV impinging on a polarised gaseous target of p or d. The experiment took place from 1995 to 2007.

In fact HERMES was the first experiment to publish results on the direct Δg/g extraction, *cf*. [67] from the analysis of high-p_T hadron pairs. However, these results were later superseded by a newer analysis, which increased the statistical precision by a factor of 10, but also claimed larger systematic uncertainties than those of [67], by a factor of 4. Therefore, here only the result of the latest analysis of HERMES [68] is presented.

In order to optimise the statistical uncertainty of the obtained results HERMES uses the whole Q^2 range. However, due to the spectrometer configuration, scattered electrons at low angles (*i.e.* coming from low Q^2 events) cannot be detected. As a result for most of the sample the kinematics of the event is not known. Instead, events with a hadron having p_T larger than 1 GeV with respect to the beam line are considered. Observe that each hadron in a given event which fulfils the p_T criterium is counted separately. Such a sample contains about 90% of the data analysed in HERMES. The data with $Q^2 > 0.1$ GeV^2, where a scattered lepton is detected and the hadron p_T can be calculated with respect to γ^* amounts to about 4% of the data sample. Finally, the third sample of events used in the analysis contains hadron pairs with $p_T^2 > 2.0$ GeV^2, calculated with respect to the beam line. To interpret these data in terms of Δg/g the PYTHIA generator [69] is used. The final result is:

$$\frac{\Delta g}{g} = 0.049 \pm 0.034_{\text{stat.}} \pm 0.010_{\text{syst.exp.}} {}^{+0.126}_{-0.099}{}_{\text{syst.models.}} \tag{3.7}$$

at average hard scale $\langle \mu^2 \rangle = 1.35\ \mathrm{GeV}^2$ and $\langle x_\mathrm{g} \rangle = 0.22$.

The summary of the LO and NLO results of the Δg/g direct extractions is presented in Fig. 3.3. While high values of the gluon polarisation are excluded by these results, the sign of the gluon polarisation can still be debated.

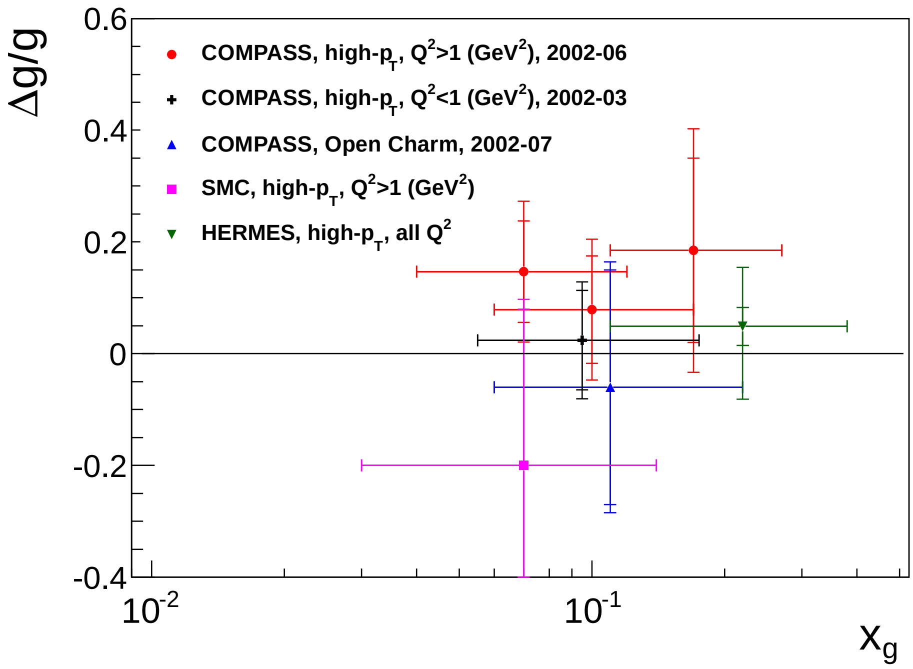

Figure 3.3: The Δg/g results from direct extractions using open charm or high-p_T hadrons (pairs) from [60, 64, 66, 68]. The internal uncertainty band marks the statistical uncertainty, while the external error bars mark the total uncertainty, where the statistical and systematic uncertainties were added in quadrature. The horizontal bar corresponds to the RMS of the probed x_g range.

3.3 Measurements of A_LL as a function of jet or hadron p_T

Studies of the gluon polarisation were also performed in p–p collisions at the Relativistic Heavy Ion Collider (RHIC). Since two compound objects collide, the interpretation of such a data is rather difficult. That is why RHIC experiments STAR and PHENIX, instead of extracting Δg/g, publish only double longitudinal spin asymmetries. These asymmetries can be interpreted in pQCD and used in global pQCD fits, see *e.g.* [70, 71]. With some modifications the A_{LL} asymmetries at high-p_{T} and low Q^2 from COMPASS can also be interpreted in the pQCD collinear formalism, *cf.* [72].

3.3.1 RHIC results

For the currently available data set, the protons in RHIC were accelerated to reach an energy of 200 GeV in the centre of mass. In the region where high p_{T} jets or hadrons (π^0) are produced the dominant processes are related to gluon-gluon and gluon-quark fusion. The first process is effectively sensitive to the square of the gluon polarisation, while in the second the sensitivity is just linear. It should be also noted that contrary to the DIS case, in hadronic collisions the event-by-event kinematics is not well known. As a result one must interpret these data globally, integrating over the available phase space.

What is measured experimentally is just a cross section asymmetry $A_{\mathrm{LL}}^{\mathrm{exp}}$ between parallel σ^{++} and antiparallel σ^{+-} collisions of polarised protons

$$A_{\mathrm{LL}}^{\mathrm{exp}} = \frac{1}{P_{\mathrm{b}}^2} \frac{\sigma^{++} - \sigma^{+-}}{\sigma^{++} + \sigma^{+-}}, \tag{3.8}$$

where the dilution due to limited beam polarisation is taken into account (P_{b}). There are several measurements of such asymmetries obtained for various final states from the two RHIC experiments: STAR and PHENIX [73–87]. In the next step theory groups use these data in their approaches, based on pQCD collinear models. It should be noted that recent global fits including RHIC data suggest that the gluon polarisation in the measured range $x_{\mathrm{g}} \in (0.05–0.20)$ is positive, see *e.g.* [92]. In that work the integral $\int_{0.05}^{0.2} \Delta \mathrm{g} \mathrm{d}x_{\mathrm{g}} = 0.10 \pm 0.07$. The extrapolated integral $\int_{0.05}^{1} \Delta \mathrm{g} \mathrm{d}x_{\mathrm{g}} = 0.20 \pm 0.07$, where the constraint of $\Delta \mathrm{g}$ in the high x_{g} region comes from the scaling violation of the g_1 structure function. Due to the lack of measurements at low x_{g} the integral $\int_{0.001}^{1} \Delta \mathrm{g} \mathrm{d}x_{\mathrm{g}}$ is poorly constrained between -0.4 and 1.1. In order to extend the range of x_{g} towards lower values, in 2013 RHIC performed measurements at higher centre-of-mass energy of 500 GeV. To the author's knowledge so far these data were not yet used in global QCD fits.

3.3.2 COMPASS results

As suggested by the authors of [72], a similar method to the one used at RHIC could be applied to the COMPASS data in the photo-production limit, where $p_{\mathrm{T}}^2 \gg Q^2$, as only one

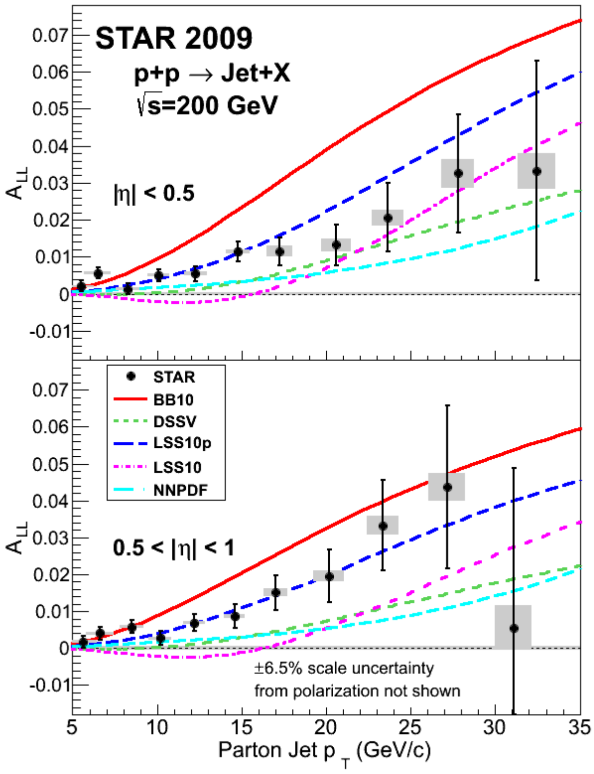

Figure 3.4: An example of RHIC results, the A_{LL} asymmetries in jet production from the STAR experiment compared to various NLO pQCD fits. See [84] for details. Figure reprinted with permission from [84], Copyright (2015) by the American Physical Society.

hard scale can be easily treated in the theory. First of all, due to the COMPASS centre-of-mass energy which is lower than RHIC, it is not clear if the model can be indeed applied in the COMPASS kinematics. The first results have shown a discrepancy by a factor 4 between the observed and the predicted cross sections for high-p_{T} hadron production. The discrepancy was reduced to an acceptable level when the so-called gluon threshold re-summation was included in the calculation [88] . The comparison between COMPASS data and the model is presented in [89]. It should be noted that these re-summations are only available for the unpolarised cross-section. For the polarised case they are still being calculated, some partial results were recently published in [90]. Therefore, for the moment one has to be careful when interpreting COMPASS A_{LL} in terms of the gluon polarisation in the nucleon.

The COMPASS results for the proton target, and their comparison with Δg curves obtained from the NLO pQCD fit are presented in Fig. 3.5. The curves marked as '$\mathrm{GRSV_{min}}$' and '$\mathrm{GRSV_{max}}$' come from [91], the 'DSSV' curve corresponds to the fit results from [92] that include the RHIC data discussed in Subsection 3.3.1. Generally COMPASS data suggest that Δg is positive in the measured region of x_{g}, the same conclusion drawn from RHIC data. For most of the results there is a good agreement between COMPASS and the DSSV fit. However, in the case of positive hadrons at low pseudo-rapidity there is a clear preference for larger values of Δg. It should be stressed that due to u quark dominance for positive hadrons and proton target the relevant asymmetry from the background processes is dominated by Δu/u term, *i.e.* the relative polarisation of the up quarks in the nucleon. Thus, data in this region should be the easiest to interpret, while exactly here the tension between data and model is found. It should be also noticed that the large value of the predicted asymmetry in the discussed region is also related to the fact that the pQCD calculation using this collinear model estimates that the fraction of events from the QCDC process (*i.e.* sensitive to Δu/u) of more than 50% in the high-p_{T} region. This value can be roughly compared with the 12% of QCDC process found in PYTHIA for the hadron pairs analysis described in Subsection 3.2.4. In any case the final conclusions concerning the Δg/g value and/or the applicability of the model from [88], can only be reached once the gluon re-summations are available for the polarised case. The details of this analysis, including results for the proton and deuteron target, can be found in [93].

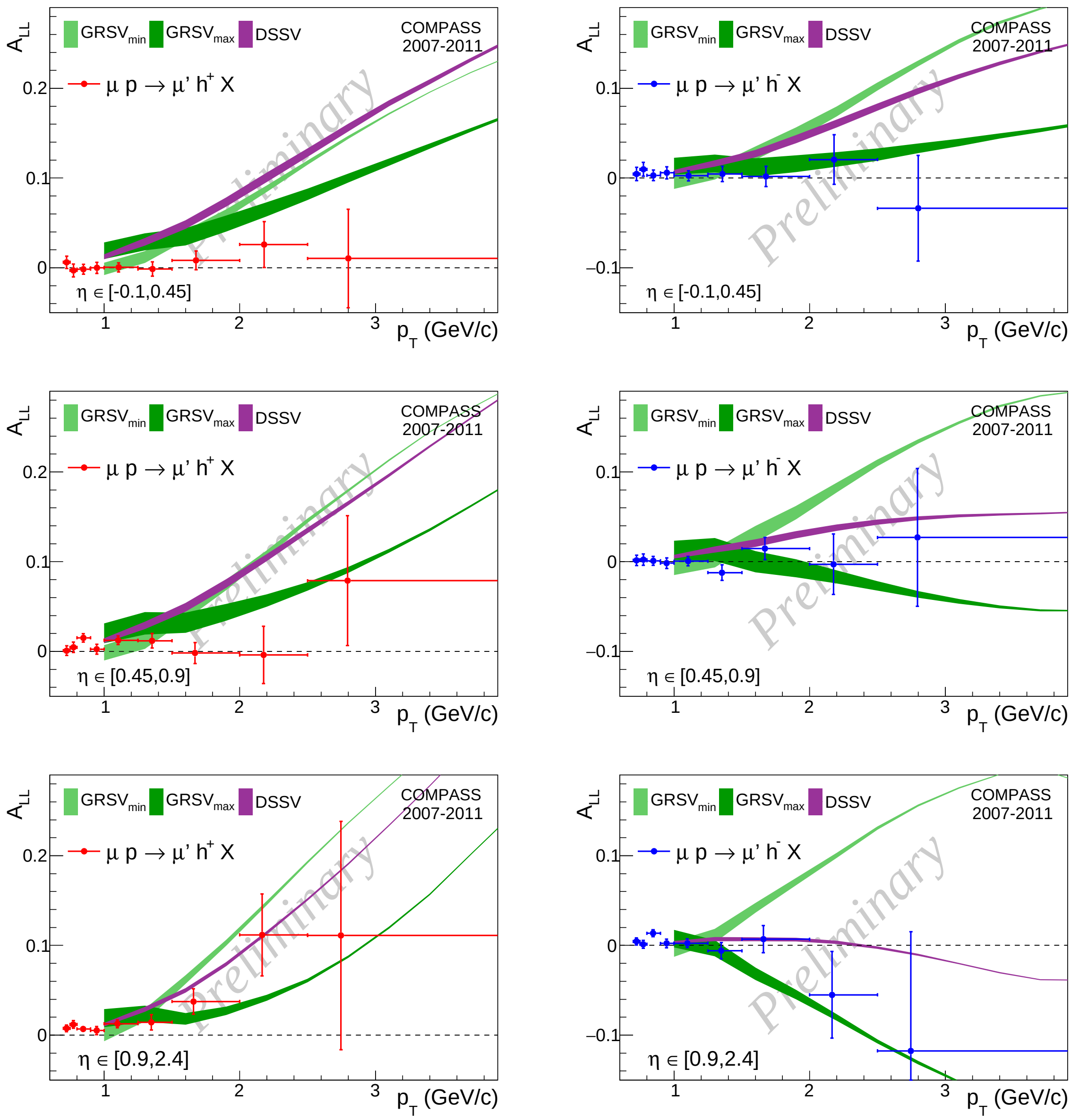

Figure 3.5: The COMPASS results of A_{LL} for the proton target as a function of pseudo-rapidity η (rows), for positive (left column) and negative hadrons (right column). The theory curves come from [91] and [92]. There is a tension observed between data and models for the positive hadrons at low pseudo rapidity. Figure made by COMPASS Collaboration.

Chapter 4

Experimental set-up

COMPASS is the fourth generation experiment in series studying the (spin) structure of the nucleon in muoproduction in DIS process at CERN. The previous experiments were the European Muon Collaboration (EMC), the New Muon Collaboration (NMC) and the Spin Muon Collaboration (SMC). All of them used the same experimental hall and the same beam line. The detailed description of the COMPASS set-up can be found in [94]. In this chapter only the most relevant information concerning the muon beam, polarised target, and the COMPASS spectrometer are given. The trigger system and the COMPASS analysis chain are also briefly discussed.

4.1 The muon beam

The COMPASS uses tertiary muon beam obtained from pion decays which were produced in the interaction of protons with a solid target. The beam is delivered in cycles called spills. About $1.2{\cdot}10^{13}$ protons per cycle are accelerated in Super-Proton-Synchrotron (SPS) to energy of about 400 GeV, the typical acceleration time being 9.6 s. After the acceleration they are extracted in about 4.8 s and hit a 500 mm long beryllium target. The secondary pions produced in the p-Be interaction are focused using set of quadrupoles, and a certain momentum range with a spread of about $\pm10\%$ is selected using three dipole magnets. The selected pions are transported through a 600 m decay tunnel, where a few percent of them decay into muons.

These muons are further focused using quadrupole magnets, while not accompanying pions are stopped using nine Be absorbers 1.1 m long each. A set of collimators selects 160 GeV muons, with a momentum spread of about 5%. The beam momentum is measured with a precision better than 1% by a set of scintillating fibre detectors, called BMS, surrounding one of the dipole magnets of the beam line. The typical beam spot, at the position of the COMPASS target is 8×8 mm^2 (Root Mean Square (RMS)). Due to radio-protection issues the maximum allowed muon flux is limited to about $2{\cdot}10^8$ per SPS cycle.

The pion decay violates parity and as a result the muons from the pion decays are polarised. The level of polarisation of the muon in the laboratory frame depends upon the energy ratio of the decay muon (E_μ) and the parent pion (E_π), their masses (m_μ, m_π) and is given by

$$P_{\mu^\pm} \approx \frac{m_\pi^2 + (1 - 2\frac{E_\pi}{E_\mu})m_\mu^2}{m_\pi^2 - m_\mu^2}. \tag{4.1}$$

Since there is a limit on the maximum muon flux, one should optimise the FOM to obtain the smallest statistical uncertainties of the performed measurement. In COMPASS the optimal beam polarisation is $-0.80 \pm 0.04\%$, which gives the parent pion mean energy of 172 GeV. The beam polarisation is not measured directly in COMPASS. Instead its estimation is based on a dedicated beam line Monte-Carlo simulation [95], whose validity was confirmed by the SMC measurement of the beam polarisation [96].

4.2 The polarised target

The measurement of the gluon polarisation was from the beginning one of the main goals of COMPASS. In order to optimise the statistical uncertainty of the measurement the optimal target material had to be chosen. Namely, the one which can be polarised to a high degree and in which the fraction of polarisable material is high. Having this in consideration the ^{6}LiD material was selected. This material can be polarised up to 50%. Moreover, the ^{6}Li can be considered as ^{4}He + D, *cf.* [97]. As a result four out of eight nucleons of the target can be polarised. Apart from the main target material there are also other target impurities like ^{1}H, ^{2}D, ^{7}Li, ^{12}C, ^{19}F, in addition ^{3}He, ^{4}He coming for the target cooling system, and ^{59}Ni and ^{64}Cu coming from the target polarisation measurement system. In total about 85% of weight of the target material is related to ^{6}LiD.

The COMPASS target was composed of two cylindrical 60 cm long and 3 cm in diameter cells. The cells are put one after another in the direction of the beam line, with a 10 cm gap between them. They are filled with ^{6}LiD in a bath of ^{3}He and ^{4}He cooling mixture. The target is kept in a strong magnetic field created by the superconducting solenoid taken from the SMC experiment [98]. The magnet system consists of a solenoid providing up to 2.5 T field and a dipole field of up to 0.5 T. The dipole field is used to reverse the target polarisation (every 8 hours) in order to cancel systematic effects related to the spectrometer acceptance and stability. The presented set-up was used for the majority of the analysed data in the years 2002 to 2004. For the 2006 year the target system was improved. Namely, in order to reduce systematic effects, instead of two target cells three cells were introduced; with a length of 30 cm-60 cm-30 cm respectively, and 5 cm gap between the cells. In addition, instead of the SMC solenoid, a dedicated COMPASS solenoid was built. The new solenoid enlarged the COMPASS angular acceptance from ± 70 mrad to ± 180 mrad.

Due to the low value of the nuclear magnetic moment, low temperature and high magnetic field are not sufficient to polarise deuterons to high degree using the Zeeman effect. For the magnetic field of 2.5 T and temperature about 0.5 K, the polarisation of deuterons would be about 0.1%. Instead, to achieve a hight level of deuteron (or nucleon) polarisation a technique called *Dynamic nuclear Polarisation* [99] is used. In COMPASS the polarisation of the ^{6}LiD target takes about 3–5 days to achieve about 50% polarisation. After the wanted level of target polarisation is reached, the target temperature is lowered to about 50 mK. In this mode, called *frozen spin mode*, the polarisation relaxation time exceeds 3000 hours.

The neighbouring target cells are polarised in opposite directions. This allows for simultaneous data taking with two target spin configurations. The aforementioned target field reversal helps to cancel acceptance effects. To further reduce systematic effects at least once per year the relative polarisation of the cells with respect to the solenoid field is also reversed. For this operation the target polarisation must be destroyed and re-built. This operation is not performed more often mostly due to the long polarisation built up time of the ^{6}LiD target.

4.3 COMPASS spectrometer

The COMPASS spectrometer was optimised to measure hadrons and muons over a large momentum range, between 0.5 and 160 GeV. It consists of a beam telescope and two spectrometers built around two dipole magnets. The first is the so-called Large Angle Spectrometer, (LAS) and the second is the Small Angle Spectrometer (SAS).

The beam telescope consisted of scintillating fibres detectors (FI) and Silicon detectors (SI). The FI have a typical resolution of about 100 μm and a time resolution of about 0.4 ns, while the SI have spatial resolution of 10 μm, and time resolution of 2.5 ns. Excellent time resolution of FI and spatial resolution of SI allow to correlate the information between the beam telescope and the momentum measurement in BMS located 100 m before the

COMPASS target.

The first spectrometer (LAS) is built around the first dipole spectrometer magnet (SM1), which is characterised by a $\int B\mathrm{d}l = 1.1$ Tm. This large angle spectrometer consists of various tracking detectors like: scintillating fibres, micromegas (MM), GEMs (GM), drift chambers (DC), straw detectors (ST) and multi wire proportional chambers (PA). The sizes of the detectors varies from 0.05×0.05 m^2 to 3.2×2.7 m^2 and resolutions from 100 μm to 1000 μm. Apart from the mentioned tracking detectors the LAS includes also a Ring Imaging Cherenkov (RICH) which allows for the identification of π, K, and p with low momentum thresholds 3 GeV, 9 GeV and 18 GeV, respectively, and up to 50 GeV. The first spectrometer ends with a Hadron Calorimeter[1], which is followed by the hadron absorber, around which dedicated tracking detectors for muon identification are placed (Muon-Wall 1). The first spectrometer allows particle momentum reconstruction with a precision of about 1–2% and the angular precision at the interaction vertex is about 0.1 mrad for a 30 GeV particle.

The second spectrometer is built around the second dipole magnet (SM2), which has $\int B\mathrm{d}l = 4.4$ Tm. This spectrometer has an angular acceptance of about 30 mrad, and mostly charged particles with momentum above 5 GeV are accepted in it. The SAS consists of larger detectors up to 5.0×2.7 m^2 with typical resolutions varying from 600 μm to 1500 μm. There are also a few GEM and FI of smaller dimensions for a precise measurement of high momentum particles emitted at low angles. The small angle spectrometer includes also an electromagnetic calorimeter (not fully constructed and not fully operational during the data taking periods used in this monograph), and a hadron calorimeter (HCAL2), followed by a 3 m long concrete hadron absorber. After the absorber, dedicated muon tracking detectors are present, as well as most of the COMPASS trigger system elements. The typical momentum resolution of the tracks accepted in SAS is about 0.5%.

The layout of the COMPASS spectrometer is presented in Fig. 4.1. COMPASS has a rather complex mix of various tracking detector types. While the complexity is not optimal from the stability point of view, it should be noted that COMPASS was/is used as a test facility for new detector concepts. For example in recent years pixelized GEM and MM detectors were included, as well as Thick GEMs. Quite a few of the ideas tested/developed in COMPASS are seriously considered for medical imaging purposes.

[1] An electromagnetic calorimeter was not yet in place for the data used in the presented analysis.

4.4 Trigger system

In order to measure the kinematics of the DIS event the scattered muon has to be reconstructed. Therefore, it is not a surprise that most of the COMPASS trigger system is dedicated to the scattered muon detection.

Three different trigger types are used in COMPASS. The most important for the presented analysis are the inclusive triggers. This means that the trigger is realised by the coincident signals in two hodoscopes which fulfil to so-called coincidence matrix. This matrix has some target pointing capability and allows to reject horizontally travelling muons from the halo of the beam. To further remove halo muons the signal from the trigger hodoscopes can be vetoed by the signal in "veto" detectors located before the target. Note that at least one of the two hodoscopes is located after the hadron absorber, therefore the vast majority of signals can be only created by muons. In the data period which is analysed in this monograph two inclusive triggers contributed about 70% to the analysed DIS sample. One of the goals of COMPASS was the measurement of Δg/g from the open charm events. These events are usually produced with rather low Q^2, which means that the muon scattering angle is low. In such case a pure inclusive trigger cannot be used, as the trigger rate would exceed the capability of the data acquisition system (DAQ). Thus, another type of trigger was needed, which in addition to the conditions of the inclusive triggers, required an energy deposit (about 4 GeV) in one of the hadron calorimeters. These are the so-called semi-inclusive triggers. Depending upon the year of data taking COMPASS used two to three such triggers. Finally, the third type of COMPASS trigger is the so-called pure calorimeter trigger. Its main purpose is to select events in which the scattered muon is produced at so large angle that it is outside of the acceptance of the largest of the hodoscopes. Such events have the largest Q^2 and in fact are not so crucial for the presented analysis. This trigger type is solely based on the signal (above 9 GeV) in hadronic calorimeters. In addition to the triggers used for physics purposes, several other triggers existed which were used for calibration and alignment like veto triggers, beam triggers and random triggers.

The muon trigger system is optimised from the point of view of efficiency rather than purity. Due to limitations of the COMPASS data acquisition system, in 2003 the typical trigger rate could not exceed 10 kHz. With the technology developments and the network connection speed increase, in later years the trigger rate could reach 30 kHz with much bigger stream of information written to tape. As a result some of the previous semi-inclusive triggers could be replaced by inclusive ones.

4.5 Data analysis chain

The raw events fulfilling the trigger condition are written to tape using the CERN CASTOR system. They can be decoded afterwards, with a special library called DaqDataDecoding. After the software calibration and alignment of the spectrometer, the decoded data are fed to the COMPASS reconstruction program CORAL. Its main purpose is to perform track and vertex reconstruction. The RICH and calorimeter clusters reconstruction as well as eventual association of the RICH and calorimeters information to a reconstructed track are also performed by CORAL. The output of CORAL has mini Data Summary Tree (mDST) format. These mDSTs are the main input for the physics analyses performed in COMPASS. A “PHysics Analysis Software Tools” (PHAST) framework provides the tools needed for the development of the analysis codes based on mDST. At this stage the final analyses are performed.

Apart from these COMPASS is also using several Monte-Carlo generator programs, *e.g.* LEPTO, PYTHIA, and HEPGEN. In the presented analysis the LEPTO event generator is used. It is a dedicated Monte-Carlo generator for DIS events. The generated events are passed through the COMPASS spectrometer simulation program COMGEANT, based on GEANT3 [100], and later by CORAL. The CORAL output of MC data can be read by PHAST. What is important is that exactly the same reconstruction and analysis code can be used on real and MC data.

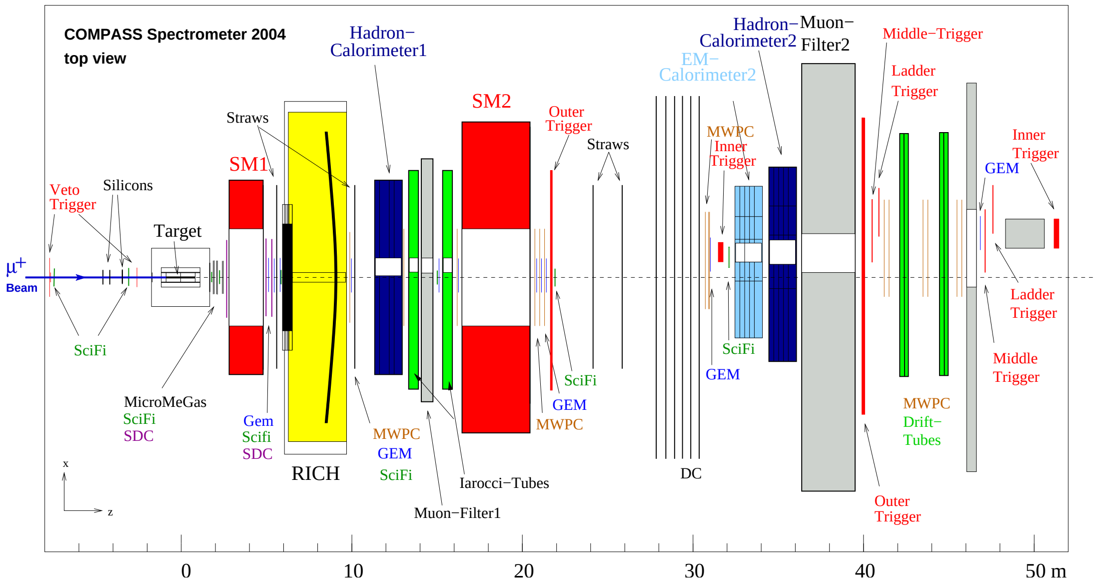

Figure 4.1: COMPASS set-up of 2004. Figure made by COMPASS Collaboration.

Chapter 5

Methods of Δg/g extraction

In this chapter the details concerning the methods used in COMPASS for the direct Δg/g extraction from DIS events with (high-p_{T}) hadron(s) produced are presented. First, the method used in [64] is described since it is the predecessor of the analysis method used in this monograph. The weaknesses of the previous method will be presented and the new method will be introduced.

5.1 Previous Δg/g extraction method

The ratio of the polarised to unpolarised differential cross sections for the production of two high-p_{T} hadrons in the DIS regime, assuming that only three processes (LP, QCDC, PGF presented in Fig. 2.5), are contributing to the cross section is given by:

$$\frac{\mathrm{d}\Delta\sigma}{\mathrm{d}\sigma} = \frac{\Delta \mathrm{g} \otimes \mathrm{d}\Delta\hat{\sigma}^{\mathrm{PGF}} \otimes H + \sum_{\mathrm{q}} e_{\mathrm{q}}^2 \Delta \mathrm{q} \otimes \mathrm{d}\Delta\hat{\sigma}^{\mathrm{LP}} \otimes H + \sum_{\mathrm{q}} e_{\mathrm{q}}^2 \Delta \mathrm{q} \otimes \mathrm{d}\Delta\hat{\sigma}^{\mathrm{QCDC}} \otimes H}{g \otimes \mathrm{d}\hat{\sigma}^{\mathrm{PGF}} \otimes H + \sum_{\mathrm{q}} e_{\mathrm{q}}^2 \mathrm{q} \otimes \mathrm{d}\hat{\sigma}^{\mathrm{LP}} \otimes H + \sum_{\mathrm{q}} e_{\mathrm{q}}^2 \mathrm{q} \otimes \mathrm{d}\hat{\sigma}^{\mathrm{QCDC}} \otimes H}, \tag{5.1}$$

where for simplicity all kinematic variable dependencies are omitted. Here, (Δ)g and (Δ)q stand for (polarised) gluon and quark PDF, respectively. The symbol $\otimes$ stands for convolution integrals and $(\Delta)\hat{\sigma}^i$ denotes the (polarised) partonic cross-section for the process type $i =$ { PGF, LP, QCDC}. The partonic cross section for different processes can be computed in QCD *cf.* [57]. The symbol H denotes fragmentation functions. These are non-perturbative objects which encode information about the parton fragmentation into hadrons. One should note that in the case of LP and of PGF one deals with the same quark fragmentation, while in the case of QCDC both quark and gluon fragmentation functions are important. Eq. 5.1 can be rewritten as

$$A_{\mathrm{LL}}^{2h}(x_{\mathrm{Bj}}) = \langle a_{\mathrm{LL}}^{\mathrm{PGF}} R_{\mathrm{PGF}} \rangle \left\langle \frac{\Delta \mathrm{g}}{\mathrm{g}}(x_{\mathrm{g}}) \right\rangle + \langle a_{\mathrm{LL}}^{\mathrm{LP}} R_{\mathrm{LP}} \rangle \left\langle A_1^{\mathrm{LP}}(x_{\mathrm{Bj}}) \right\rangle + \left\langle a_{\mathrm{LL}}^{\mathrm{QCDC}} R_{\mathrm{QCDC}} \right\rangle \left\langle A_1^{\mathrm{QCDC}}(x_{\mathrm{C}}) \right\rangle, \tag{5.2}$$

where the leading process inclusive asymmetry A_1^{LP} is equivalent to A_1^{QCDC} and is given by the ratio of spin-dependent and spin-independent quark distribution functions, weighted by the squared electric charge and summed over all quark flavours

$$A_1^{\mathrm{LP}} \equiv A_1^{\mathrm{QCDC}} \equiv \frac{\sum_{\mathrm{q}} e_{\mathrm{q}}^2 \Delta \mathrm{q}}{\sum_{\mathrm{q}} e_{\mathrm{q}}^2 \mathrm{q}}. \tag{5.3}$$

The R_i and a_{LL}^i in Eq. (5.2) are the fractions of the process i and corresponding analysing powers (*i.e.* the asymmetry of the partonic cross sections ratios $\Delta\hat{\sigma}^i/\hat{\sigma}^i$), respectively. The variables x_{g}, x_{Bj} and x_{C} are the nucleon momentum fraction carried by gluons in the PGF process, the nucleon momentum fraction carried by a quark in the LP process and the nucleon momentum fraction carried by a quark in the QCDC process, respectively. The averages present in Eq. (5.2) are defined in the following way:

$$\langle a_{\mathrm{LL}}^{\mathrm{PGF}} R_{\mathrm{PGF}} \rangle \equiv \frac{a_{\mathrm{LL}}^{\mathrm{PGF}} g \otimes \mathrm{d}\hat{\sigma}^{\mathrm{PGF}} \otimes H}{\mathrm{d}\sigma}, \tag{5.4}$$

$$\left\langle \frac{\Delta \mathrm{g}}{\mathrm{g}} \right\rangle \equiv \frac{\Delta \mathrm{g}/\mathrm{g}\, a_{\mathrm{LL}}^{\mathrm{PGF}}\, g \otimes \mathrm{d}\hat{\sigma}^{\mathrm{PGF}} \otimes H}{a_{\mathrm{LL}}^{\mathrm{PGF}}\, g \otimes \mathrm{d}\hat{\sigma}^{\mathrm{PGF}} \otimes H}, \tag{5.5}$$

$$\langle a_{\mathrm{LL}}^{\mathrm{LP}} R_{\mathrm{LP}} \rangle \equiv \frac{a_{\mathrm{LL}}^{\mathrm{LP}} \sum_{\mathrm{q}} e_{\mathrm{q}}^2\, \mathrm{q} \otimes \mathrm{d}\hat{\sigma}^{\mathrm{LP}} \otimes H}{\mathrm{d}\sigma}, \tag{5.6}$$

$$\left\langle A_1^{\mathrm{LP}} \right\rangle \equiv \frac{A_1^{\mathrm{LP}} a_{\mathrm{LL}}^{\mathrm{LP}} \sum_{\mathrm{q}} e_{\mathrm{q}}^2\, \mathrm{q} \otimes \mathrm{d}\hat{\sigma}^{\mathrm{LP}} \otimes H}{a_{\mathrm{LL}}^{\mathrm{LP}} \sum_{\mathrm{q}} e_{\mathrm{q}}^2\, \mathrm{q} \otimes \mathrm{d}\hat{\sigma}^{\mathrm{LP}} \otimes H}, \tag{5.7}$$

$$\langle a_{\mathrm{LL}}^{\mathrm{QCDC}} R_{\mathrm{QCDC}} \rangle \equiv \frac{a_{\mathrm{LL}}^{\mathrm{QCDC}} \sum_{\mathrm{q}} e_{\mathrm{q}}^2 \mathrm{q} \otimes \mathrm{d}\hat{\sigma}^{\mathrm{QCDC}} \otimes H}{\mathrm{d}\sigma}, \tag{5.8}$$

$$\left\langle A_1^{\mathrm{QCDC}} \right\rangle \equiv \frac{A_1^{\mathrm{QCDC}} a_{\mathrm{LL}}^{\mathrm{QCDC}} \sum_{\mathrm{q}} e_{\mathrm{q}}^2 \mathrm{q} \otimes \mathrm{d}\hat{\sigma}^{\mathrm{QCDC}} \otimes H}{a_{\mathrm{LL}}^{\mathrm{QCDC}} \sum_{\mathrm{q}} e_{\mathrm{q}}^2 \mathrm{q} \otimes \mathrm{d}\hat{\sigma}^{\mathrm{QCDC}} \otimes H}. \tag{5.9}$$

Note that Eqs. (5.4)–(5.9) correspond to weighted averages, with a weight factor equal to $a_{\mathrm{LL}}^i R_i$ of the corresponding process i.

Taking into account that $A_1^{\rm LP}$ mostly depends upon $x_{\rm Bj}$ and assuming that in the range where the averages of $\Delta g/g$ and $A_1^{\rm QCDC}$ are computed these functions can be approximated by a linear function, Eq. (5.2) can be further simplified to

$$A_{\rm LL}^{2h}(x_{\rm Bj}) = \langle a_{\rm LL}^{\rm PGF} R_{\rm PGF}\rangle \frac{\Delta g}{g}(\langle x_{\rm g}\rangle) + \langle a_{\rm LL}^{\rm LP} R_{\rm LP}\rangle A_1^{\rm LP}(x_{\rm Bj}) + \langle a_{\rm LL}^{\rm QCDC} R_{\rm QCDC}\rangle A_1^{\rm LP}(\langle x_{\rm C}\rangle). \tag{5.10}$$

Here, the average values of $x_{\rm g}$ and $x_{\rm C}$ [1] are weighted by the corresponding $a_{\rm LL}^i R_i$. Eq. (5.2) is valid in the DIS regime at LO and under the assumption of spin-independent fragmentation. Note that possible spin dependencies, as discussed in [101], are expected to be small in the COMPASS kinematic domain. It should be also noted that $a_{\rm LL}^i$ are proportional to the depolarisation factor D, which is the fraction of the muon beam polarisation transferred to the virtual photon, and in addition that $a_{\rm LL}^{\rm LP} \equiv D$.

In order to extract $\Delta g/g$ from Eq. (5.2) the asymmetry related to background processes has to be estimated and subtracted. $A_{\rm LL}^{\rm LP}$ is evaluated from the inclusive lepton-nucleon asymmetry $A_{\rm LL}^{\rm incl}$. This asymmetry can be decomposed in a similar way as $A_{\rm LL}^{\rm 2h}$

$$A_{\rm LL}^{\rm incl}(x_{\rm Bj}) = \langle R_{\rm PGF}^{\rm incl} a_{\rm LL}^{\rm incl,PGF}\rangle \frac{\Delta g}{g}(\langle x_{\rm g}\rangle) + \langle R_{\rm LP}^{\rm incl} a_{\rm LL}^{\rm incl,LP}\rangle A_1^{\rm LP}(x_{\rm Bj}) + \langle R_{\rm QCDC}^{\rm incl} a_{\rm LL}^{\rm incl,QCDC}\rangle A_1^{\rm LP}(\langle x_{\rm C}\rangle). \tag{5.11}$$

A similar decomposition is performed for $A_{\rm LL}^{\rm incl}(x_{\rm C})$, where replacements of $x_{\rm Bj} \to x_{\rm C}$, $x_{\rm g} \to x'_{\rm g}$ and $x_{\rm C} \to x'_{\rm C}$ are done in Eq. (5.11). Combining Eqs. (5.2), (5.11) and the analogue of (5.11) but for $A_{\rm LL}^{\rm incl}(x_{\rm C})$ and in addition neglecting small terms, one obtains

$$\Delta g/g(x_{\rm g}^{\rm av}) = \frac{A_{\rm LL}^{\rm 2h}(x_{\rm Bj}) - a^{\rm corr}}{\lambda_1 - \lambda_2}. \tag{5.12}$$

Here,

$$x_{\rm g}^{\rm av} = \frac{\lambda_1 \langle x_{\rm g}\rangle - \lambda_2 \langle x'_{\rm g}\rangle}{\lambda_1 - \lambda_2},$$

$$\lambda_1 = \langle a_{\rm LL}^{\rm PGF} R_{\rm PGF}\rangle - \langle a_{\rm LL}^{\rm incl,PGF} R_{\rm PGF}^{\rm incl}\rangle \frac{\langle R_{\rm LP}\rangle}{\langle R_{\rm LP}^{\rm incl}\rangle}, \qquad \lambda_2 = \langle a_{\rm LL}^{\rm incl,PGF} R_{\rm PGF}^{\rm incl}\rangle \frac{\langle a_{\rm LL}^{\rm QCDC} R_{\rm QCDC}\rangle}{\langle D R_{\rm LP}^{\rm incl}\rangle},$$

and

$$a^{\rm corr} = A_{\rm LL}^{\rm incl}(x_{\rm Bj}) \frac{\langle R_{\rm LP}\rangle}{\langle R_{\rm LP}^{\rm incl}\rangle} + A_{\rm LL}^{\rm incl}(\langle x_C\rangle) \left(\frac{\langle a_{\rm LL}^{\rm QCDC} R_{\rm QCDC}\rangle}{\langle D R_{\rm LP}^{\rm incl}\rangle} - \frac{\langle a_{\rm LL}^{\rm incl,QCDC} R_{\rm QCDC}^{\rm incl}\rangle}{\langle D R_{\rm LP}^{\rm incl}\rangle} \frac{\langle R_{\rm LP}\rangle}{\langle R_{\rm LP}^{\rm incl}\rangle} \right) - A_{\rm LL}^{\rm incl}(\langle x'_{\rm C}\rangle) \frac{\langle a_{\rm LL}^{\rm incl,QCDC} R_{\rm QCDC}^{\rm incl}\rangle}{\langle D R_{\rm LP}^{\rm incl}\rangle} \frac{\langle a_{\rm LL}^{\rm QCDC} R_{\rm QCDC}\rangle}{\langle D R_{\rm LP}^{\rm incl}\rangle}.$$

[1] Averaging of $x_{\rm Bj}$ is not needed, but effectively it is done experimentally since only a given range of $x_{\rm Bj}$ is studied.

In the presented method to obtain Δg/g from the $A_{\rm LL}^{\rm 2h}$ asymmetries, one effectively "corrects" the latter asymmetry by a factor $a_{\rm corr}$. Observe that for $x_{\rm Bj}$ about 0.01–0.02 the $A_1^{\rm d,incl}$ asymmetry is indeed small and could be neglected. However, for the same events the typical $\langle x_{\rm C}\rangle$ is about 0.12, and since $A_1^{\rm d,incl}(0.12) \approx 0.08$ one cannot neglect $a_{\rm corr}$ term in the analysis.

The other observation is related to the denominator of Eq. (5.12), to which the statistical uncertainty of the extracted Δg/g is proportional. The value of $\langle R_{\rm PGF} a_{\rm LL}^{\rm PGF}\rangle$ is reduced by a factor proportional to the value of $\langle R_{\rm PGF}^{\rm incl}\rangle$, *i.e.* to the PGF content in the inclusive sample. The presence of PGF in the inclusive sample effectively results in an increase of the statistical uncertainty of the extracted Δg/g. On several occasions it was suggested that the analysis would be greatly simplified if one would use LO PDFs from world data fits to obtain $A_{\rm LL}$. The problem with this suggestion is related to the notion of what 'LO' means. Namely, the LO method for Δg/g extraction presented deals with QCD diagrams up to α_S. At the same time the LO analysis of PDFs uses just LP to describe the whole asymmetry, effectively assuming $R_{\rm PGF}^{\rm incl} = R_{\rm QCDC}^{\rm incl} = 0$. As can be deduced from the denominator of Eq. (5.12), such an assumption leads to an incorrect decrease of the statistical uncertainty of Δg/g. In the case of the presented analysis the obtained statistical uncertainty of Δg/g would be by 20%–30% smaller comparing to the case of correct treatment of $R_{\rm PGF}^{\rm incl}$ and $R_{\rm QCDC}^{\rm incl}$. Similarly, in the COMPASS kinematics one cannot use the low-$p_{\rm T}$ data and assume that they just correspond to $A_{\rm LL}^{\rm LP}$ as in [68]. Such a method introduces smaller bias than the aforementioned LO PDF usage, because regions enriched in PGF and QCDC are removed from the sample. Nevertheless for a sample with $p_{\rm T} < 0.8$ GeV used to calculate $A_1^{\rm LP}$, the bias in the Δg/g uncertainty in the COMPASS case can reach 15%–25%.

The number of observed DIS events is proportional to the beam flux (Φ), the acceptance (a), the number of scattering centres in the target (n) and the unpolarised cross-section (σ_0). To extract Δg/g from the COMPASS data the employed method was similar to the one of [102], where data are combined in a way such that ($\Phi a n \sigma_0$) cancels. Namely, the neighbouring target cells are polarised in opposite directions. This allows for the simultaneous measurement of the two spin states, effectively cancelling the σ_0 factor. However, due to the different z position of cells along the beam line they have different acceptances and in addition they may have different number of scattering centres. In order to cancel the an factors, the spin orientations of the target cells were reversed on a regular basis. To cancel the beam flux in the offline analysis only the events for which the extrapolation of the beam track crosses entirely all target cells are kept. Labelling the target cells as u, d (upstream and downstream) before and u', d' after the field reversal

[2] one can conclude that the factors $\Phi a n \sigma_0$ cancel in the double ratio $(N_u N'_d)/(N'_u N_d)$, where N_i is the number of events observed in a given target cell.

In experimental conditions it may happen that $(a_u a'_d)/(a'_u a'_d) \neq 1$ for example, due to detector failures or mechanical detector movements caused by day/night temperature variations, *etc.* In such case, false asymmetries are generated and the physics asymmetry results are biased. More details concerning the estimation of false asymmetries are presented in Section 8.3.

The double ratio $(N_u N'_d)/(N'_u N_d)$ can be expressed as a second-order equation for $\Delta g/g$. To increase the precision of the measurement the weighted method of asymmetry extraction is used. The $\Delta g/g$ is obtained from the following equation:

$$\frac{p_u p_{d'}}{p_{u'} p_d} = \frac{(1 + \langle A_u^{\mathrm{corr}} \rangle_w + \langle \Lambda_u \rangle_w \ \Delta g/g(x_{\mathrm{g}}^{\mathrm{av}}))(1 + \langle A_{d'}^{\mathrm{corr}} \rangle_w + \langle \Lambda_{d'} \rangle_w \ \Delta g/g(x_{\mathrm{g}}^{\mathrm{av}}))}{(1 + \langle A_{u'}^{\mathrm{corr}} \rangle_w + \langle \Lambda_{u'} \rangle_w \ \Delta g/g(x_{\mathrm{g}}^{\mathrm{av}}))(1 + \langle A_d^{\mathrm{corr}} \rangle_w + \langle \Lambda_d \rangle_w \ \Delta g/g(x_{\mathrm{g}}^{\mathrm{av}}))}, \tag{5.13}$$

where p_j is the sum of event weights w from sample $j = u, u', d, d'$ and $\langle A_j^{\mathrm{corr}} \rangle_w$ and $\langle \Lambda_j \rangle_w$ are the weighted means of $f P_{\mathrm{b}} P_{\mathrm{t}} a^{\mathrm{corr}}$ and $f P_{\mathrm{b}} P_{\mathrm{t}}(\lambda_1 - \lambda_2)$, respectively. The weight is defined as $w = f P_{\mathrm{b}}(\lambda_1 - \lambda_2)$. Note that the weight does not contain the target polarisation, since the value of p_{T} changes with time. A time dependence of the weight may introduce an asymmetry bias in the analysis. It should be also noticed that $\Delta g/g(x_{\mathrm{g}}^{\mathrm{av}})$ is directly obtained from Eq. (5.13), without an intermediate extraction of the $A_{\mathrm{LL}}^{2\mathrm{h}}(x_{\mathrm{Bj}})$ asymmetry. However, in [64] the values of $A_{\mathrm{LL}}^{2\mathrm{h}}(x_{\mathrm{Bj}})$ were separately obtained in bins of x_{Bj} and p_{T}, to allow their future use as input to NLO analyses of $\Delta g/g$, once the corresponding theory will be sufficiently developed.

The extraction of $\Delta g/g$ using this method relies on the knowledge of R_i, a_{LL}^i and x_i. As already indicated in Section 3.2 generally these quantities cannot be obtain from data. In the case of a high-p_{T} hadron analysis only x_{Bj} and $a_{\mathrm{LL}}^{\mathrm{LP}}$ are obtained from data. To estimate the remaining parameters a model has to be used, *e.g.* LEPTO used in [60, 64]. In the previous analyses [60, 66] only the mean values of R_i and a_{LL}^i obtained from MC were used. For the method published in [64] due to a more advanced usage of artificial neural networks (NN) trained on MC data, it was possible to estimate R_i and a_{LL}^i on an event-by-event basis. As a result, R_i and a_{LL}^i could be included in the weight, leading to an improvement of FOM. Moreover, in the same way the value of x_{g} could be estimated on an event-by-event basis. Thanks to this, the $\Delta g/g$ values were for the first time obtained in three bins of x_{g}. Details concerning the MC and the NN approach will be presented in Chapter 7.

[2] For 2006 data, where there were three cells, the outer ones are denoted as u while the centre cell is denoted as d.

5.1.1 Limitations of the analysis method

The presented method was a step forward in the direct analyses of Δg/g. However, soon it became obvious that some elements of the analysis could be further improved. Here is a short and incomplete list of various ideas and observations which shaped the analysis method explained in the next section.

Tests have shown that using information only from the leading hadron in p_T to train the NN resulted in only marginally worse ($\approx 2\%$) final uncertainty of Δg/g. The fact that the second hadron carries so few information might seem surprising, but this is largely due to the fact that COMPASS studies only charged hadrons. Tests performed on MC data have shown that in 70% of the cases the selected sub-leading hadron in p_T was not the correct one. It was therefore concluded that one can safely neglect the second hadron in the analysis. By doing so, one gets additional events with high-p_T leading hadron for which no second high-p_T hadron was found, so there is a gain in FOM. In addition, the analysis becomes less MC dependent as less information from the generator is used.

One difficulty was that the weight used in the analysis was somewhat complex. The estimation of systematic uncertainties, specially those related to the MC model dependence, was rather difficult, since there were many combinations of parameters extracted from MC to consider.

Another issue was related with the appearance in the a_corr term of not only x_C but also x'_C. In fact the uncertainty related to assumptions concerning the relation of x_C with x'_C gave rise to the second highest systematic uncertainty in [64]. One could try to avoid the use of A_1^incl and instead find another way to estimate the A_1^LP asymmetry.

The presented analysis method is model dependent. However, besides the ratios of data to MC the method does not offer any other means to verify if *e.g.* R_QCDC is correct. One can just hope/assume that if the data are well described by a MC model, the values of R_i obtained from the model are indeed close to reality. It would be beneficial for the trustworthiness of the Δg/g result if some additional tests could further support the selected LEPTO model.

5.2 The all-p_T method

Let us re-write Eq. (5.10) for the one hadron case,

$$A_\mathrm{LL}^\mathrm{1h}(x_\mathrm{Bj}) = \langle R_\mathrm{PGF} a_\mathrm{LL}^\mathrm{PGF} \rangle \frac{\Delta \mathrm{g}}{\mathrm{g}}(\langle x_\mathrm{g} \rangle) + \langle R_\mathrm{LP} a_\mathrm{LL}^\mathrm{LP} \rangle A_1^\mathrm{LP}(x_\mathrm{Bj}) + \langle R_\mathrm{QCDC} a_\mathrm{LL}^\mathrm{QCDC} \rangle A_1^\mathrm{QCDC}(\langle x_\mathrm{C} \rangle). \tag{5.14}$$

Keeping in mind that R_i and a^i_{LL} are estimated on an event-by-event basis, if there would be enough variation of the product $R_i a^i_{\mathrm{LL}}$ over the whole kinematic domain one could simply extract simultaneously Δg/g and A_1^{LP} from the same data set. In such case x'_{g} and x'_{C} would not appear and the parametrisation of A_1^{incl} would also not be used, *i.e.* two systematic uncertainties of [64] would be immediately eliminated. Moreover, as described later in the chapter, the weight would have a simpler form, allowing for easier and more stable estimation of systematic uncertainties. Since the two asymmetries are then extracted simultaneously, they are affected by the same spectrometer instabilities. As a result the potential false asymmetries of Δg/g are also reduced. Finally, the careful reader may have noticed that instead of $A_1^{\mathrm{LP}}(\langle x_{\mathrm{C}}\rangle)$ as in Eq. (5.10), here $A_1^{\mathrm{QCDC}}(\langle x_{\mathrm{C}}\rangle)$ is used. This distinction is kept only to emphasise an additional fact present in the simultaneous extraction method. Namely, one can separately extract A_1^{LP} and A_1^{QCDC} and by means of a statistical test verify that they are indeed equal for the same x value. The simplest cases in which such test would fail is if the incorrect values of $R_i a^i_{\mathrm{LL}}$ were used or if higher-order corrections were important. The simultaneous extraction method gives some additional hints concerning the quality of the model beyond the data/MC comparison plots. More details on these systematic studies are presented in Subsection 8.6.1.

To minimise the statistical uncertainty of the extracted value of Δg/g in a simultaneous fit one should have a sample where the range of R_i is as wide as possible. Thus, the full p_{T} range of the hadron leading in p_{T} is used, instead of a restricted region as in [64]. The idea behind is simple, the low-p_{T} range is a rather clean sample of LP process, while in the high-p_{T} region the sample is enriched in PGF and QCDC processes. The idea of the all-p_{T} analysis faced some initial doubts. Namely, the main criticism was that the method uses a region with very low values of R_{PGF} which has large statistics. Naively, it would seem that these 'bad' events may largely contribute to Δg/g, thus making the final result questionable. However, in reality the situation is opposite. Let us consider an academic example, where one compares the asymmetries in the low-p_{T} and in the high-p_{T} regions, assuming for simplicity that only PGF and LP contribute. We consider two situations where in the low-p_{T} region R_{PGF} is either small or zero, and also for simplicity we assume that the asymmetry measured in the low-p_{T} range has zero uncertainty:

$$
\begin{aligned}
&0.4\,\Delta\mathrm{g/g} + 0.6\,A_1^{\mathrm{LP}} = x \pm 0.10, && 0.4\,\Delta\mathrm{g/g} + 0.6\,A_1^{\mathrm{LP}} = x \pm 0.10,\\
&0.1\,\Delta\mathrm{g/g} + 0.9\,A_1^{\mathrm{LP}} = y \pm 0.00, && 0.0\,\Delta\mathrm{g/g} + 1.0\,A_1^{\mathrm{LP}} = y \pm 0.00.
\end{aligned}
$$

Combining the equations one obtains the Δg/g uncertainty of 0.30 and 0.25 for the data in the left and the right columns, respectively. As can be seen, the presence of R_{PGF} at low-p_{T} *increases* the statistical error of the extracted Δg/g. Thus, it acts in an opposite way with respect to the raised concerns. Even if at low-$p_{\rm T}$ $R_{\rm PGF}$ is small and has large relative error, it is still important. One cannot neglect the presence of $R_{\rm PGF}$ at low-$p_{\rm T}$, as otherwise the statistical uncertainty of Δg/g becomes underestimated[3].

The ideas on how to simultaneously extract signal and background asymmetries using the weighted method were presented in [103]. The COMPASS experiment has already used this method in the extraction of Δg/g from open charm events, see [55]. The method presented in [103] had to be adapted to the all-$p_{\rm T}$ case. A short summary, based on [30], is presented below.

The predicted number of events $N^{\rm pre}(x_{\rm Bj})$ can be calculated from the SIDIS cross sections of LP, QCDC, and PGF as:

$$\begin{aligned} N^{\rm pre}(x_{\rm Bj}) = an\Phi\sigma_0\Big(1 + \big\langle fP_{\rm b}P_{\rm t}a_{\rm LL}^{\rm PGF}R_{\rm PGF}\ \frac{\Delta {\rm g}}{\rm g}(x_{\rm g})\big\rangle + \big\langle fP_{\rm b}P_{\rm t}a_{\rm LL}^{\rm LP}R_{\rm LP}\ A_1^{\rm LP}(x_{\rm Bj})\ \big\rangle \\ +\big\langle fP_{\rm b}P_{\rm t}a_{\rm LL}^{\rm QCDC}R_{\rm QCDC}\ A_1^{\rm QCDC}(x_{\rm C})\ \big\rangle\Big). \end{aligned} \tag{5.15}$$

Similarly to Eq. (5.2) all variables but $x_{\rm Bj}$ were integrated over. As mentioned before, the two symbols $A_1^{\rm LP}$ and $A_1^{\rm QCDC}$ denote the same asymmetry and the distinction is kept only to emphasise the fact that in the new method there are two estimators of the same quantity. As in the method described previously, Eq. (5.15) is valid at LO QCD, assuming spin-independent fragmentation. The equation can be written in a shorter form as:

$$N^{\rm pre}(x_{\rm Bj}) = \alpha\left(1 + \sum_i \big\langle\beta_i\ A^i(x_i)\big\rangle\right). \tag{5.16}$$

Here, $\alpha = an\Phi\sigma_0$, $\beta_i = fP_{\rm b}P_{\rm t}a_{\rm LL}^iR_i$. The $\langle\beta_iA^i(x_i)\rangle$ denotes the average of $\beta_iA^i(x_i)$ over the experimental kinematic domain. For simplicity the x_i dependence of β_i is omitted.

In order to extract simultaneously Δg/g and $A_1^{\rm LP}$ (and $A_1^{\rm QCDC}$), the event yields are considered separately for the three processes i. Since the asymmetries are x_i dependent, and to avoid integration over a region with large asymmetry changes the analysis is performed in several bins of the corresponding x_i variable (indexed by m). For each configuration $k = u$, d, u', d' the weighted event yields "predicted", $\mathcal{N}^{\rm pre}_{i_m,k}$, and "observed", $\mathcal{N}^{\rm obs}_{i_m,k}$, are calculated. The weight is defined as $w = fP_{\rm b}a_{\rm LL}R$. The target polarisation changes with time, thus it cannot be included in the weight. As pointed out in [104], one could use a more optimal weight and by means of an iterative procedure decrease the statistical uncertainty of the obtained asymmetries. The method described in [104] was

[3]The situation is analogous to the discussed use of LO polarised PDFs for the analysis in [64], in Section 5.1.

tried, but the gain in FOM was found negligible, changing the uncertainty of Δg/g only on the 4th significant digit. The observed weighted yield of events for the process i in the m-th bin of x_i is given by

$$\mathcal{N}^{\mathrm{obs}}_{i_m,k} = \sum_{n=1}^{N_k} \epsilon_{m,i} w_{i,n} = \sum_{n=1}^{N_k} \epsilon_{m,i} f_n P_{\mathrm{b},n} a^i_{\mathrm{LL},n} R_{i,n}. \tag{5.17}$$

The sum runs over the number of events N_k observed for the configuration k, and $\epsilon_{m,i} = 1$ if the given event x_i belongs to its m-th bin, and $\epsilon_{m,i} = 0$ otherwise. Since only estimators of the probability R_i that the event originated from a particular partonic process are known, each event contributes to all three event yields $\mathcal{N}^{\mathrm{obs}}_{\mathrm{PGF}_m,k}$, $\mathcal{N}^{\mathrm{obs}}_{\mathrm{QCDC}_{m'},k}$, and $\mathcal{N}^{\mathrm{obs}}_{\mathrm{LP}_{m''},k}$. This fact is schematically presented in Fig. 5.1. To avoid double counting, as the same events are used multiple times in the analysis, the correlation between these event yields is taken into account by the covariance matrix $\mathrm{cov}_{i_m j_{m'},k} = \sum_{n=1}^{N_k} \epsilon_{m,i}\epsilon_{m',j} w_{i,n} w_{j,n}$.

The predicted weighted yields of events of each type, $\mathcal{N}^{\mathrm{pre}}_{i_m,k}$, are approximated by

$$\mathcal{N}^{\mathrm{pre}}_{i_m,k} \approx \alpha_{k,w_{i_m}} \left(1 + \sum_j \sum_{m'} \langle \beta_{j_{m'}} \rangle_{w_{i_m}} \langle A^j(x_j) \rangle_{m'} \right), \tag{5.18}$$

where $\alpha_{k,w_{i_m}}$ is the weighted value of α_k, and

$$\langle \beta_{j_{m'}} \rangle_{w_{i_m}} \approx \frac{\sum_{n=1}^{N_k} \epsilon_{m,i}\epsilon_{m',j} \beta_{j,n} w_{i,n}}{\sum_{n=1}^{N_k} \epsilon_{m,i} w_{i,n}}. \tag{5.19}$$

In these equations an additional assumption is used, namely $\langle \beta_j A^j(x_j) \rangle \simeq \langle \beta_j \rangle \langle A^j(x_j) \rangle$. If the spectrometer is stable enough one can assume that $\alpha_{u,w_{i_m}}/\alpha_{d,w_{i_m}} = \alpha_{u',w_{i_m}}/\alpha_{d',w_{i_m}}$.

With these inputs the standard χ^2 can be defined as $\chi^2 = (\boldsymbol{\mathcal{N}}^{\mathbf{obs}} - \boldsymbol{\mathcal{N}}^{\mathbf{pre}})^T \mathrm{cov}^{-1} (\boldsymbol{\mathcal{N}}^{\mathbf{obs}} - \boldsymbol{\mathcal{N}}^{\mathbf{pre}})$. Here $\boldsymbol{\mathcal{N}}^{\mathbf{obs}}$ and $\boldsymbol{\mathcal{N}}^{\mathbf{pre}}$ are vectors with the components $\mathcal{N}^{\mathrm{obs}}_{i_m,k}$ and $\mathcal{N}^{\mathrm{pre}}_{i_m,k}$, respectively. The MINUIT programme [105] is used for the χ^2 minimisation. To increase precision and stability of the uncertainty determination the HESSE method from the same package is used. It should be noticed that so far there is no free parameter in the fit, *i.e.* there is one unique solution for Δg/g, A_1^{LP} and A_1^{QCDC}. The analysis is performed in 12 bins in x_{Bj}, 6 in x_{C} and either 1 or 3 bins in x_{g}. The six highest bins in x_{Bj} have the same numerical limits as the 6 bins in x_{C}. In COMPASS, a kinematic limit $x_{\mathrm{C}} \gtrapprox 0.06$ holds.

One can eliminate several parameters from the fit, thus increasing number of degrees of freedom, by using the relation $A_1^{\mathrm{LP}}(x) = A_1^{\mathrm{QCDC}}(x)$. Under this assumption the correlations between parameters obtained in the fit are reduced. As a consequence the uncertainty of the extracted parameters, including Δg/g, is also reduced. The difference between the $\Delta g/g$ results obtained with/without the assumption $A_1^{\mathrm{LP}}(x) = A_1^{\mathrm{QCDC}}(x)$ will be discussed in Chapter 8. It should be stressed that for a given event x_{Bj} and x_{C} will be still different, see Fig. 5.1. What happens is that there is a group of events which under an assumption of being LP belong to certain x_{Bj} bin, and there is another group of events which under an assumption of being QCDC has x_{C} in the same range as x_{Bj} of the previous group. The equality of $A_1^{\mathrm{LP}}(x) = A_1^{\mathrm{QCDC}}(x)$ will be used for these groups, *i.e.* six groups presented in Fig. 5.1 starting from $x_i > 0.06$.

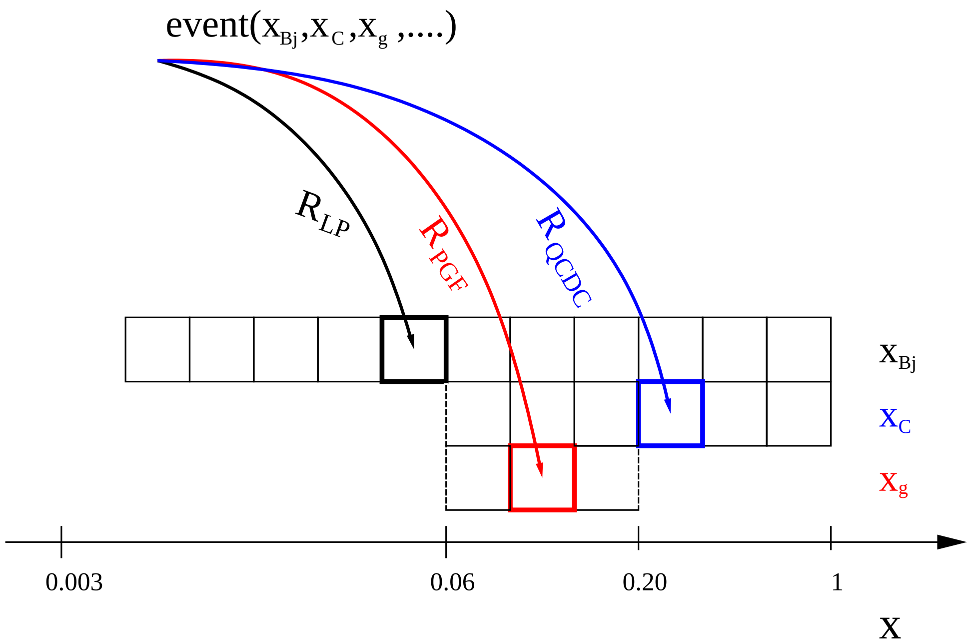

Figure 5.1: For the purpose of simultaneous extraction of $\Delta g/g$ and background asymmetries the same event is counted three times for different processes in its corresponding x_i bin. See text for details.

Chapter 6

Data selection and experimental inputs

In this chapter the selection criteria applied to the data sample used for the $\Delta g/g$ extraction are presented, as well as the experimental inputs like P_{t}, P_{b}, f and D. The remaining factors required for $\Delta g/g$ extraction, namely R_i, a^i_{LL}, x_{g} and x_{C}, are obtained from MC and are discussed in the next chapter.

6.1 Data selection

First the quality of data is examined. The periods with questionable data quality are identified by the so-called "bad run" and "bad spill" list. These lists are collections of runs and spills for which spectrometer instabilities were detected. These instabilities can be related to problems in a particular detector and reflected into global parameters like the number of reconstructed tracks per event. Runs and spills in these lists are removed from the analysis. In addition only runs present in the so-called grouping list are used. As described in Section 5.2, to extract $\Delta g/g$ one has to combine data before and after a field reversal. The double ratio of acceptances should fulfil $(a_u a'_d)/(a'_u a'_d) = 1$, as otherwise false asymmetries are generated. The "grouping list" consists precisely of groups of runs for which stability tests assure that the equation $(a_u a'_d)/(a'_u a'_d) = 1$ holds. These pre-selection criteria remove on average 7% of the sample.

In the next step of data selection the cuts related mostly with muon kinematic are applied. The interaction vertex (IV) has to be reconstructed and its position be located inside the target cells. The interaction vertex must contain the beam and scattered muons (μ, μ') as well as at least one potential hadron candidate. The beam momentum is restricted to the range 140−180 GeV, where the usage of the program to simulate values of the beam polarisation is justified. Additionally, to ensure muon flux cancellation in the double ratio, for a given incoming muon track its extrapolation has to cross fully inside all the target cells.

After the pre-selection step the following kinematic cuts are applied. In order to ensure that the analysis is performed in the perturbative region a $Q^2 > 1$ GeV^2 cut is applied. This cut removes about 90% of the whole data sample, more than all other cuts together. The analysis is restricted to a region of $0.1 < y < 0.9$. The lower limit is related with the correlated low values of $D \rightarrow a^i_{\mathrm{LL}}$, resulting in increased sensitivity to the time instabilities of the spectrometer. The upper limit removes events strongly affected by radiative effects. Finally, only events for which $x_{\mathrm{Bj}}< 1$ are kept in the analysis.

The remaining cuts apply to the hadron candidates. The hadron candidate should have a number of crossed radiation lengths smaller than 15 and should not be detected in a zone downstream of the hadron absorber, in order to exclude muons. To avoid contamination by low-momentum tracks, with poorly reconstructed momentum (using just the fringe-field of SM1), the track trajectory must not end before the SM1 magnet. Some additional quality criteria are also applied, like $\chi^2/ndf < 20$ and that the track should not cross the target solenoid walls (large multiple scattering).

Special care is taken to reject diffractive events. Namely, diffraction can be considered as a higher twist effect and it is not described in the formalism of LP, QCDC and PGF used in this analysis. To largely reduce the contamination of the sample by these events, two additional criteria for event selection are applied. The fraction of photon energy carried by a hadron candidate, z, must be below 0.85, otherwise the whole event is discarded. Moreover, a special procedure is established for events with exactly two oppositely charged tracks. In case their $z_1 + z_2 > 0.95$ the event is discarded. This cut mostly removes events from diffractive ρ^0 production, which is a dominant diffraction channel in the COMPASS kinematic domain.

From the selected hadrons in an event, the one with the highest p_{T} is selected. As explained in Section 5.2, in the all-p_{T} method no p_{T} limit is required for the leading hadron. However, from the comparison of data and MC, it was decided to restrict the region of analysis to $(0.05 < p_{\mathrm{T}} < 2.5)$ GeV. In the region of $p_{\mathrm{T}} < 0.05$ GeV the sample is largely contaminated by electrons and positrons coming from radiative events. On the other hand in the region $p_{\mathrm{T}} > 2.5$ GeV the two programs to simulate secondary interactions in the target give inconsistent results. More details concerning the upper p_{T} cut will be given in Subsection 7.1.1.

The data reduction flow after each cut is presented in Table 6.1. The total number of events used in the analysis is 113 millions, out of almost 8 billions available. The kinematic distributions for the selected sample are presented in Fig. 6.1 , where inclusive variables x_{Bj}, Q^2, and y are shown. In Fig. 6.2 the p_{T}, p_{L}, and z of the hadron leading in p_{T} are presented.

Table 6.1: Impact of cuts on the selected data sample.

cut	# events	%
mDST w/o bad spill	7775267710	1.000
pre-cuts	7228214533	0.930
best IV	6645240448	0.855
μ' in IV	3911238848	0.503
beam momentum cuts	3883660260	0.499
$Q^2 > 1$ GeV^2	344337850	0.044
$0.1 < y < 0.9$	232716361	0.030
$x_{\mathrm{Bj}} < 1.0$	232715292	0.030
cross cell cut	172943191	0.022
IV in target	141438410	0.018
all $z < 0.85$	139433634	0.018
good hadron	118009913	0.015
$z_1 + z_2 > 0.95$	115707098	0.015
$0.05 < p_{\mathrm{T}}, 1 < 2.5$	113491065	0.015

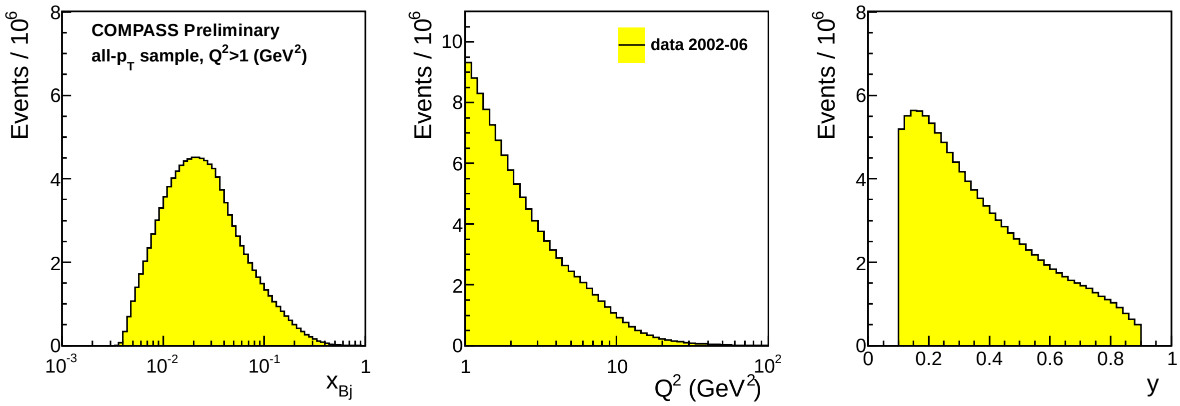

Figure 6.1: Distributions of x_{Bj}, Q^2, and y for the selected sample.

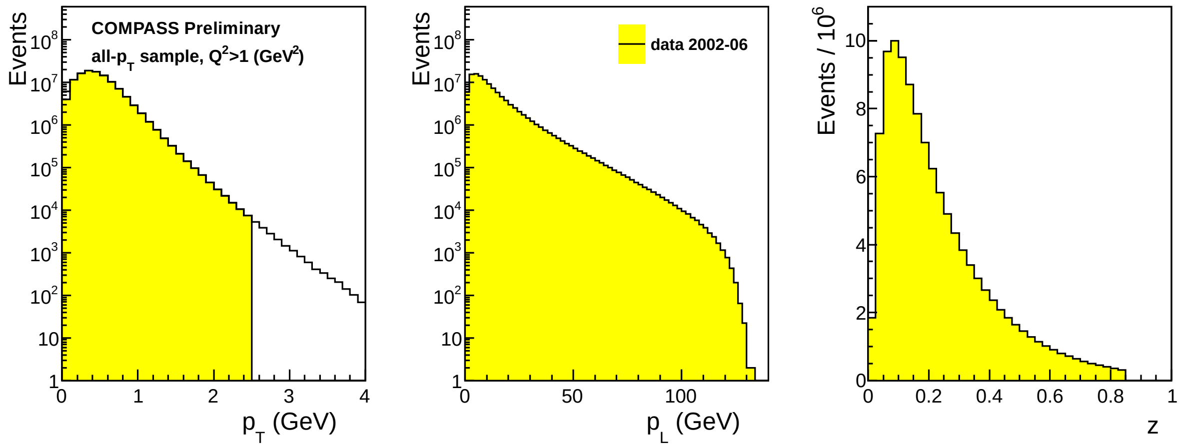

Figure 6.2: Distribution of p_{T}, p_{L}, and z, of the hadron leading in p_{T}.

6.2 Analysis inputs from the experimental data

In order to extract $\Delta g/g$ using the method presented in Section 5.2, several inputs are obtained from the physics data or from dedicated measurements. These are, x_{Bj}, Q^2, D, P_{b}, P_{t} and f.

For the measurement of x_{Bj} and Q^2 the four-vectors of the incoming and scattered muons are used. The typical relative precision of the extracted values is about 4%. The main uncertainty is related with multiple scattering of the μ and μ' in the target material, which affects the precision of the scattering angle measurement.

The average beam polarisation is -0.80 ± 0.04. The actual polarisation value depends strongly upon the beam momentum and is presented in the top panel of Fig. 6.3. Observe that in COMPASS the beam polarisation is not measured directly. Instead, only the beam momentum is measured and a simulation is used to correlate the measured beam momentum with the beam polarisation. As mentioned in Section 4.1, the actual measurement of the beam polarisation as well as the validation of the simulation program used nowadays in COMPASS were done at the SMC experiment, *cf.* [96].

The target polarisation is measured using a NMR system, *cf.* [94]. For the longitudinal data the target polarisation can be constantly monitored. The typical beam polarisation obtained for the deuteron target is about 50%. The relative uncertainty of the target polarisation is taken as 5%. The main contribution to the systematic uncertainty is related to the fact that the polarisation of the target is not uniform. Besides, for the data used in this analysis the NMR system was not covering the whole target[1].

The target dilution factor takes into account the fact that only a fraction of the nucleons in the target are polarizable. In a rough estimate the ^{6}Li nucleus can be considered as a ^{4}He core and a quasi-free D, see [97]. Thus, in the ^{6}LiD molecule about 50% of the nucleons can be polarised. The dilution factor which is actually used in the analysis is defined as

$$f_{\mathrm{raw}}(x, Q^2) = \frac{n_{\mathrm{d}}}{n_{\mathrm{d}} + \sum_{A \neq d} n_A \left(\frac{\sigma_A^T(x,Q^2)}{\sigma_d^T(x,Q2} \right)}, \tag{6.1}$$

where n_i corresponds to the number of nuclei of type-i, and σ_i^T is the double differential cross-section of μ on i unpolarised scattering. The total cross sections ratio σ_A^T/σ_d^T was experimentally measured at NMC (He, C, Ca, Li) [106, 107], at EMC (Cu) [108] and at E665 (Xe) [109].

The dilution factor in Eq. (6.1) is further multiplied by a factor of $C_1 \approx 1.9$, which takes into account the aforementioned fact that effectively there are two deuterons in the ^{6}LiD molecule, the purity of Li and D, and the fraction of time that the spins of quasi-free p, n in Li remain aligned with respect to each other (*i.e.* while they can be treated as deuteron). Finally, another correction entering that C_1 factor is that the free deuteron is found in both S and D states. While the procedure may seem complex, the uncertainty of the dilution factor in the measured region is only about 1–2%.

So far in Eq. (6.1) only the total cross sections were mentioned, but in fact, it is convenient to correct also the dilution factor to take into account the unpolarized radiative corrections [110], such that the obtained results can be interpreted in the 1γ formalism used in DIS. In this analysis, the so-called semi-inclusive radiative corrections are used, since a hadron is observed in each event. Contrary to the inclusive measurements, if a hadron is present in the event, contrary to the inclusive measurements, such event cannot be misidentified with radiative tails of elastic and quasi-elastic μ–A or μ–N interactions. As a result $RC_{\mathrm{SIDIS}} < RC_{\mathrm{incl}}$.

Unfortunately, up to now these corrections could be only calculated as a function of x_{Bj} and y being so far unavailable as a function of hadron z or p_{T}. There is a dedicated discussion of this problem in Section 8.7. For that reason the uncertainty of the effective dilution factor used in the analysis, *i.e.* the one corrected by radiative effects, is taken as 5%. It should be noted that the uncertainty of the dilution factor acts only as a scaling factor and therefore is not that important. The value of the effective dilution factor is presented on the bottom panel of Fig. 6.3. Its average is $\langle f \rangle = 0.38$.

[1]In more recent years, the NMR system was improved and extended to the whole target, resulting in a decrease of the relative uncertainty of the target polarisation to a level of 2–3%.

The depolarisation factor is defined in [111] and reads

$$D = \frac{y[(1+\gamma^2 y/2)(2-y) - 2y^2 m^2/Q^2]}{y^2(1-2m^2/Q^2)(1+\gamma^2) + 2(1-y-\gamma^2 y^2/4)(1+\gamma^2)(1+R)}, \tag{6.2}$$

where m is the lepton mass, and all other variables were defined in Chapter 2. Neglecting small corrections to the COMPASS kinematics due to the high beam energy and corrections which depend on m^2/Q^2, which is also small for $Q^2 > 1$ GeV^2, the depolarisation factor can be approximated as

$$D \approx \frac{y(2-y)}{y^2 + 2(1-y)(1+R)}. \tag{6.3}$$

Formally, the values of $R(x_{\mathrm{Bj}}, Q^2)$, defined in Section 2.2 are experimentally measured. However, in the LO pQCD approximation only transversely polarised photons interact with the quark and the function $R = \sigma_L/\sigma_T = 0$. Moreover, this ratio is process dependent and it was never measured for PGF or QCDC. Therefore, in all COMPASS analyses of $\Delta g/g$ it is assumed that $R = 0$, and the systematic uncertainty of D related to the uncertainty of R is not considered. Another uncertainty of D comes from the limited precision on the average y measurement. This uncertainty is related with a possible mismatch between the μ and μ' momentum measurements. However, dedicated tests have shown that this uncertainty can be safely neglected. For the uncertainty estimation only the first derivatives $\partial D/\partial y$ are used. In this case the fact that on the event-by-event basis the y value is known with limited precision does not contribute to the uncertainty of D.

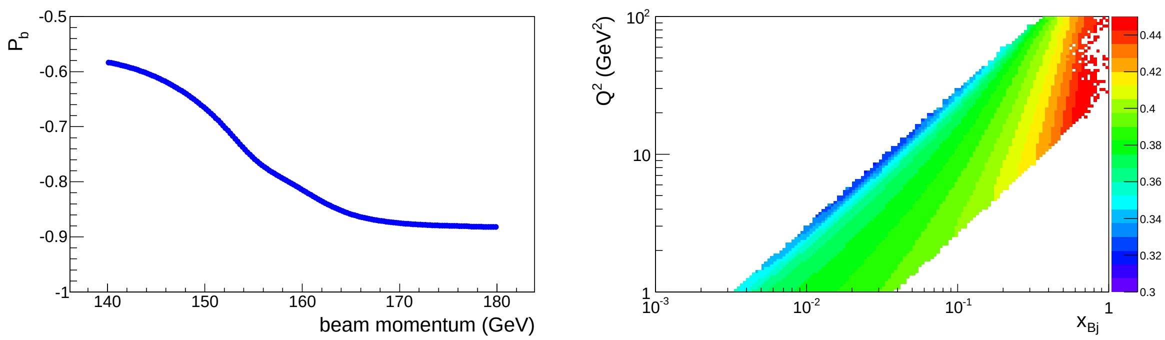

Figure 6.3: Left panel: The value of beam polarisation (P_{b}) used in the analysis as a function of beam momentum. Right panel: The value of the dilution factor (f) for the ^{6}LiD target, presented in the z-axis, as a function of x_{Bj} and Q^2.

Chapter 7

Monte Carlo and neural network

As any other method of direct Δg/g extraction, the one proposed in this monograph is model dependent. In the analysis the simulation of hard processes is done using the LEPTO Monte Carlo (MC) generator [44], while parton hadronisation is performed by the JETSET package. The generated events are processed by the COMPASS spectrometer simulation program COMGEANT (based on GEANT 3), and they are further reconstructed in the same way as real data by CORAL. The same cuts as for data are applied on MC. Based on the MC truth bank, for a process of type $i = \{\mathrm{PGF}, \mathrm{QCDC}, \mathrm{LP}\}$, a^i_{LL} and x_i are determined from the reconstructed MC data. These values are parametrised by an artificial neural network and can be estimated on an event-by-event basis, and used in the Δg/g extraction, according to the formalism presented in section 5.2.

7.1 Monte Carlo

In the analysis LEPTO version 7.51 together with JETSET version 4.74 were used. To properly describe COMPASS data, in [64] a few parameters of the JETSET fragmentation model were tuned. In the present analysis that same fragmentation tuning was used. For consistency the same PDF set as in [64] was used, namely MSTW08L [112]. The data are only well described by MC if in the latter the so-called parton shower option is switched on. Parton showers simulate higher-order corrections, so in the analysis a considerable fraction of NLO corrections is accounted for. A similar situation is found for the F_{L} function, ($F_{\mathrm{L}} = F_2 - 2xF1$). Formally, $F_L = 0$ in LO, but considerable improvement in the data description by MC was found at the high y region when the F_L function from LEPTO was used. The COMPASS polarised target has about 0.5 nuclear interaction lengths, therefore it is frequent that hadrons re-interact along the target, and if not, they will do so in the spectrometer. To simulate these secondary interactions a FLUKA program [113] was used. In order to compare real and MC data, radiative corrections calculated using the TERAD programme [110] were applied to MC data.

The comparison of data and MC is presented in the top panels of Fig. 7.1 for inclusive variables and in the top panels of Fig. 7.2 for p_{T}, p_{L} and z of the hadron leading in p_{T}. In the bottom panels of both figures the ratio of data/MC is shown. The real and MC data are normalised to the number of events in each sample and not to the cross-section. The overall agreement is reasonable. It should be noted that the tuning of fragmentation parameters in [64] was performed on the high-p_{T} sample which accounts for only 6% of the sample currently used in the analysis. Yet, the tuning seems to work well in the extended phase space region, and it is now commonly used in other COMPASS analyses. The largest discrepancy between data and MC is observed in the low p_{T} region, where LP is dominant, but this region has limited impact for Δg/g extraction. The presented MC was selected for the final Δg/g extraction as it gives the best description of data.

To study the model dependence of the analysis method several other MCs were produced. The summary of all eight MCs used in the analysis is presented in Table 7.1. For simplicity various MCs are denoted by a 5 digit code, in which each digit represents the following choice of simulation parameters (from left to right): 1st fragmentation tuning ([64] or default LEPTO); 2nd switching on or off parton shower mechanism; 3rd PDF selection (MSTW08L or CTEQ5L [114]); 4th LEPTO F_L used or not used; 5th program to simulate re-interactions in the target (FLUKA or GEISHA). The code '00000' corresponds to the main MC used for the final Δg/g extraction and described earlier in this section. The digit '1' at a certain position means that a different parameter/option was used as compared to the main MC. While not shown here, the data/MC ratio especially for the p_{T} dependence can reach a factor of 2–3 for certain MCs from Table 7.1 (*e.g.* default fragmentation tuning without usage of parton shower mechanism). A large observed data/MC variation for different samples assures that the MC model was tested in sufficiently large phase space. The average values of R_i and a^i_{LL}/D for $x_{\mathrm{Bj}}< 0.05$ and p_{T} above and below 1 GeV are presented in Table 7.2. Detailed studies concerning the model dependence of the Δg/g results are presented in Subsection 8.6.2.

7.1.1 FLUKA and GEISHA

The default program to simulate secondary interactions in GEANT is GEISHA. However, in [89] it was found out that GEISHA seems to produce too many secondary interactions in the COMPASS target and spectrometer as compared to real data. Therefore, a different

Table 7.1: Summary of MC used for final $\Delta g/g$ extraction and systematic studies. See text for details.

Sample	code	fragmentation	Parton Shower	PDF	LEPTO F_L	re-interaction
1	00000	[64]	ON	MSTW08L	ON	FLUKA
2	00001	[64]	ON	MSTW08L	ON	GEISHA
3	01001	[64]	OFF	MSTW08L	ON	GEISHA
4	00101	[64]	ON	CTEQ5L	ON	GEISHA
5	00011	[64]	ON	MSTW08L	OFF	GEISHA
6	10101	default	ON	CTEQ5L	ON	GEISHA
7	10001	default	ON	MSTW08L	ON	GEISHA
8	11001	default	OFF	MSTW08L	ON	GEISHA

Table 7.2: MC samples characterised in therms of Rs and a_{LL}s.

	$p_{\mathrm{T}} < 1$ GeV			$p_{\mathrm{T}} > 1$ GeV				
Sample	R_{LP}	R_{QCDC}	R_{PGF}	R_{LP}	R_{QCDC}	R_{PGF}	$a_{\mathrm{LL}}^{\mathrm{QCDC}}/D$	$a_{\mathrm{LL}}^{\mathrm{PGF}}/D$
1	0.85	0.09	0.06	0.56	0.23	0.21	0.80	-0.58
2	0.85	0.09	0.06	0.57	0.23	0.20	0.80	-0.59
3	0.84	0.09	0.07	0.51	0.30	0.19	0.78	-0.59
4	0.81	0.10	0.09	0.52	0.25	0.23	0.80	-0.58
5	0.86	0.09	0.05	0.61	0.21	0.18	0.80	-0.59
6	0.81	0.11	0.08	0.46	0.26	0.28	0.80	-0.58
7	0.84	0.10	0.06	0.52	0.25	0.23	0.80	-0.59
8	0.83	0.10	0.07	0.41	0.33	0.26	0.78	-0.59

program, FLUKA [113], was tested. In the case of [89] the simulation with FLUKA gave better agreement between data and MC. For the present analysis the two programs were also tested. The ratio of data to MC using either FLUKA or GEISHA for the p_{T} of the hadron leading in p_{T} is presented in Fig. 7.3. In the high-p_{T} region FLUKA is able to describe the data up to 2.5 GeV, which is a slightly wider range than GEISHA. Above this value none of the programs describe the data well. It was decided that for the main result the FLUKA program will be used, while GEISHA will be used for systematic studies. However, the discrepancy between data and MC for $p_{\mathrm{T}} > 2.5$ GeV was the reason to exclude this range from the analysis.

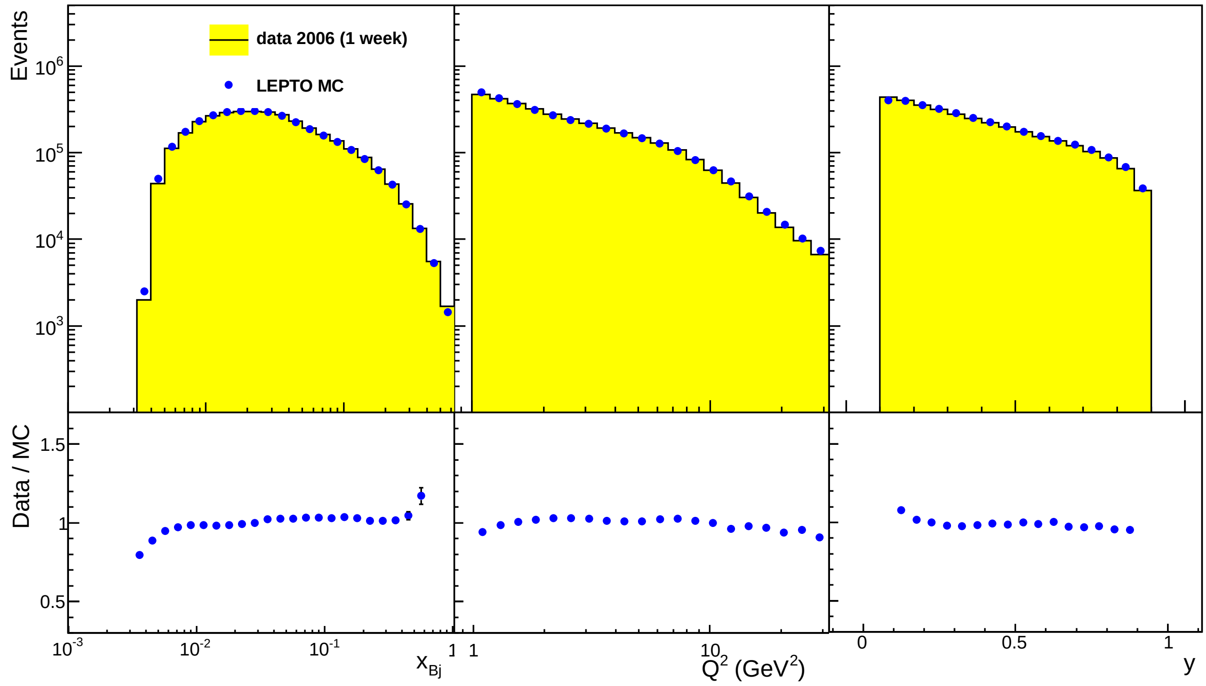

Figure 7.1: Top panels: Data and MC comparison for inclusive variables x_{Bj}, Q^2, and y, respectively. Bottom panels: The corresponding ratio of data and MC.

7.1.2 Global normalisation of data and MC

In the early years of COMPASS the experimental setup was not optimised for cross-section measurements. For example DIS inclusive cross section was measured with a precision of about 10%, where the dominant systematic uncertainty was coming from the precision of the luminosity measurement. The extracted results were not published as the obtained uncertainty was too large comparing to the world data. For the same reason in many analyses, including the one presented here and as well in [64], the cross-sections are not measured and data/MC plots are normalised to the number of events.

The lack of cross section measurement in the analyses dealing with $\Delta g/g$ extraction was often criticised by the community. Since the selected sample in [64] contained only 6% of the full data sample it could happen that in this particular corner of the phase space the ratio plots were flat, but the global normalisation could be wrong, say by a factor of two. However, such a criticism cannot be used for the current analysis, where hadrons from a much wider phase-space region are analysed. Namely, in case a charged hadron would be produced in each DIS event, the measured (p_{T} integrated) cross-section for a hadron leading in p_{T} would correspond to the inclusive cross-section. According to

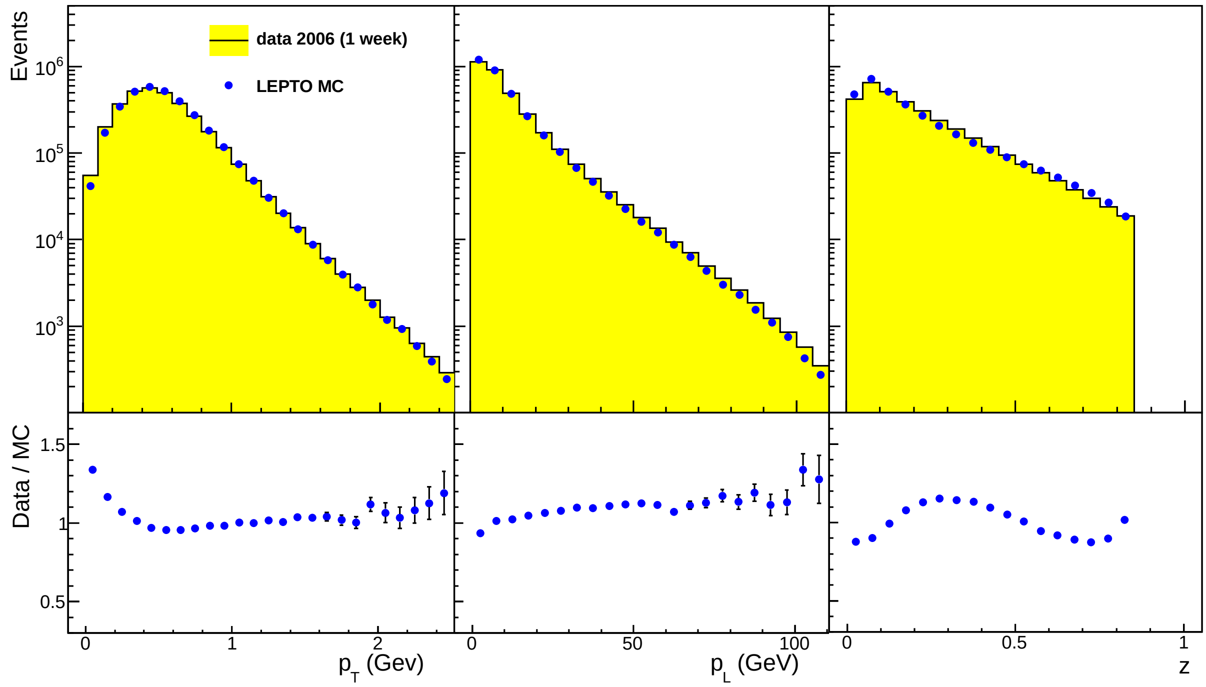

Figure 7.2: Top panels: Data and MC comparison for p_{T}, p_{L}, and z of the hadron leading in p_{T}, respectively. Bottom panels: The corresponding ratio of data and MC.

the COMPASS MC simulation in about 97% of the events a charged hadron should be observed. The actual number observed in the real data is about 95%, taking into account also radiative corrections. Considering further complications, like the fact that not all COMPASS triggers are inclusive and the use of p_{T} cuts, one can conclude that the global normalisation of data and MC cannot be off by more than about 15%. Moreover, this uncertainty is dominated by the precision of the luminosity measurement.

7.2 Neural networks

In order to minimise the statistical uncertainty of $\Delta g/g$ the values of R_i, a^i_{LL} and x_i should be known event-by-event. Since the kinematic dependence of these variables can be quite complex a multidimensional parametrisation as function of various experimental observables has to be found. An ideal tool to perform such a parametrisation is an artificial neural network (NN). In this work the multilayer perception NN type was used [115]. The details concerning the working principles of NN are beyond the scope of this monograph and can be found elsewhere [116]. Here, a history of NN usage in the $\Delta g/g$ extraction is

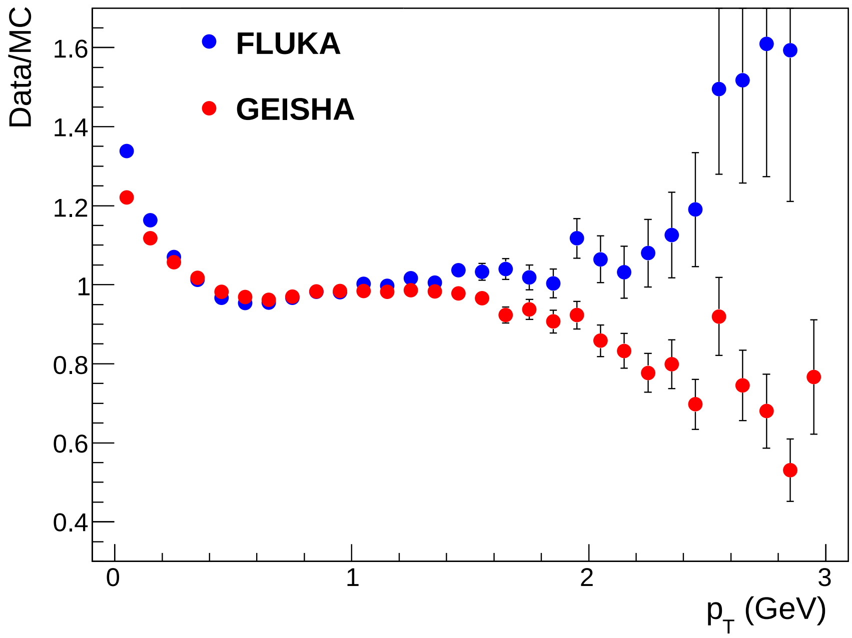

Figure 7.3: Data to MC ratio as a function of p_T of the hadron leading in p_T using two different programs to simulate secondary interactions, *i.e.* FLUKA and GEISHA. See text for details.

shortly presented. The results of the NN training to parametrise the MC output are also discussed. Whenever in the text a clear distinction is needed between a value from the MC truth bank and its estimation by the NN parametrisation, a superscript 'NN' will be added to the variable name *e.g.* R_i^{NN} for the latter case.

7.2.1 Neural networks usage in Δg/g extraction

Artificial neural networks were used in $\Delta g/g$ analyses since SMC times [60,61]. The main purpose of the NN usage was to separate signal (PGF) from background (QCDC and LP). At that time the value of the NN output had no physics interpretation. One could just parametrise *e.g. Figure of Merit* as a function of NN output and select the optimal working point. The events for which the NN output was above the working point were accepted in the analysis, while the ones with the NN output below the working point were rejected, see also [117].

The approach to NN usage was modified when the author realised that for a specific setting of the NN parameters the output has a special meaning. Namely, it corresponds to the fraction of the signal process in the sample, *i.e.* R_i. This specific NN setting is discussed below.

In a typical signal-background separation problem the expectation value of the NN output is set to 1 for signal, and 0 for background. At the same time the output values of the NN are internally restricted, *e.g.* by the sigmoid function, to the 0–1 range. While this may seem to be the natural choice, in reality it introduces a bias in case one wants to estimate R_i. Since NN are trained on finite MC samples, for each event the output of the NN has a certain uncertainty. If in a given phase-space point the value $\langle R_i \rangle$ is close to 0 or 1, the NN output range restriction will effectively bias $\langle R_i \rangle$ towards higher or lower values, respectively. In order to avoid this problem, the restriction on NN has been removed and the so-called linear NN output must be used [1]. The goal of the NN is to minimise the so-called "error function", which describes how well a given NN parametrisation follows the expected output. In case the error function is selected as MSE, *i.e.* the error contribution from a given event is calculated as the square of the difference between the value obtained in the NN parametrisation and the expected one, the total NN "error" is given by

$$\mathrm{NN}_{\mathrm{error}} = \sum_{N_S, N_B} (\exp - \mathrm{obs})^2 = N_S(1-o)^2 + N_B(0-o)^2. \tag{7.1}$$

The aim of the NN is to find the output 'o' which minimises the NN error, so:

$$\frac{\mathrm{dNN}_{\mathrm{error}}}{\mathrm{d}o} = 0 = -2N_S(1-o) + 2N_B o \to o = \frac{N_S}{N_S + N_B} = R_S. \tag{7.2}$$

As shown, in the aforementioned special conditions, the expectation values of the NN output correspond to the fraction of signal in the sample *i.e.* R_S. Instead of just signal and background separation the NN can be trained to parametrise the expectation values of R_i as a function of the input parameters. Obtained in this way R_i can be used as a part of the weight for the Δg/g extraction. This in turn largely increase the FOM and allows for the implementation of more sophisticated methods of Δg/g extraction, including the one presented in this monograph.

7.2.2 Neural network training results

In the current analysis there are only 4 input parameters used for NN training, namely two inclusive variables x_{Bj}, Q^2, and two hadron variables p_{T}, and p_{L} of the hadron leading in p_{T}. More complex NN were tested, including even with up to 19 input parameters.

[1] As a consequence for a clean background sample the NN ouput had a Gaussian shape, centered at zero with small RMS (of the order of 0.01).

However, the gain in statistical precision of the obtained $\Delta g/g$ was only 5%, thus it did not compensate, given the large increase in NN complexity and increased dependence on the MC. As explained in the previous section, the output of the NN is set to correspond to the expectation value of the parametrised quantity, *e.g.* R_i or a_{LL} in a given phase space point of the input variables. The MC data were divided into two subsamples, to provide learning and testing sets. The two sets are needed to avoid NN over-training. To optimise the stability of the NN output the learning process is repeated twice and in addition the training and learning sets are swapped. The final NN output is taken as a mean value of 4 parametrisations. To be sure that the obtained NNs are correct and their usage will not bias $\Delta g/g$, the output of NN have to pass two tests. In the first test the NN output has to be compared with the expectation values as function of input parameters. To pass the test the mean values of the two distributions must agree. In the second test, bins are created in the NN output, and using the MC truth bank information the real composition of the sample is verified. It is expected that the composition of the sample corresponds to the mean value of the NN output. For example, a sub-sample is selected for which the NN output fulfils the condition $R_{\mathrm{PGF}}^{\mathrm{NN}} \in (0.10, 0.14)$. Then using the MC truth bank it is verified that in this sub-sample the fraction of PGF is indeed about 0.12. From all performed NN trainings the parametrisation of R_i is the most complex, since all three fractions are obtained simultaneously. This is a two-dimensional problem, as the three fractions must sum up to 1. As an example for the first test, in Fig. 7.4 the fraction of R_i from NN and MC are compared as a function of p_{T}. In the top panels the NN parametrisation and the MC are compared, while in the bottom panels the difference between NN and MC is shown. The errors correspond only to statistical errors of the MC sample. A very good agreement between MC and NN parametrisation is observed for all three processes. It is also noticeable that for higher p_{T} the fractions of PGF and QCDC are increasing, as expected from [59]. An example of the result for the second test is presented in Fig. 7.5, where in bins of R_i^{NN} the true MC composition is verified. A very good correlation between the two values is observed. Thus, the NN parametrisation passed successfully the two tests and can be used for $\Delta g/g$ extraction. In Fig. 7.6 the values of R_i are also shown in bins of p_{T}, p_{L} in the top panel, and in bins of x_{Bj}, Q^2 in the bottom panel. As can be seen, the strongest dependence of R_i as a function of p_{T} is observed. However, some dependencies are also observed as a function of x_{Bj} and effectively y. In general, while keeping x_{Bj} constant and increasing y, the fractions of PGF and QCDC are increasing. Similarly one notices that on average the PGF is observed for lower x_{Bj} values than QCDC. These observed differences allow for the separation of the three processes and for the simultaneous extraction of $\Delta g/g$ and A_1^{LP} asymmetry.

The values of a^i_{LL} and x_i are also parametrised using a NN. The typical correlation between the expected output and the NN parametrisation is about 60%–70% for $a^{\mathrm{PGF}}_{\mathrm{LL}}$, x_{C}, and x_{g} and only about 20% for $a^{\mathrm{QCDC}}_{\mathrm{LL}}$. The correlation plots between the NN parametrisation and the true values are presented in Fig. 7.7. It should be noticed that a low value for the correlation of $a^{\mathrm{QCDC}}_{\mathrm{LL}}$ does not mean that the extracted $\Delta g/g$ or A^{LP}_1 is biased. It just means that with more knowledge one could still increase the statistical precision of the obtained results. The low correlation means that $a^{\mathrm{QCDC}}_{\mathrm{LL}}$ does not depend upon the input variables, contrary to $a^{\mathrm{PGF}}_{\mathrm{LL}}$. Since in the formulae usually we have a product $a^i_{\mathrm{LL}}R_i$ appearing, the different behaviour of a_{LL} for PGF and QCDC allows for an easier separation of the two related asymmetries. Last but not least, with much more than four input parameters to the NN training the correlation for $a^{\mathrm{QCDC}}_{\mathrm{LL}}$ was still at the level of 20%–25%. It looks like the partonic variables on which $a^{\mathrm{QCDC}}_{\mathrm{LL}}$ depend are not easily reconstructed using the available information on the hadron level.

In Fig. 7.8, $a^{\mathrm{PGF}}_{\mathrm{LL}}$ as a function of Q^2 and p_{T} is presented. A much stronger Q^2 dependence (rather than p_{T} dependence) of $a^{\mathrm{PGF}}_{\mathrm{LL}}$ is observed. This explains for example why in Table 7.2 the value of $a^{\mathrm{PGF}}_{\mathrm{LL}}$ is stable for different MCs. Namely, that Q^2 is an inclusive variable not affected by *e.g.* the fragmentation tuning or the parton shower on/off options selected in the MC generator.

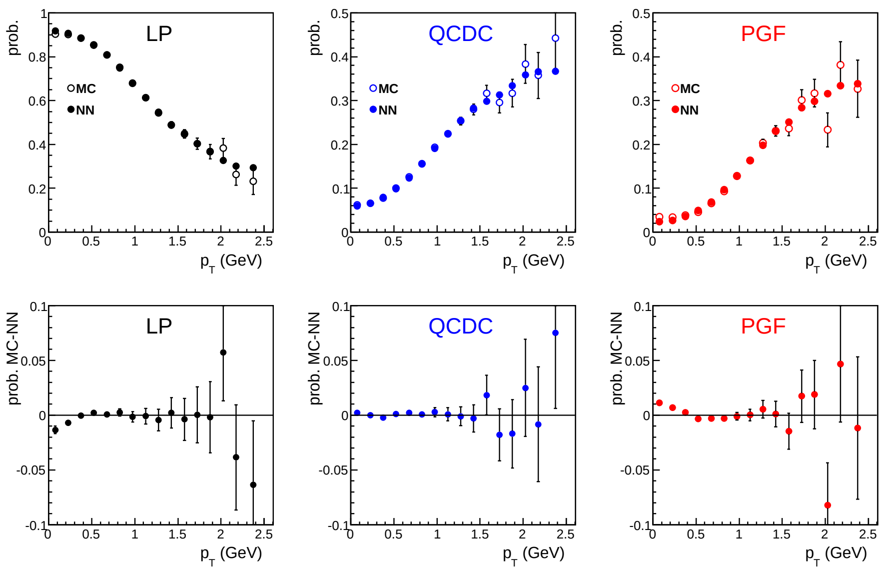

Figure 7.4: Top panels: Comparison of MC and NN output for R_i as a function of p_{T} of the hadron leading in p_{T}. Bottom panels: The difference of MC and NN output for R_i as a function of p_{T} of the hadron leading in p_{T}.

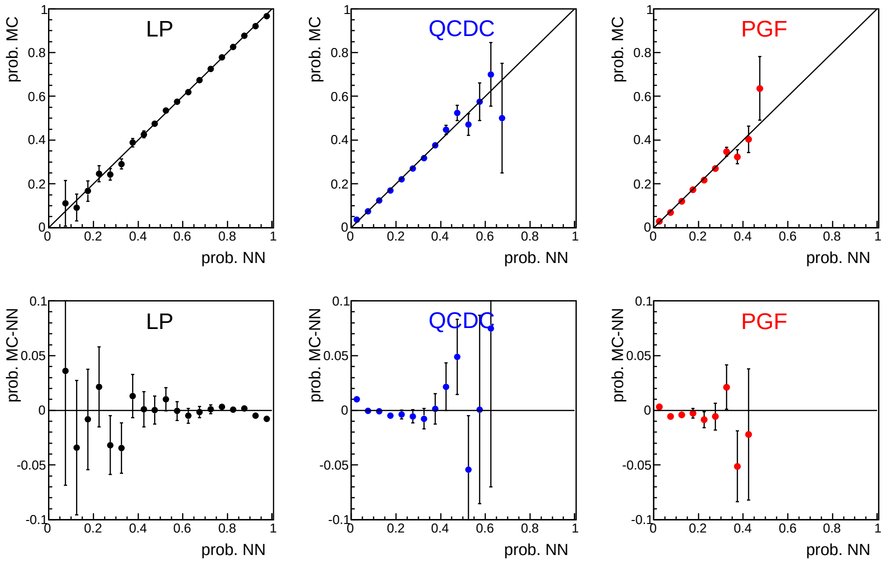

Figure 7.5: Top panels: The R_i in MC obtained in bins of R_i^{NN}. A very good correlation is observed. Bottom panels: The difference of R_i between MC and NN parametrisation in bins of R_i^{NN}.

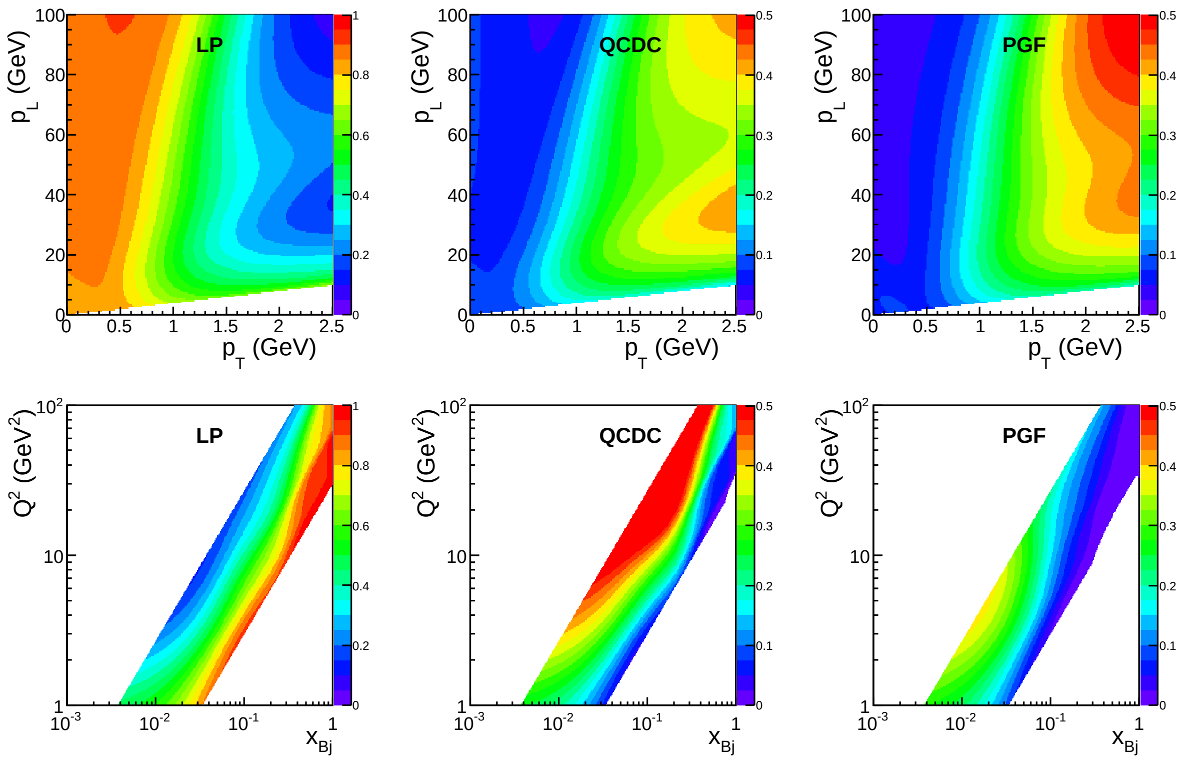

Figure 7.6: Top panels: The fraction of R_i as a function of p_{T} and p_{L} of the hadron leading in p_{T} for x_{Bj}= 0.01 and Q^2= 2 GeV^2. Bottom panels: The fraction of R_i as a function of x_{Bj} and Q^2 for p_{T}= 1.5 GeV and p_{L} = 30 GeV for different processes.

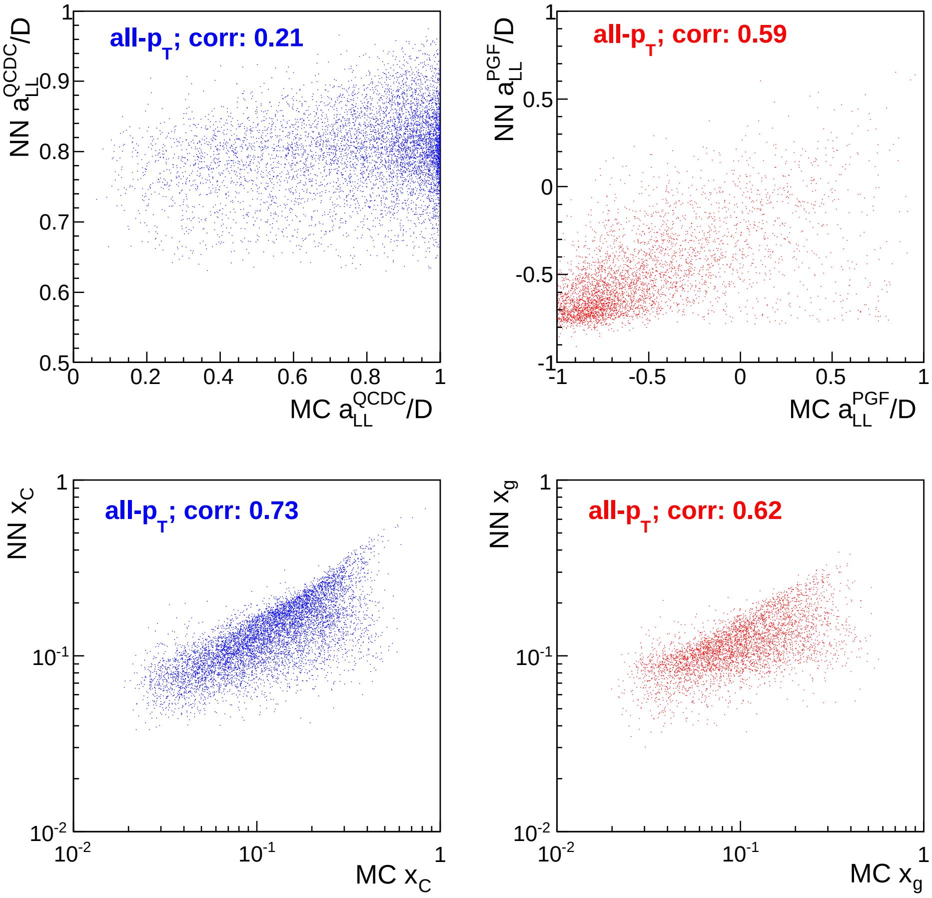

Figure 7.7: The correlation of a_{LL}^{i}/D (top) and x_i (bottom) between MC and NN parametrisation for QCDC (left) and PGF (right).

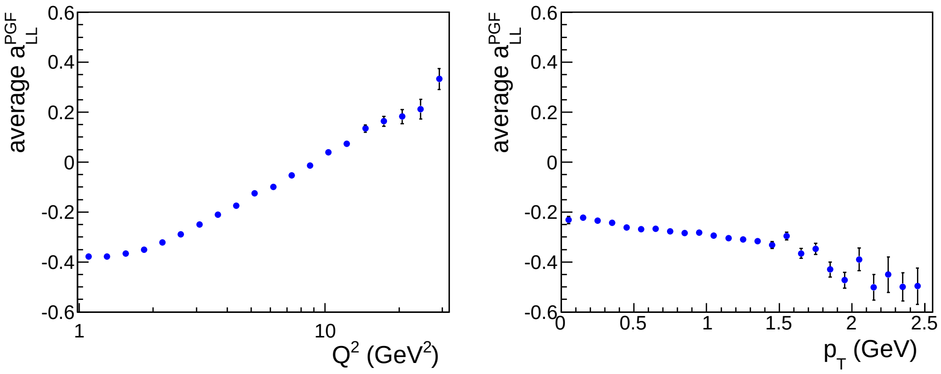

Figure 7.8: The average value of $a_{\mathrm{LL}}^{\mathrm{PGF}}/D$ as a function of Q^2 (left) and p_{T} (right).

Chapter 8

Systematic studies

Extended systematic studies were performed for the analysis presented in [64]. Many conclusions reached there are valid also for the new analysis method. Therefore, studies which in the past gave negligible systematic contribution to the $\Delta g/g$ were generally not repeated. Here, only the most important systematic contributions are presented. These include the impact of resolved photon contribution, the non-pion contamination, and the usage of MC for 2006 data for earlier data sets (2002–2004). Certain systematic uncertainties present in the method used in [64] are not appearing in the current one. Namely, the contribution from the parametrisation of A_1^d and the assumptions about the relation between x_{C} and x'_{C}. In addition the proposed method of $\Delta g/g$ extraction allows for some tests of the underlying model. These tests are also described in this chapter.

8.1 MC tests of the new method

The implementation of the new method of $\Delta g/g$ extraction was verified using a MC sample. Raw asymmetries were injected in the MC sample. For the LP asymmetry, $A_1^{\mathrm{LP}}(\mathrm{Bj}) = x_{\mathrm{Bj}}$, and a constant value of 0.3 for $\Delta g/g(x_{\mathrm{g}})$ were assumed. To generate an asymmetry the true MC values of a_{LL}^i were used. In addition using the MC truth bank one knows which process took place. The same MC was later used in NN training to obtain parametrisations of R_i, a_{LL}^i, and x_i. These parametrisations were later used in order to extract $\Delta g/g$ and A_1^{LP} using the proposed method.

While in the first try biased results were obtained, in a second attempt the extracted values of $\Delta g/g$ and A_1^{LP} agreed within errors with the injected asymmetry. The observed bias in the first try was not negligible, up to 20% of the A_1^{LP} value at high x_{Bj}, and was due to having set the product $fP_{\mathrm{b}}P_{\mathrm{t}} = 1$ for simplicity reasons. However, the extraction method works for $fP_{\mathrm{b}}P_{\mathrm{t}}a_{\mathrm{LL}}\,A \ll 1$. Such a condition was originally not fulfilled for the simulated high x_{Bj} data. The bias turned out to be quadratic in $fP_{\mathrm{b}}P_{\mathrm{t}}a^{i}_{\mathrm{LL}}\,A^{i}$. A closer investigation revealed that in experimental conditions, where $\langle fP_{\mathrm{b}}P_{\mathrm{t}}\rangle \approx 0.16$ the bias is negligible even if Δg/g and A_1^{LP} would be close to 1.

8.2 Global vs consecutive configuration

In order to reduce the impact of the spectrometer instabilities, the target polarisation was reversed either once or three times a day, *cf.* Section 4.2. The optimal condition to extract an asymmetry is to use two such consecutive periods of data (consecutive configurations). The other, less preferred, option is to extract the asymmetry from a so-called data period, which roughly corresponds to one week of data taking and contains several consecutive configurations. During the given period the experimental area is closed, thus the spectrometer performance should be also rather stable. This is the so-called global configuration.

Contrary to the expectations the studies have shown that for the proposed analysis the global configuration must be used. The reason behind is that the proposed method of Δg/g extraction has a lot in common with the 2nd-order asymmetry extraction method. In such a method a double ratio of event yields is considered, namely $N_uN'_d/N_dN'_u$. In case the number of observed/expected events is too small a bias is introduced. The source of the bias is related with the non-equality of the expectation values, $1/\langle N_i\rangle \neq \langle 1/N_i\rangle$. The number of events, especially of the QCDC type at high x_{C}, was found indeed to be too small when using the consecutive configuration. In Table 8.1, extracted values of A_1^{LP} for global and consecutive configurations are presented for 12 x_{Bj} intervals. In the last column the χ^2 is calculated, taking into account the correlation between the samples, $\chi^2 = (A_{\mathrm{con}} - A_{\mathrm{gl}})^2/(\delta A^2_{\mathrm{con}} - \delta A^2_{\mathrm{gl}})$. A clear difference between the results is seen for high x_{Bj}. It is worth mentioning that the observed discrepancy on A_1^{LP} has a negligible impact on the Δg/g extraction. The Δg/g values differ by less than 0.003 between the two ways of data grouping.

8.3 False asymmetries

The possible false asymmetries are related with instabilities of the spectrometer for the data taken before and after field reversal. As a result a bias for the extracted asymmetries can be introduced, as the assumed acceptance cancellation, $(a_u a'_d)/(a'_u a'_d) = 1$, may not

Table 8.1: Comparison of A_1^{LP} for global and consecutive data grouping. A large difference at high x_{Bj} is observed, due to the bias in the consecutive configuration. This test was performed on the early stage of the analysis. Thus, the presented here A_1^{LP} does not correspond to the final result presented in Chapter 9.

x_{Bj} range	Global	Consecutive	χ^2
<0.006	0.0074 ± 0.0056	0.0059 ± 0.0058	1.3
0.006–0.01	-0.0005 ± 0.0043	-0.0012 ± 0.0045	0.4
0.01–0.02	-0.0009 ± 0.0039	-0.0013 ± 0.0040	0.2
0.02–0.03	0.0097 ± 0.0053	0.0091 ± 0.0055	0.2
0.03–0.04	0.0027 ± 0.0073	0.0039 ± 0.0076	0.4
0.04–0.06	0.0056 ± 0.0075	0.0072 ± 0.0078	0.7
0.05–0.10	0.0238 ± 0.0086	0.0270 ± 0.0089	2.1
0.10–0.15	0.0938 ± 0.0123	0.0916 ± 0.0127	0.5
0.15–0.20	0.1405 ± 0.0182	0.1399 ± 0.0188	0.0
0.20–0.30	0.1724 ± 0.0205	0.1515 ± 0.0213	14.3
0.30–0.40	0.2484 ± 0.0383	0.1969 ± 0.0400	20.0
>0.40	0.3582 ± 0.0515	0.3065 ± 0.0537	11.3

be fulfilled. In previous COMPASS analyses of Δg/g false asymmetries were studied using the so-called extended data sample. For example in [64], the full sample without p_{T} cuts and with extended Q^2 range ($Q^2 > 0.7$ GeV^2) was used. In this way the systematic error of Δg/g was not limited by the statistical one. Observe that by using such an extended sample, one effectively assumes that false asymmetries are p_{T} independent, which may not be true.

The data currently used in the analysis were effectively already checked against false asymmetries in [64]. While the studies of false asymmetries were repeated for this work, it is not a surprise that the same conclusions as before were reached. Namely, except of the so-called microwave false asymmetry and for the hadron ϕ angle asymmetry (affecting data at low momenta and/or low p_{T}) the false asymmetries are consistent with zero. The microwave false asymmetry is related to the fact that the polarisation of a given target cell in a given data taking period has fixed direction with respect to the solenoid magnetic field. When the target solenoid field is reversed (in order to change the sign of the polarisation in the target cells), the acceptance may change slightly and a false asymmetry be generated. To cancel this asymmetry, a few times per year the relative polarisation of the given cell with respect to the solenoid field is changed (the target polarisation has to be destroyed and built up again in the opposite direction using different MW frequencies, see also Section 4.2). The hadron ϕ angle asymmetry is also related with the direction of the solenoid field. This false asymmetry was reproduced in MC and found to cancel in case the data is integrated over ϕ (as in the present analysis). Therefore, the two observed false asymmetries effectively do not contribute to the uncertainty of $\Delta g/g$.

8.3.1 False asymmetries and simultaneous extraction of $\Delta g/g$ and A_1^{LP}

In the analysis of [64] the A_1^{incl} asymmetry was assumed to be known, and the spectrometer instabilities generating false asymmetries were affecting only $\Delta g/g$. The situation is different when the simultaneous extraction of all asymmetries is performed. In such case any asymmetry bias affects not only $\Delta g/g$ but also A_1^{LP}. Generally the same spectrometer instability affects much less $\Delta g/g$ extracted in the current method than using the method from [64].

For example, a test was performed where the acceptance in one out of four spin configurations used for the asymmetry extraction was changed by 1%. Using the method of [64] the extracted value of $\Delta g/g$ was biased by 0.35. At the same time in the new method the bias was below 0.01. However, a bias of about 0.05 was seen for A_1^{LP}. Such a large bias could be easily detected during standard false asymmetry studies, *cf*. statistical precision of A_1^{LP} in Table 8.1.

8.3.2 $A_1(x_{\mathrm{Bj}}, p_{\mathrm{T}}, z)$ consistency problem

In the analysis one assumes spin-independent fragmentation, but in the most general case the possible spin dependence is expected to be function of z. Using data we can verify that the asymmetries extracted in bins of z are consistent [1], an additional test to strengthen the analysis. Such a test was successfully performed using the 2-dimensional asymmetries $A_1(x_{\mathrm{Bj}}, z)$. However, problems were noticed when the 3-dimensional asymmetries $A_1(x_{\mathrm{Bj}}, p_{\mathrm{T}}, z)$ were analysed.

The original extraction of asymmetries was performed in 12 bins of x_{Bj}, 5 bins of p_{T} and two bins of z. In Table 8.2 a condensed table with 3 x_{Bj} bins and 2 bins in z and p_{T} is presented. The results in the two z ranges do not agree with each other. The observed χ^2/ndf is 27.8/6. Multiple studies were performed to understand the observed

[1] This is expected for an isoscalar target, except for a very small difference present because $D_{\mathrm{s}}^{\mathrm{h}} \neq D_{\mathrm{u}}^{\mathrm{h}}$.

effect, including an analysis of all data without $Q^2 > 1$ GeV^2 cut, as well as the analysis of proton data taken in 2007 and 2011. The problematic regions were seen to be only in about 5% of the sample. In the remaining phase space the data compatibility is acceptable, $\chi^2/ndf = 9.4/6$. At the same time the obtained value of $\Delta g/g$ increased by 0.029. Despite of all efforts, the origin of the problem was not understood. The final result is quoted without "bad regions" removal. The difference $\delta(\Delta g/g)_{\mathrm{false}} = 0.029$ between results extracted with and without the problematic regions is taken into account as an additional source of false asymmetries. The limit for other false asymmetries is negligible compared to the one obtained here. Note that, contrary to previous methods of false asymmetry estimation, in the present case the false asymmetry is not assumed to be p_{T} independent. This is the reason why the obtained limit for false asymmetries is higher here than in [64].

Table 8.2: Comparison between $A_1^h(x_{\mathrm{Bj}}, p_{\mathrm{T}})$ for two bins of z.

		$z < 0.3$	$z > 0.3$	χ^2
	$0.004 < x_{\mathrm{Bj}} < 0.03$	0.0024±0.0017	-0.0094±0.0036	9.0
$p_{T1} < 1$	$0.03 < x_{\mathrm{Bj}} < 0.15$	0.0258±0.0037	0.0253±0.0069	0.0
	$0.15 < x_{\mathrm{Bj}} < 1.0$	0.1758±0.0126	0.1455±0.0248	1.2
	$0.004 < x_{\mathrm{Bj}} < 0.03$	-0.0170±0.0078	0.0069±0.0088	4.1
$p_{T1} > 1$	$0.03 < x_{\mathrm{Bj}} < 0.15$	0.1011±0.0197	0.0062±0.0175	13.0
	$0.15 < x_{\mathrm{Bj}} < 1.0$	0.0884±0.0745	0.1532±0.0574	0.5
			Total χ^2/ndf	27.8/6

8.3.3 Stability of $\Delta g/g$ and A_1^{LP} extraction

The data used in this analysis were grouped into 40 periods where the spectrometer was considered to be stable, *i.e.* fulfilling acceptance cancellation condition, $(a_u a'_d)/(a'_u a'_d) = 1$. The $\Delta g/g$ and A_1^{LP} are extracted from each of the 40 periods of analysed data. To obtain the final values a weighted average is used. The period by period results were compared with the averaged value of $\Delta g/g$, the obtained χ^2/ndf being about 34/39. Similar results, $\chi^2/ndf = 35/39$, were obtained for A_1^{LP} in the bin with the highest statistics, $0.01 < x_{\mathrm{Bj}} < 0.02$. Therefore, the results obtained from different periods are consistent. In addition the $\Delta g/g$ results for each year of data taking are presented in Fig. 8.1. A good agreement between results of various years is seen.

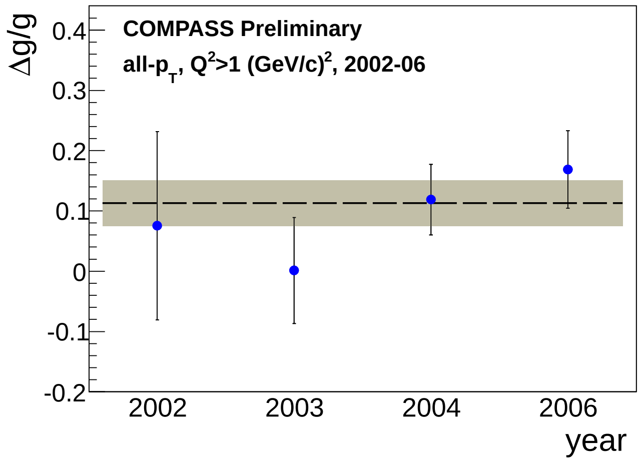

Figure 8.1: Comparison of $\Delta g/g$ obtained for 4 years of data. Good agreement is seen.

8.4 Neural network stability

The example of tests to the neural network parametrisations was presented in Section 7.2. As mentioned there, there are 4 NNs for each of the parametrised variable, mixing learning and testing sets. The output of these 4 NNs is averaged, and used for the final $\Delta g/g$ extraction. From the RMS of $\Delta g/g$ obtained separately from the 4 NNs, one concludes that the systematic error related to the NN, $\delta(\Delta g/g)_{\mathrm{NN}}$, is about 0.007. It was also found that there are small differences (*ca.* 10^{-4}) in the output of NN depending upon the computer system on which NN is being run and/or usage of double/single precision. As a result there is about 0.05% events that can be reconstructed in different x_{g} bins. A difference between $\Delta g/g$ obtained in these various scenarios is included in the systematic uncertainty.

8.5 $f, P_{\mathrm{b}}, P_{\mathrm{t}}$ uncertainties

Relative uncertainties of 5% for f, P_{b}, and P_{t} are assumed. In the current method the error of $\Delta g/g$ is proportional to the errors of $f, P_{\mathrm{b}}, P_{\mathrm{t}}$, resulting in $\delta(\Delta g/g)_{f,P_{\mathrm{b}},P_{\mathrm{t}}} = 0.010$. It is often noted that the present uncertainty is about a factor two higher than in [64]. The reason is that in case of [64] there is no direct proportionality between the uncertainties of $f, P_{\mathrm{b}}, P_{\mathrm{t}}$ and $\Delta g/g$, because of the a_{corr} term present in Eq. (5.12). For small positive values of $\Delta g/g$ indeed the former method is less affected by the uncertainties of f, P_{b} and P_{t}.

8.6 MC studies

The presented analysis method of Δg/g extraction is model dependent. Therefore, the uncertainty of Δg/g related to the model dependence must be carefully studied. In this section several such studies are shown.

8.6.1 The A_1 compatibility tests

As explained in Section 5.2, in the new method one can fit separately $A_1^{\mathrm{QCDC}}(x_{\mathrm{C}})$ and $A_1^{\mathrm{LP}}(x_{\mathrm{Bj}})$. However, from the physics point of view we do expect that $A_1^{\mathrm{QCDC}}(x_{\mathrm{C}}) = A_1^{\mathrm{LP}}(x_{\mathrm{Bj}})$ for $x_{\mathrm{C}} = x_{\mathrm{Bj}}$. Using a simple χ^2 test the compatibility between A_1^{QCDC} and A_1^{LP} can be verified. It may fail in case of *e.g.* incorrect values of R_i and $a_{\mathrm{LL}}s$ are used in the extraction of asymmetries and/or that higher-order corrections are sizeable. In this way the presented test can be used to discriminate between various models.

The comparison of the two asymmetries is done for the 6 bins of x_{C} and corresponding x_{Bj}. An example of extracted asymmetries in case a constraint $A_1^{\mathrm{QCDC}} = A_1^{\mathrm{LP}}$ was not used is presented in Table 8.3. In this particular case, the results for a MC sample used for the final Δg/g extraction are shown. It should be noted that, to calculate correctly the χ^2 value, the full covariance matrix (not shown here) has to be taken into account. With six degrees of freedom one can reject a model/tuning behind a given MC sample on 95% CL if the resulting χ^2 is larger than 12.6. For the discussed MC sample one has $\chi^2 = 8.1$, much smaller than the aforementioned limit. Therefore, one cannot reject the hypothesis that $A_1^{\mathrm{QCDC}}(x_{\mathrm{C}}) = A_1^{\mathrm{LP}}(x_{\mathrm{Bj}})$ and thus the model used for final Δg/g extraction has passed the consistency test. The obtained values of χ^2 for all 8 MC samples are summarised in Table 8.4. There is one MC sample, number six, with $\chi^2 = 13.1$ (thus formally above the 12.6 limit). Therefore, on 95% CL one could reject this MC sample from the analysis.

8.6.2 Δg/g results for eight MC samples

The Δg/g results obtained using the eight MC samples under the assumption that the asymmetries are equal for QCDC and LP processes are presented in Fig. 8.2. There are two striking features when inspecting this figure. First of all the results are very stable, the RMS being only 0.017. At the same time the uncertainty of Δg/g varies by up to a factor of two.

The second observation is easier to explain. Namely, in different MC samples also the value of R_{PGF} changes by up to a factor two, *cf.* Table 8.2. At first order the statistical

Table 8.3: Comparison between A_1^{LP} and A_1^{QCDC} for the final MC tuning. Observe that there are negative correlations involved and the final χ^2 is much lower than in case the data sets are treated as independent ones.

x range	A_1^{LP}	A_1^{QCDC}
$0.06 < x < 0.10$	0.009 ± 0.011	0.093 ± 0.035
$0.10 < x < 0.15$	0.086 ± 0.016	0.150 ± 0.034
$0.15 < x < 0.20$	0.131 ± 0.024	0.221 ± 0.042
$0.20 < x < 0.30$	0.200 ± 0.032	0.159 ± 0.054
$0.30 < x < 0.40$	0.273 ± 0.058	0.191 ± 0.113
$x > 0.40$	0.423 ± 0.087	0.208 ± 0.208
	TOTAL χ^2	8.1

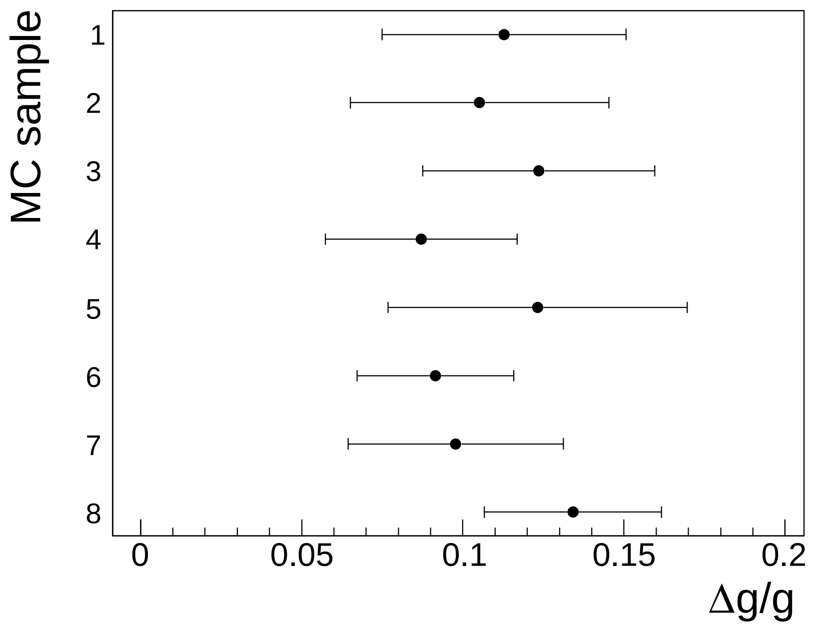

Figure 8.2: Summary of Δg/g obtained for eight MC samples.

uncertainty of Δg/g is proportional to $1/\langle R_{\mathrm{PGF}}\rangle$, hence large variations of the statistical uncertainty are observed for different MC samples.

Within the formalism of the proposed method it is also easy to understand why the Δg/g results are so stable, while at the same time large differences in the statistical

Table 8.4: The values of χ^2 from the compatibility test for eight MC samples. The ordering of MC samples correspond to the one used in Table 7.1.

MC sample	$\chi^2(ndf = 6)$
1	8.1
2	8.8
3	3.9
4	10.1
5	6.9
6	13.1
7	10.7
8	9.9

uncertainty of $\Delta g/g$ are observed. Assuming that the observed hadron asymmetry $A^h_{\rm LL}/D$ at high $p_{\rm T}$ and $A_1^{\rm LP}$ cancel each other, Eq. (5.14) can be approximated as

$$\Delta g/g = -\frac{a_{\rm LL}^{\rm QCDC} R_{\rm QCDC}}{a_{\rm LL}^{\rm PGF} R_{\rm PGF}} A_1^{\rm LO}(\langle x_{\rm C}\rangle). \tag{8.1}$$

At obtained $\langle x_{\rm C}\rangle = 0.14$ the asymmetry is about 0.087, and $(\langle a_{\rm LL}^{\rm QCDC} R_{\rm QCDC}\rangle)/(\langle a_{\rm LL}^{\rm PGF} R_{\rm PGF}\rangle) \approx 1.5$, *cf.* Table 7.2. Within such an approximation $\Delta g/g = 0.130$, not so far away from the full calculation presented in Chapter 9. Thus, the usage of Eq. (8.1) is justified to understand the surprising stability of $\Delta g/g$ results presented in Fig. 8.2.

Analysing Eq. (8.1) one can conclude that a rather small systematic uncertainty can be attributed to the ratio $a_{\rm LL}^{\rm QCDC}/a_{\rm LL}^{\rm PGF}$. It comes from the fact that in LO both $a_{\rm LL}$s are quite stable for different MC samples. As discussed in Subsection 7.2.2, $a_{\rm LL}^{\rm PGF}$ depends mostly on Q^2, and so it doesn't matter if we use MC with parton shower ON or OFF, or how fragmentation parameters are tuned. The stability of $a_{\rm LL}$s for various MC samples can also be verified in Table 7.2.

Therefore, the only relevant contribution to the systematic uncertainty is related to the ratio $R_{\rm QCDC}/R_{\rm PGF}$. Observe that both QCDC and PGF are higher order in α_S processes, meaning that the large uncertainty of α_s, which is present at low scale, cancels. Moreover, in both cases the $p_{\rm T}$ of hadron is dominated by the hard process. The quark fragmentation and intrinsic parton transverse momentum, $k_{\rm T}$, acts as additional smearing. Observe that the PGF and QCDC $p_{\rm T}$ dependent cross-section can be calculated in LO pQCD. Based on these arguments one expects the ratio $R_{\rm QCDC}/R_{\rm PGF}$ to be more stable than *e.g.* $R_{\mathrm{LP}}/R_{\mathrm{PGF}}$ or R_{PGF} itself. This explains why using very different MC samples the Δg/g results obtained are stable.

It is also interesting to notice that the observed similarity between values of A^h_{LL}/D and A_1^{LP} is an experimental, largely model-independent fact. Therefore, one could assume that an equation similar to Eq. (8.1) may also hold in NLO. In case one observes a positive value of Δg/g in the LO analysis it is very difficult that the NLO analysis would lead to a sign change of Δg/g. Except for $a_{\mathrm{LL}}^{\mathrm{PGF}}$ all other variables must be positive. It is rather unlikely that suddenly $a_{\mathrm{LL}}^{\mathrm{PGF}}$ becomes positive in NLO. At least LO and NLO values of $a_{\mathrm{LL}}^{\mathrm{PGF}}$ calculated in the photoproduction limit in [72] are both negative.

8.6.3 Comparison of Δg/g from a free versus a constrained fit

The results of Δg/g obtained with or without the assumption about $A_1^{\mathrm{LP}} = A_1^{\mathrm{QCDC}}$ are compared in Table 8.5 for all eight MC tunings. In the first column the MC sample number as explained in Table 7.1 is indicated. In the next two columns the Δg/g results with and without the $A_1^{\mathrm{LP}} = A_1^{\mathrm{QCDC}}$ condition are presented, while in the fourth column the χ^2 difference between the two results is given. Here, it is assumed that the error of the difference is $\sqrt{\delta(\Delta\mathrm{g/g})^2_{\mathrm{col3}} - \delta(\Delta\mathrm{g/g})^2_{\mathrm{col2}}}$. In the fifth column the previously calculated χ^2 of the compatibility test is given; finally the last column shows the sum of the two χ^2s. This last value is rather informative, as the full covariance matrix is not known. One can easily give an example where the χ^2 values in columns 3 and 4 give the same information. In these circumstances the presented sum of χ^2s can be considered as an upper limit. The results of Δg/g obtained for a free fit are in all eight cases higher than the ones obtained with the constrained fit. The difference is of the order of 2.2σ for the MC sample used for the final Δg/g extraction, *i.e.* the two results are compatible. It should be noticed that tuning number 3, which has the smallest χ^2 value at the compatibility test, gives also the best agreement between Δg/g obtained with or without the assumption $A_1^{\mathrm{QCDC}} = A_1^{\mathrm{LP}}$.

8.6.4 Hints from data about the product $a_{\mathrm{LL}}^{\mathrm{QCDC}} R_{\mathrm{QCDC}}$

In Subsection 8.6.1 the compatibility of A_1^{QCDC} and A_1^{LP} was discussed. The level of compatibility is mostly related to the value of $a_{\mathrm{LL}}^{\mathrm{QCDC}} R_{\mathrm{QCDC}}$ used in the analysis. In the presented method of Δg/g extraction, for a given MC sample it is possible to introduce a scaling factor, η_{QCDC}, for $a_{\mathrm{LL}}^{\mathrm{QCDC}} R_{\mathrm{QCDC}}$, as a free parameter in the fit. One can study the χ^2 value of the compatibility test as a function of η_{QCDC}. The results of this exercise are presented in Fig 8.3 for the MC sample used for the final Δg/g extraction. In the x-axis the η_{QCDC} is given, which multiplies the weight of the QCDC events. The obtained χ^2

Table 8.5: Summary of $\Delta g/g$ obtained for eight MC tunings, with and without the assumption about $A_1^{\rm QCDC} = A_1^{\rm LP}$.

Tune	$A_1^{\rm QCDC} = A_1^{\rm LP}$	free fit	$\chi^2_{\rm diff.}$	$\chi^2_{\rm QCDC}$	$\chi^2_{\rm limit}$
1	0.1128 ± 0.0379	0.1827 ± 0.0489	5.1	8.1	13.2
2	0.1052 ± 0.0401	0.1729 ± 0.0516	4.4	8.8	13.1
3	0.1236 ± 0.0360	0.1491 ± 0.0454	0.9	3.9	4.8
4	0.0871 ± 0.0298	0.1237 ± 0.0375	2.6	10.1	12.7
5	0.1232 ± 0.0464	0.1921 ± 0.0590	3.6	6.9	10.4
6	0.0915 ± 0.0243	0.1201 ± 0.0315	2.0	13.1	15.1
7	0.0978 ± 0.0334	0.1836 ± 0.0446	8.4	10.7	19.1
8	0.1342 ± 0.0275	0.1537 ± 0.0390	0.5	9.9	10.4

values in the compatibility test are presented on the y-axis. The blue colour corresponds to the χ^2 obtained only for comparison of $A_1^{\rm QCDC}$ vs $A_1^{\rm LP}$, while the red colour takes into account also the compatibility of $\Delta g/g$ between fits with and without the A_1 constraint. Note that in this case the χ^2 value should be considered as an upper limit, as discussed in the previous section. In both cases the χ^2 value obtained for $\eta_{\rm QCDC} = 1$ is close to minimum. This gives additional confidence in the model used in the analysis.

Here, only the simplest exercise was presented. In more complex ones, *e.g.* the shape of $R_{\rm QCDC}$ and $R_{\rm LP}$ was changed as a function of $p_{\rm T}$. In all performed exercises, the χ^2 value of the fit without modification was within a reasonable distance from the χ^2 minimum. However, a general tendency was observed to have larger values (by about 20%) of $a_{\rm LL}^{\rm QCDC} R_{\rm QCDC}$ when compared to the unmodified MC. This observation is somehow in line with the results obtained in the previous section, where for all MC samples $\Delta g/g$ in the free fit was higher than in case a constraint $A_1^{\rm LP} = A_1^{\rm QCDC}$ was used.

From the difference of $\chi^2_{\rm min}$ and $\chi^2_{\rm min} + 1$ presented in Fig. 8.3 one can conclude that the uncertainty of extraction of $a_{\rm LL}^{\rm QCDC} R_{\rm QCDC}$ from data is about 30%. If indeed one trusts such a result one can assume that $R_{\rm PGF}$ predicted by MC is also known with such a precision.

8.6.5 The final systematic error related to MC

Within the framework of the new method the stability of $\Delta g/g$ results obtained with different tunings is better understood than previously. The largest contribution to the systematic uncertainty is related to the ratio $R_{\rm QCDC}/R_{\rm PGF}$; arguments were given to

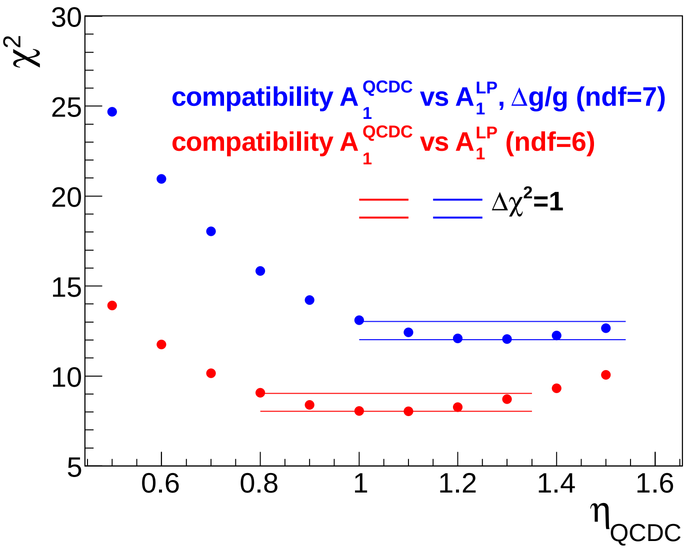

Figure 8.3: The χ^2 profile as a function of η_{QCDC} i.e. scaling factor for the weight of QCDC events. Red: Only compatibility of A_1 QCDC vs LP is verified. Blue: In addition compatibility of $\Delta g/g$ is added.

explain why this ratio is more stable than *e.g.* $R_{\mathrm{LO}}/R_{\mathrm{PGF}}$.

The stability of $a_{\mathrm{LL}}^{\mathrm{QCDC}} R_{\mathrm{QCDC}}$ for various MC samples is about 30%, and in fact a similar result was obtained in the previous section directly from the data. The full error propagation reveals that $\Delta g/g$ is changed by 0.015 in such circumstances. It is about a factor two lower than expected from Eq. (8.1); this is because QCDC events are also used to extract A_1^{LP}. The 30% uncertainty assumed on R_{PGF} changes both the error and the value of $\Delta g/g$ by this amount *i.e.* it acts as a multiplicative factor. One of the possibilities is to claim an additive uncertainty of about 0.015 and a multiplicative one of 30%. However, in such case one does not take into account the fact that R_{PGF} and R_{QCDC} are correlated, *i.e.* $\sqrt{0.015^2 + (0.3 \times 0.113)^2} = 0.037$, while the maximum difference between $\Delta g/g$ obtained from any of the MC sample and the final one is only 0.026.

Another possible solution is to take the difference between $1/2(\Delta g/g_{\mathrm{max}} - \Delta g/g_{\mathrm{min}}) = 0.024$. However, here the danger is that one outlier defines the uncertainty. One has to keep in mind that the errors must be calculated separately for the three x_{g} bins as well as in the future for the proton data. The third possibility is to use the same procedure as in [64], which leads to an uncertainty of 0.028. However, this uncertainty just reflects the large fluctuation of the obtained errors of Δg/g for various MC tunings, while in the present method it was better understood why the Δg/g results themselves are stable. The other solution for the uncertainty estimation was mentioned before: to take the RMS of the Δg/g from the eight MC samples (0.017). Such an RMS value has no real probabilistic interpretation, it just gives information about the typical stability of the obtained Δg/g. Having apparently no better choice, indeed the RMS of Δg/g obtained from the eight MC samples is taken as an estimate of the model uncertainty.

8.7 Radiative corrections

The radiative corrections which depend on (x_{Bj}, y) were included in the dilution factor, see Section 6.2. However, due to the photon radiation the kinematics of the event changes, thus also z and p_{T} of the hadron are affected by the radiation process. In order to treat radiative corrections in a more proper way there was an attempt to simulate radiative events using the MC programme RADGEN [118]. It was found out that the inclusive (x_{Bj}, y) correction is very similar to the one obtained in TERAD. However, more detailed studies revealed that most probably the photon spectrum generated by the RADGEN programme, especially the hard part, does not describe the data.

The majority of the hard photons is emitted in the lepton scattering plane, *cf*. Fig. 3 in [118]. From the point of view of the analysis presented in this monograph part of the emitted photons converts into electrons/positrons which may be misidentified with hadrons. By studying the ϕ_{h} angle of hadron production with respect to the lepton scattering plane one can identify such events. The data/MC comparison is shown in Fig. 8.4. The hadron spectrum as a function of the absolute value of ϕ_{h} in the region $0 < \phi_{\mathrm{h}} < 1$ is presented. The data and MC are normalised to be consistent at high ϕ_{h} values, including in the not shown $\phi_{\mathrm{h}} \in (1 - 2\pi)$ range. In the left panel hadrons with $z > 0.1$ are shown. There is a discrepancy between data and MC of the order of 1.8. In the middle panel an additional cut is used, namely $y > 0.7$, and the discrepancy between data and MC becomes even larger. Finally in the right panel the comparison is presented for hadrons with $p_{\mathrm{T}} > 2$ GeV, *i.e.* in the most important region from the point of view of Δg/g extraction. At low ϕ_{h} values data and MC clearly do not agree. It should be added that there are phase-space regions where in real data electrons from conversions were observed, but not in RADGEN, *e.g.* $p_{\mathrm{T}} < 0.05$ GeV. To overcome presented problem, naively, one could exclude this region of low ϕ_{h} from the analysis. However, as RADGEN seems to produce too many hard photons, it means that it produces too few of them at lower energies. As a result even if the low ϕ_{h} region is excluded the corrections predicted by RADGEN would not be correct.

The observed discrepancies in Fig. 8.4 might be also related with a wrong description of photon conversion in MC and/or wrong association of electrons to the interaction point. There were additional studies performed for low-energy electrons in the low y region. In this region radiative corrections are low and electrons can be identified in the RICH detector. There was a good agreement observed between data and MC.

Whether there is a problem with photon generation in RADGEN, with gamma conversion or with the electron reconstruction, the fact is that the RADGEN MC is effectively not able to reliably describe the COMPASS data. Therefore, results obtained using this program cannot be used in the analysis. Very recently, a different program to estimate RC was employed in COMPASS, namely DJANGOH [119]. The first preliminary studies show that indeed the hard photon spectrum generated in DJANGOH has a very different shape from that of RADGEN. Most importantly DJANGOH predicts much less hard photons, the large number of which was the biggest concern with RADGEN.

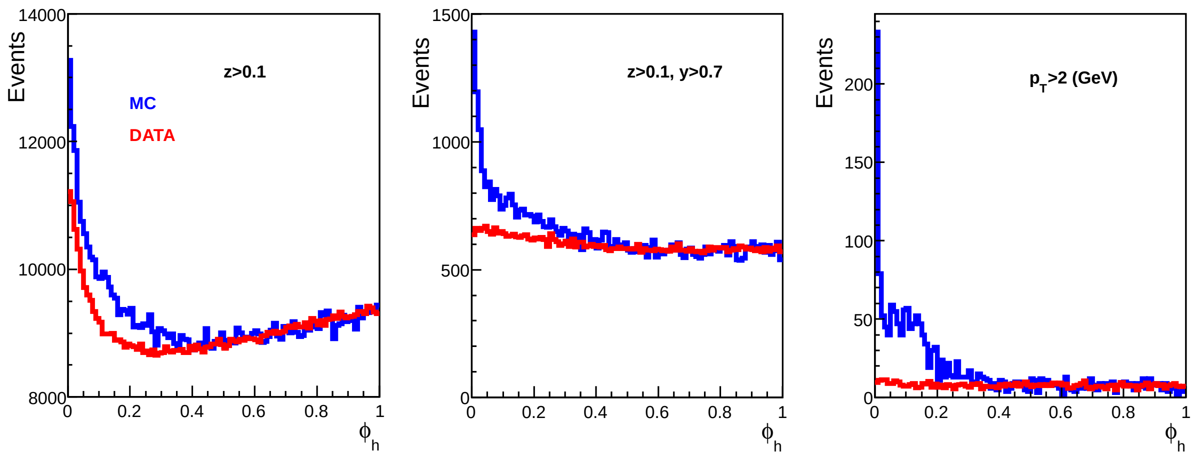

Figure 8.4: Comparison of data and MC with RADGEN. Large kinematic dependent discrepancies are observed, see text for details.

8.8 Summary of systematic uncertainties

In Table 8.6 the systematic uncertainty for total $\Delta g/g$ integrated in the full x_g range and in each of three x_g bins is presented. The systematic uncertainty of the $\Delta g/g$ results obtained in the full x_g range is lower than in [64] by a factor 1.8. The presented novel method of Δg/g extraction indeed allowed for a considerable reduction of the systematic uncertainty. Not only certain systematic uncertainties were reduced or eliminated, but it was also possible to perform additional systematic tests of the MC model assumed in the analysis.

Table 8.6: Summary of contributions to the systematic uncertainty of Δg/g.

Syst. error	Full x_{g} range	$x_{\mathrm{g}} < 0.10$	$0.10 < x_{\mathrm{g}} < 0.15$	$x_{\mathrm{g}} > 0.15$
$\delta(\Delta g/g)_{\mathrm{false}}$	0.029	0.039	0.022	0.014
$\delta(\Delta g/g)_{\mathrm{NN}}$	0.007	0.007	0.007	0.018
$\delta(\Delta g/g)_{f,P_{\mathrm{b}},P_{\mathrm{t}}}$	0.010	0.008	0.013	0.013
$\delta(\Delta g/g)_{\mathrm{MC}}$	0.017	0.017	0.041	0.044
TOTAL	0.036	0.044	0.049	0.051

Chapter 9

Results

The final $\Delta g/g$ result, with its statistical and systematic uncertainties, is

$$\left\langle \frac{\Delta g}{g} \right\rangle = 0.113 \pm 0.038_{\text{stat.}} \pm 0.036_{\text{syst.}}, \tag{9.1}$$

and suggests that $\Delta g/g$ is positive in the measured range. It was obtained in LO pQCD, at averaged scale $\mu^2 = \langle Q^2 \rangle = 3\ \text{GeV}^2$ and at weighted average value of nucleon momentum fraction carried by gluons $\langle x_g \rangle \approx 0.10$ as reported in [30]. A correction for the probability of the deuteron to be in a D-wave state [120] was applied.

The present result is in excellent agreement with the previous analysis from [64], $\Delta g/g = 0.125 \pm 0.060 \pm 0.065$. The difference is 0.012 ± 0.046, where the uncertainty is assumed to be $\sqrt{0.060^2 - 0.038^2}$. The statistical uncertainty, with the new method, got improved by a factor of 1.6. About half of the gain can be attributed to the new method. The other part of the gain is related with the fact that a larger sample was used. Namely, a sample with $p_T > 1.5$ GeV for the hadron leading in p_T and $p_T < 0.4$ GeV for the next to leading hadron which is still a rather clean source of PGF. However, these events were not used in the analysis presented in [64]. The systematic uncertainty of the new result is also considerably reduced, by a factor of 1.8. Not only certain systematic effects present in [64] are not existing in the present method, but due to the simpler event weighting the systematic uncertainty related to MC can be also studied in more detail.

The comparison of the new result with other available LO direct extraction of $\Delta g/g$ from SMC [60], HERMES [68], and COMPASS [55,66] is presented in Fig. 9.1. For clarity in this figure the results obtained in [64] are not shown. The present result agrees very well with the world data. It should be stressed that the new result has the smallest total uncertainty.

The results of $\Delta g/g$ were also obtained in three bins of x_g^{NN}, which correspond to three

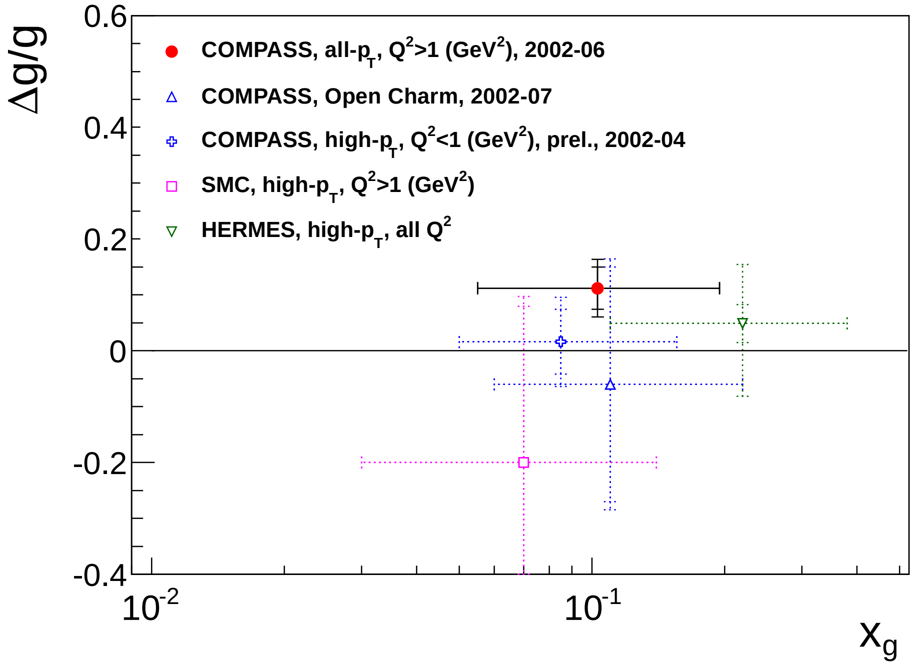

Figure 9.1: Comparison of the present $\Delta g/g$ results in the measured x_g range with world LO analyses of SMC [60], HERMES [68], and COMPASS [55, 66]. For figure clarity the result published in [64] is not shown.

ranges in x_g. These ranges are partially overlapping. This is related to the fact that the correlation between x_g^{NN} and x_g obtained during the NN training was about 60% and not 100%. The obtained results are summarised in Table 9.1. In the measured x_g range and within the obtained uncertainties there is no sign of strong x_g dependence of $\Delta g/g$.

It is important to notice that the events in the three bins of x_g^{NN} are statistically independent. However, a correlation may arise during the fit between results of $\Delta g/g$ obtained in different bins because a common set of 12 A_1^{LP} asymmetry is extracted. One could obtain separately 12 A_1^{LP} for each of the three x_g^{NN} bins. In such case the $\Delta g/g$ results in different x_g^{NN} bins would be statistically independent. However, the statistical uncertainty of $\Delta g/g$ would not be optimal. For the extracted values of $\Delta g/g$ the only observed non zero correlation is between the 1st and the 2nd x_g^{NN} bin and it amounts to 30%.

The new $\Delta g/g$ results obtained in three x_g ranges are compared with the previous results in Fig. 9.2. The inner error bands correspond to the statistical uncertainty while the outer ones correspond to the quadratic sum of statistical and systematic uncertainties.

Table 9.1: The value of $\langle \Delta g/g \rangle$ in three x_g^{NN} bins. The result for the full x_g range is also shown.

x_g^{NN} bin	$\langle x_g \rangle$	x_g range (RMS)	$\langle \Delta g/g \rangle$
0−0.10	0.08	0.04–0.13	$0.087 \pm 0.050 \pm 0.044$
0.10−0.15	0.12	0.07–0.21	$0.149 \pm 0.051 \pm 0.049$
0.15−1	0.19	0.13–0.28	$0.154 \pm 0.122 \pm 0.051$
0−1	0.10	0.05–0.20	$0.113 \pm 0.038 \pm 0.036$

As in the case of the extraction in a single bin, a very good agreement between the two results is seen. The reduction of uncertainties is clearly visible. In addition a shift of the $\langle x_g \rangle$ points is noticeable. There are two reasons why the x_g is higher in the new analysis; first: in the enlarged phase space of the all-p_T analysis higher x_g is preferred; second: in the new method a given event is characterised by one x_g value, while previously some subtraction of the so-called x'_g had to be done, *cf*. Eq. (4) of [64].

The comparison of the new results in three x_g ranges with all world LO direct extraction of $\Delta g/g$ is presented in Fig. 9.3. The world data are exactly the same as in the right panel of Fig. 9.1, namely from SMC [60], HERMES [68], and COMPASS [55, 66]. Again, for figure clarity, the results obtained in [64] are skipped in Fig. 9.3. The present results given in three x_g ranges agree very well with the world data. However, all three points are slightly higher than all previous $\Delta g/g$ results.

It is also interesting to compare the present results with the pQCD fits to inclusive g_1, see Section 3.1. One should keep in mind that these results are calculated in LO, while recent fits are performed at least in NLO precision. For example in Fig. 9.4 the new COMPASS results are compared with COMPASS NLO pQCD fit to world g_1 data, *cf*. [50]. In this fit two solutions for $\Delta g/g$ are found: a positive and a negative one, however, with a large systematic uncertainty. The present results strongly disagree with the negative solution of the COMPASS $\Delta g/g$ fit. The comparison of obtained $\Delta g/g$ with more QCD fits is presented in Table 9.2. In the first column the name of the fit is given, in the next three columns the predicted values of $\Delta g/g$ for x_g corresponding to COMPASS averages x_g for the three ranges are shown. In the last column the values of χ^2 are given. Here only the COMPASS statistical uncertainties were used for χ^2 calculation. In addition, the aforementioned correlation between $\Delta g/g$ results obtained in the first and the second x_g ranges was also taken into account. Needless to say, there is an excellent agreement observed between the present results and the various pQCD fits. Only in the case of

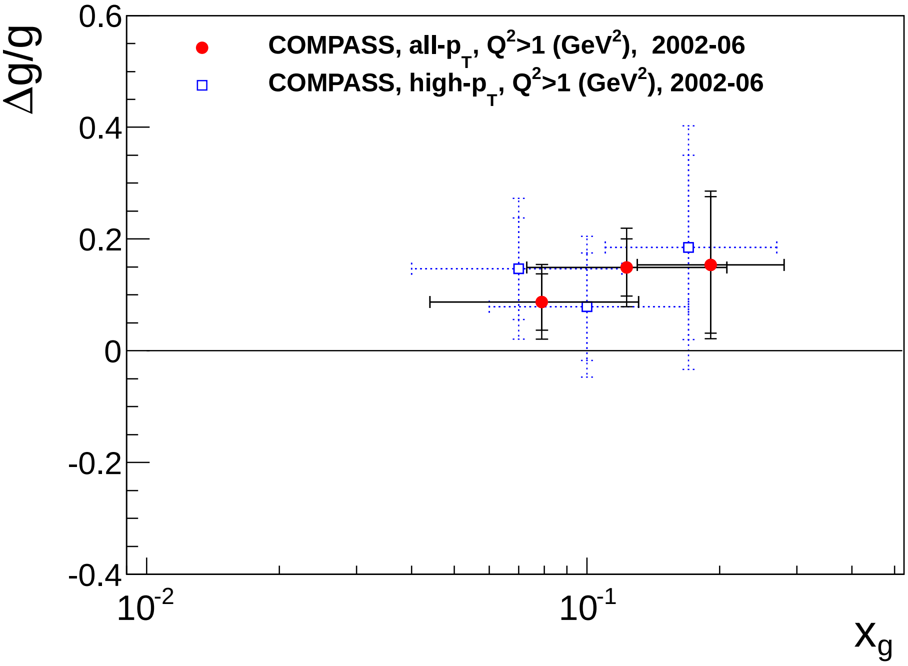

Figure 9.2: Comparison of the present results in 3 x_g ranges with results presented in [64]. See text for details.

COMPASS and LSS negative solutions and the DSSV fit there is a clear discrepancy visible. It is also interesting to notice that one of the best χ^2 values is obtained for a LO GRVS fit. One can also verify that for GRVS there is a very small difference between NLO and LO predictions. This gives some more confidence that the comparison of LO results of present analysis to the NLO QCD fits is justified to some extent. In addition, to obtain the final Δg/g value the MC with parton shower option on was used. Therefore, some part of the NLO correction is in fact taken into account in the present analysis.

So far only the results of Δg/g were discussed. The results of the simultaneously extracted A_1^{LP} are presented in Fig. 9.5. They are compatible with zero for low x_{Bj} values and rise at high x_{Bj}. It should be noted that A_1^{LP} is a major contributor to the measured inclusive asymmetry $A_{1,\mathrm{d}}^{\mathrm{incl}}$. Therefore, the two asymmetries are expected to have similar trends. Indeed the extracted values of A_1^{LP} are very similar to COMPASS measurements of inclusive $A_{1,\mathrm{d}}^{\mathrm{incl}}$ [48, 121].

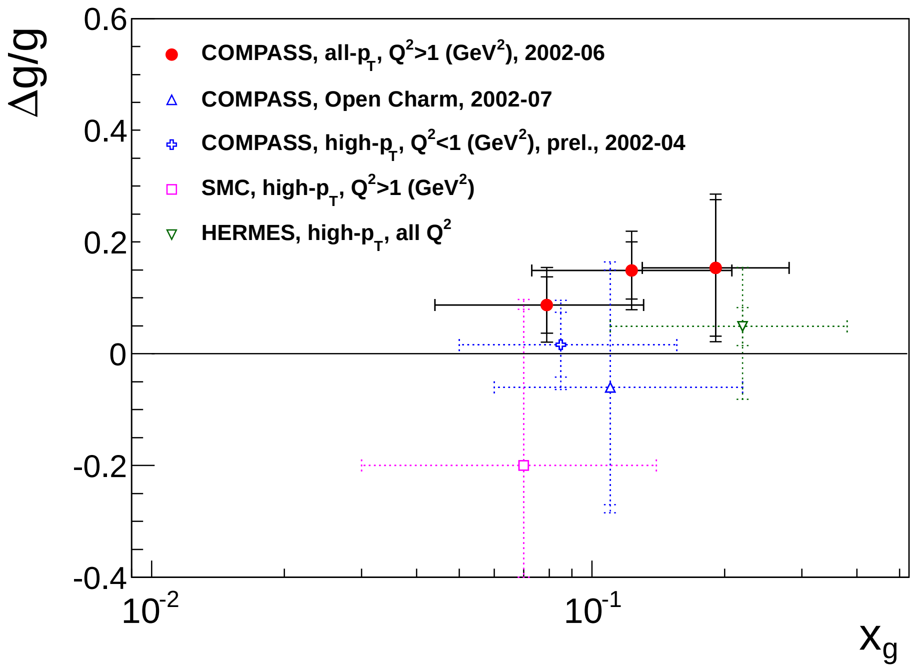

Figure 9.3: Comparison of the present $\Delta g/g$ results in 3 x_g ranges with world LO analyses of SMC [60], HERMES [68], and COMPASS [55, 66]. For figure clarity the results published in [64], and shown in Fig. 9.2, are not shown here.

9.1 Possible reduction of the statistical uncertainty of $\Delta g/g$

In the present analysis method, the A_1^{LP} is extracted in each of the x_{Bj} bins. However, one could also parametrise the asymmetry by a functional form. The same can be done for $\Delta g/g$. By using a functional form one gains additional degrees of freedom, and reduces the correlation between A_1^{LP} and $\Delta g/g$, resulting in improved uncertainties of $\Delta g/g$ and A_1^{LP}. However, the results depend upon the functional form assumed. Moreover, by using a parametrisation the extracted results are more prone to possible false asymmetries.

Several exercises were performed to verify possible gains, here only two of them are reported. For the simplest functional form of $A_1^{\mathrm{LP}} = x^\alpha$, the extracted gluon polarisation is: $\Delta g/g = 0.130 \pm 0.026$; thus there is a reduction of about 50% in the statistical uncertainty, comparing to the main result. The obtained χ^2/ndf is 752/697 with a probability of 7%. In case a functional from is selected as $A_1^{\mathrm{LP}} = x^\alpha + \mathrm{const}$, the result of $\Delta g/g$ is 0.075 ± 0.036, while const $= -0.004 \pm 0.003$ is comparable with zero. There is a clear

Table 9.2: The comparison of the COMPASS LO $\Delta g/g$ results with (mostly) NLO QCD fits. The hard scale of 3 GeV^2 was chosen for a comparison as it is average scale of the COMPASS data. Note that for [92] fit parameters were not published, the shown values are for the hard scale of 10 GeV^2 as given in the paper.

	Reference	$x_{g,1}$	$x_{g,2}$	$x_{g,3}$	χ^2
GRVS LO	[122]	0.10	0.15	0.21	0.3
GRVS NLO	[122]	0.10	0.14	0.21	0.4
GRVS LO$_v$	[122]	0.15	0.22	0.30	3.9
GRVS NLO$_v$	[122]	0.12	0.17	0.27	1.4
COMPASS $\Delta G > 0$	[50]	0.06	0.10	0.19	1.1
COMPASS $\Delta G < 0$	[50]	−0.19	−0.27	−0.37	86.9
LSS positive	[123]	0.04	0.06	0.11	3.5
LSS negative	[123]	−0.10	−0.13	−0.07	34.8
DSSV	[70]	−0.05	−0.05	−0.01	18.4
DSSV14	[92]	0.05	0.09	0.17	1.4
ACC positive	[124]	0.09	0.16	0.28	1.1
ACC mixed	[124]	0.02	0.11	0.29	3.0
COMPASS $\Delta g/g$		0.09	0.15	0.15	-

change of the $\Delta g/g$ result between the two fits. In addition the 50% gain in statistical precision is basically lost as soon as the constant term is added to the fit. The χ^2/ndf of the latter fit is 700/656, with a probability 11% and thus not much better than for the simple functional form $A_1^{\mathrm{LP}} = x^{\alpha}$.

In summary, while a decrease of the $\Delta g/g$ statistical uncertainty by using a functional form of A_1^{LP} is possible, the gain in the statistical precision does not compensate the increased systematic uncertainties.

9.2 Analysis of the proton data

In this work COMPASS data of 2002–2006 taken on deuteron target were presented. However, due to the $A_1(x_{\mathrm{Bj}}, z, p_{\mathrm{T}})$ problem described in Subsection 8.3.2 some systematic studies of proton data taken in 2007 and 2011 have been performed. The PGF is mostly present at lower x_{Bj} values, where there is not so large difference between proton and deuteron. Therefore, one may use the existing NN to have a good estimate of what to

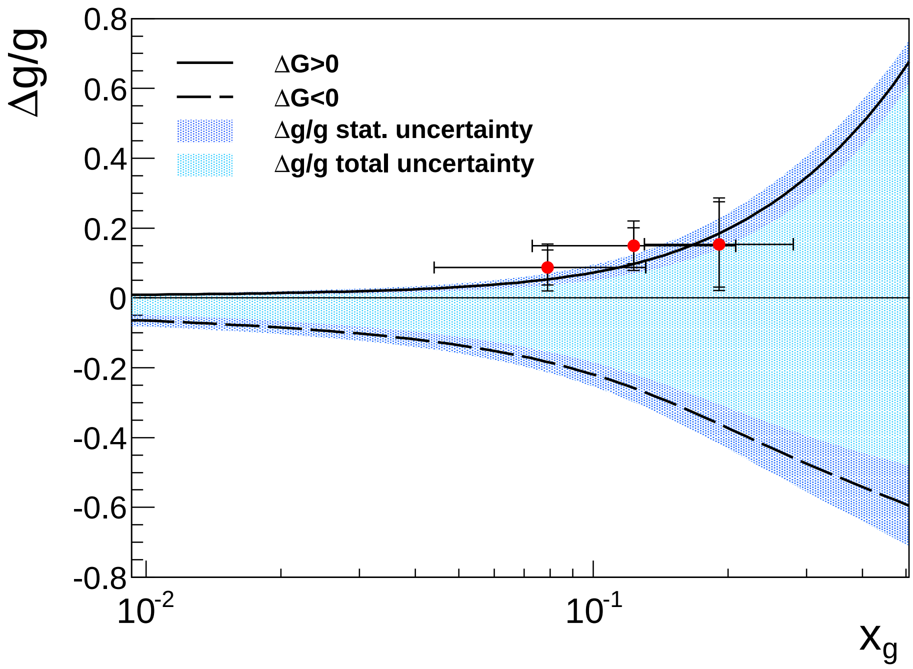

Figure 9.4: Comparison of present $\Delta g/g$ results with COMPASS NLO QCD fit [50], see text for details.

expect for the $\Delta g/g$ analysis of the proton data. Such an exercise was indeed performed; the result is $\Delta g/g = 0.147 \pm 0.045$. Although the analysis of proton data was oversimplified, there is a good agreement between $\Delta g/g$ results for proton and deuteron data. The statistical uncertainty of $\Delta g/g$ from the proton data is about 20% higher than that from the deuteron. Combining the two results one gets

$$\left\langle \frac{\Delta g}{g} \right\rangle = 0.127 \pm 0.029_{\text{stat.}}. \tag{9.2}$$

What makes proton data even more interesting is the A_1 compatibility test, described in Subsection 8.6.1. The sensitivity of the test depends on the ratio of $A_1^{\text{QCDC}}/\delta A_1^{\text{QCDC}}$. In case of proton data, for a given x_{Bj} the value of A_1^{QCDC} is larger than in the deuteron case (about a factor 3 at $x_{\text{Bj}} \approx 0.10$.) At the same time, due to more limited statistics, the expected uncertainty of A_1^{QCDC}, δA_1^{QCDC}, is only 20% worse for the proton data. Therefore, it is expected that the proton data will be more sensitive than the deuteron one in distinguishing among various models. In spite of this fact and the not optimal MC used in the analysis, the results of the A_1 compatibility test for the proton data give very reasonable value of $\chi^2/ndf = 7.9/6$. Therefore, it is rather unlikely that the MC tuning

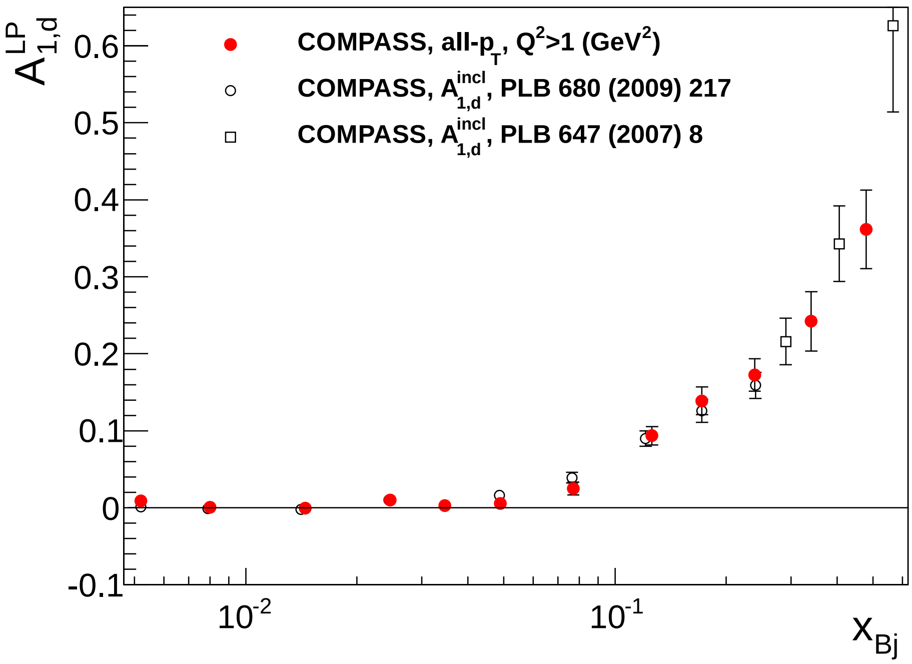

Figure 9.5: Extracted values of A_1^{LP} as a function of x_{Bj}, and COMPASS inclusive asymmetries $A_{1,\mathrm{d}}^{\mathrm{incl}}$ [48, 121].

used in the present analysis will be rejected when proton data are properly analysed. This result gives additional confidence to the assumed MC model for $\Delta g/g$ extraction.

Chapter 10

Summary and outlook

In this work a novel method of direct extraction of $\Delta g/g$ from a all-p_T data sample was presented. The method was developed by the author, responsible for this analysis in COMPASS. The resulting value is $\Delta g/g = 0.113 \pm 0.038_{\text{stat.}} \pm 0.036_{\text{syst.}}$ for average nucleon momentum fraction carried by the gluon about 0.10 and average hard scale of 3 GeV^2. The present analysis decreased by factors of 1.6 and 1.8 the statistical and the systematic uncertainties, respectively, compared to the previous COMPASS analysis published in *Phys. Lett. B* **718** (2013), 922. The present result has the lowest total uncertainty from all world data on direct extraction of $\Delta g/g$.

The present method of $\Delta g/g$ extraction is model dependent, as is any other method of direct $\Delta g/g$ extraction used so far. However, it allows additional systematic checks to the self-consistency of the assumed model. These self-consistency checks were successfully passed by the model assumed in the analysis.

The obtained $\Delta g/g$ result points towards a positive gluon contribution to the spin of the nucleon. The positive value of the gluon polarisation is further confirmed by the somewhat preliminary analysis of the proton data, with a combined result based on proton and deuteron data leading to $\Delta g/g = 0.127 \pm 0.029_{\text{stat.}}$. The obtained results are in-line with the most recent QCD fits in which the newest RHIC data are included. The present results are consistent with a nucleon picture where about 30% of spin of the nucleon is carried by quarks, about 40%–80% of the spin of the nucleon is carried by gluons and, possibly sizeable orbital angular momenta of u and d quarks largely cancel each other.

The uncertainty of the gluon and quark contributions to the nucleon spin will be further reduced when data from the future Electron-Ion-Collider are available. This accelerator will give an access to lower values of nucleon momentum fraction carried by gluons and quarks. This accelerator is not yet approved for construction. The first data are eventually to be expected only around 2025–2030. The presented method of direct Δg/g extraction could also be used in a future analysis of Electron-Ion-Collider data. Such analyses would act as an independent cross-check of the results obtained in QCD fit. To decrease the uncertainty of the direct Δg/g extractions at high values of the nucleon momentum fraction carried by gluons an experiment with lower beam energy is needed. For example, COMPASS could measure asymmetries using beam energy of 80–100 GeV instead of 160 GeV. Similarly, the presented method of Δg/g extraction could also be used in the HERMES experiment where even lower beam energy, of only 27 GeV, was used.

In view of a possible usage of the proposed method in other experiments one should point the following: The presented analysis was done using the hadron with highest p_{T} per event. It was verified that such a choice in the COMPASS case was close to optimal. The main reason behind this observation was the lack of reasonable π^0

detection capability of the COMPASS spectrometer, such that π^0 could not be considered. In case π^0 can be efficiently detected, it would be worthwhile to include more hadrons in the analysis. This would better constrain the parton kinematics, especially the value of x_{g} and also it would allow a better separation between PGF, QCDC and LP so that the presented method would be even more effective than in the COMPASS case.

Bibliography

[1] W. Prout (anonimously), *Annals of Philosophy* **6** (1815), 321; *Annals of Philosophy* **7** (1816), 111.

[2] E. Rutherford, *Phyll. Mag.* **21** (1911), 669.

[3] J. Chadwick, *Nature* **129** (1932), 312.

[4] M. Gell-Mann, *Phys. Lett.* **8** (1964), 214.

[5] G. Zweig (1964), in: D. B. Lichtenberg (Ed.), S. P. Rosen (Ed.), *Developments In The Quark Theory Of Hadrons, Vol. 1* (1964), 22.

[6] D. H. Perkins *Introduction to High Energy Physics*, 4th edition Cambridge University Press, 2000.

[7] J. I. Friedman, *The Road to the Nobel Prize.* Lecture in Hue University, Vietnam.

[8] E. D. Bloom *et al.*, *Phys. Rev. Lett.* **23** (1969), 930.

[9] M. Breidenbach *et al.*, *Phys. Rev. Lett.* **23** (1969), 935.

[10] S. L. Glashow, J. Iliopoulos, and L. Maiani, *Phys. Rev. D* **2** (1970), 1285.

[11] J. J. Aubert *et al.*, *Phys. Rev. Lett.* **33** (1974), 1404.

[12] J. E. Augustin *et al.*, *Phys. Rev. Lett.* **33** (1974), 1406; *Adv. Exp. Phys.* **5** (1976), 141.

[13] R. P. Feynman, *Phys. Rev. Lett.* **23** (1969), 1415.

[14] J. D. Bjorken and E. A. Paschos, *Phys. Rev.* **185** (1969), 1975.

[15] TASSO, R. Brandelik *et al.*, *Phys. Lett. B* **86** (1979), 243.

[16] M. J. Alguard *et al.*, *Phys. Rev. Lett.* **37** (1976), 1261.

[17] M. J. Alguard *et. al.*, *Phys. Rev. Lett.* **41** (1978), 70.

[18] J. D. Bjorken, *Phys. Rev.* **179** (1969), 1547.

[19] J. Ellis, R. L. Jaffe, *Phys. Rev. D* **9** (1974), 1444; *Phys. Rev. D* **10** (1974), 1669.

[20] EMC, J. Ashman *et al., Phys. Lett. B* **206** (1988), 364; *Nucl. Phys. B* **328** (1989), 1.

[21] F. E. Close and R. G. Roberts, *Phys. Lett. B* **316** (1993), 165.

[22] SMC, B. Adeva *et al., Phys. Rev. D* **58** (1998), 112001.

[23] HERMES, A. Airapetian *et al.*, *Phys. Lett. B* **442** (1998), 484.

[24] E142, P. L. Anthony *et al.*, *Phys. Rev. D* **54** (1996), 6620.

[25] E143, K. Abe *et al.*, *Phys. Rev. Lett.* **75** (1995), 25.

[26] E154, K. Abe *et al.*, *Phys. Rev. Lett.* **79** (1997), 26.

[27] X.-D. Ji, *Phys. Rev. Lett.* **78** (1997), 610; *Phys. Rev. D* **58** (1998), 056003.

[28] S. L. Adler, *Phys. Rev.* **177** (1969), 2426.

[29] J. S. Bell and R. Jackiw, *Nuovo Cim. A* **60** (1969), 47.

[30] COMPASS, C. Adolph *et al.*, accepted *Eur. Phys. J. C*, *hep-ex 1512.05053.*

[31] C. A. Aidala, S. D. Bass, D. Hasch and G. K. Mallot, *Rev. Mod. Phys.* **85** (2013), 655.

[32] P. Hoodbhoy, R. L. Jaffe and A. Manohar, *Nucl. Phys. B* **312** (1989), 571.

[33] H. Khan, P. Hoodbhoy, *Phys. Lett. B* **298** (1993), 181.

[34] SMC, D. Adams *et al., Phys. Lett. B* **336** (1994), 125.

[35] E143, K. Abe *et al., Phys. Rev. Lett.* **76** (1996), 587

[36] E155, P. L. Anthony *et al., Phys. Lett. B* **458** (1999), 529.

[37] E155, P. L. Anthony *et al., Phys. Lett. B* **553** (2003), 18.

[38] C. G. Callan and D. J. Gross, *Phys. Rev. Lett.* **22** (1969), 156.

[39] Y. L. Dokshitzer, *Sov. Phys. JETP* **46** (1977), 641.

[40] V. N. Gribov and L. N. Lipatov, *Sov. J. Nucl. Phys.* **15** (1972), 438.

[41] G. Altarelli and G. Parisi, *Nucl. Phys. B* **126** (1977), 298.

[42] H1 and ZEUS, H. Abramowicz *et al.*, *Eur. Phys. J. C* **75** (2015), 580.

[43] A. Bravar, K. Kurek and R. Windmolders, *Comput. Phys. Commun.* **105** (1997), 42.

[44] G. Ingelman, A. Edin and J. Rathsman, *Comput. Phys. Commun.* **101** (1997), 108.

[45] A. Accardi *et al.*, arXiv:1212.1701; BNL-98815-2012-JA; JLAB-PHY-12-1652.

[46] SMC, B. Adeva *et al.*, *Phys. Rev. D* **58** (1998), 112002.

[47] E155, P. L. Anthony *et al.*, *Phys. Lett. B* **493** (2000), 19.

[48] COMPASS, V. Yu. Alexakhin *et al.*, *Phys. Lett. B* **647** (2007), 8.

[49] HERMES, A. Airapetian *et al.*, *Phys. Rev. D* **75** (2007), 012007.

[50] COMPASS, C. Adolph *et al.*, *Phys. Lett. B* **753** (2016), 18.

[51] E143, K. Abe *et al.*, *Phys. Rev. D* **58** (1998), 112003.

[52] E155, P. L. Anthony *et al.*, *Phys. Lett. B* **463** (1999), 339.

[53] HERMES, C. Ackerstaff *et al.*, *Phys. Lett. B* **404** (1997), 383.

[54] COMPASS, M. G. Alekseev *et al.*, *Phys. Lett. B* **690** (2010), 466.

[55] COMPASS, C. Adolph *et al.*, *Phys. Rev. D* **87** (2013), 052018.

[56] C. Franco Ph.D. thesis, Universidade Tecnica de Lisboa, 2011; *https://wwwcompass.cern.ch/compass/publications/theses/2011_phd_franco.pdf*

[57] K. Kurek, Habilitation thesis, National Centre of Nuclear Research, Swierk, 2011; *https://wwwcompass.cern.ch/compass/publications/theses/2011_hab_kurek.pdf.*

[58] J. Riedl, M. Stratmann and A. Schafer, *Eur. Phys. J. C* **73** (2013), 2360.

[59] A. Bravar, D. von Harrach and A. Kotzinian, *Phys. Lett. B* **421** (1998), 349.

[60] SMC, B. Adeva *et al.*, *Phys. Rev. D* **70** (2004), 012002.

[61] K. Kowalik, E. Rondio, R. Sulej and K. Zaremba, *Acta Phys. Polon. B* **32** (2001), 2929.

[62] K. Klimaszewski, Ph.D. thesis, Soltan Institute for Nuclear Studies, Warsaw, 2010; *https://wwwcompass.cern.ch/compass/publications/theses/2010_phd_klimaszewski.pdf.*

[63] L. Silva, Ph.D. thesis, Universidade Tecnica de Lisboa, 2011; *https://wwwcompass.cern.ch/compass/publications/theses/2011_phd_silva.pdf.*

[64] COMPASS, C. Adolph *et al.*, *Phys. Lett. B* **718** (2013), 922.

[65] S. Procureur, Ph.D. thesis, Universite Paris XI, March 2006; *https://wwwcompass.cern.ch/compass/publications/theses/2006_phd_procureur.pdf.*

[66] COMPASS, E. S. Ageev *et al.*, *Phys. Lett. B* **633** (2005), 25.

[67] HERMES, A. Airapetian *et al.*, *Phys. Rev. Lett.* **84** (2000), 2584.

[68] HERMES, A. Airapetian *et al.*, *JHEP* **08** (2010), 130.

[69] T. Sjöstrand *et al., JHEP* **0605** (2006), 026.

[70] D. de Florian, R. Sassot, M. Stratmann, and W. Vogelsang, *Phys. Rev. Lett.* **101** (2008), 072001.

[71] D. de Florian, R. Sassot, M. Stratmann, and W. Vogelsang, *Phys. Rev. D* **80** (2009), 034030.

[72] B. Jager, M. Stratmann and W. Vogelsang, *Eur. Phys. J. C* **44** (2005), 533.

[73] STAR, B. I. Abelev *et al.*, *Phys. Rev. Lett.* **97** (2006), 252001.

[74] PHENIX, S. Adler *et al.*, *Phys. Rev. D* **73** (2006), 091102.

[75] PHENIX, A. Adare *et al.*, *Phys. Rev. D* **76** (2007), 051106.

[76] PHENIX, A. Adare *et al.*, *Phys. Rev. D* **79** (2009), 012003.

[77] STAR, B. I. Abelev *et al.*, *Phys. Rev. D* **80** (2009), 111108.

[78] PHENIX, A. Adare *et al.*, *Phys. Rev. Lett.* **103** (2009), 012003.

[79] PHENIX, A. Adare *et al.*, *Phys. Rev. D* **83** (2011), 032001.

[80] STAR, L. Adamczyk *et al.*, *Phys. Rev. D* **89** (2014), 012001.

[81] PHENIX, A. Adare *et al.*, *Phys. Rev. D* **90** (2014), 012007.

[82] PHENIX, A. Adare *et al.*, *Phys. Rev. D* **84** (2011), 012006.

[83] STAR, L. Adamczyk *et al.*, *Phys. Rev. D* **86** (2012), 032006.

[84] STAR, L. Adamczyk *et al.*, *Phys. Rev. Lett.* **115** (2015), 092002.

[85] PHENIX, A. Adare *et al.*, *Phys. Rev. Lett.* **106** (2011), 062001.

[86] STAR, M. Aggarwal *et al.*, *Phys. Rev. Lett.* **106** (2011), 062002,

[87] STAR, L. Adamczyk *et al.*, *Phys. Rev. Lett.* **113** (2014), 072301.

[88] D. de Florian, M. Pfeuffer, A. Schafer and W. Vogelsang, *Phys. Rev. D* **88** (2013), 014024.

[89] COMPASS, C. Adolph *et al.*, *Phys. Rev. D* **88** (2013), 091101.

[90] C. Uebler, A. Schfer, and W. Vogelsang, *Phys. Rev. D* **92** (2015), 094029.

[91] M. Glueck, E. Reya, M. Stratmann and W. Vogelsang, *Phys. Rev. D* **53** (1996), 4775.

[92] D. de Florian, R. Sassot, M. Stratmann and W. Vogelsang, *Phys. Rev. Lett.* **113** (2014), 012001.

[93] COMPASS, C. Adolph *et al.*, *Phys. Lett. B* **753** (2016), 573.

[94] COMPASS, V. Yu. Alexakhin *et al.*, *Phys. Lett. B* **647** (2007), 8.

[95] N. Doble *et al.*, *Nucl. Instrum. Meth. A* **328** (1994), 351.

[96] SMC, B. Adeva *et al.*, *Nucl. Instrum. Meth. A* **443** (2000), 1.

[97] N. W. Schellingerhout, L. P. Kok, S. A. Coon and R. M. Adam, *Phys. Rev. C* **48** (1993), 2714; Erratum: *Phys. Rev. C* **52** (1995), 439.

[98] SMC, D. Adams *et al.*, *Nucl. Instrum. Meth. A* **437** (1999), 23.

[99] A. Abragam and M. Goldman, *Nuclear Mangentism: Order and Disorder*, Clarendon Press, Oxford 1982.

[100] R. Brun *et al.*, *CERN-DD-EE-84-1.*

[101] A. Kotzinian, *Eur. Phys. J. C* **44** (2005), 211.

[102] COMPASS E. S. Ageev *et al.*, *Phys. Lett. B* **612** (2005), 154.

[103] J. Pretz and J.-M. Le Goff, *Nucl. Instrum. Meth. A* **602** (2009), 594.

[104] J. Pretz, *Nucl. Instrum. Meth. A* **659** (2011), 456.

[105] F. James and M. Roos, *Comput. Phys. Commun.* **10** (1975), 343.

[106] NMC, P. Amaudruz *et al.*, *Nucl. Phys. B* **441** (1995), 3.

[107] NMC, M. Arneodo *et al.*, *Nucl. Phys. B* **481** (1996), 3.

[108] EMC, J. Ashman *et al.*, *Z. Phys. C* **57** (1993), 211.

[109] E665, M. R. Adams *et al.*, *Phys. Rev. Lett.* **68** (1992), 3266.

[110] A. A. Akhundov *et al.*, *Fortschr. Phys.* **44** (1996), 373.

[111] SMC, B. Adeva *et al.*, *Phys. Rev. D* **60** (1999), 072004; Erratum: *Phys. Rev. D* **62** (2000), 079902.

[112] A. D. Martin, W. J. Stirling, R.S. Thorne and G. Watt, *Eur. Phys. J. C* **64** (2009), 653.

[113] A. Ferrari, P. R. Sala, A. Fasso and J. Ranft, *CERN-2005-010*, *SLAC-R-773*, *INFN-TC-05-11*

[114] CTEQ, H.L. Lai *et al.*, *Eur. Phys. J. C* **12** (2000), 375.

[115] R. Sulej, *http://www.ire.pw.edu.pl/ rsulej/NetMaker.*

[116] D. Kriesel *A Brief Introduction to Neural Networks*, *http://www.dkriesel.com/_media/science/neuronalenetze-en-zeta2-1col-dkrieselcom.pdf* and references therin.

[117] R. Sulej, K. Zaremba, K. Kurek and E. Rondio, *Meas. Sci. Technol.* **18** (2007), 2486.

[118] I. Akushevich, H. Bottcher and D. Ryckbosch, *hep-ph/9906408.*

[119] H. Spiesberger, *http://wwwthep.physik.uni-mainz.de/ hspiesb/djangoh/djangoh.html*

[120] R. Machleidt *et al.*, *Phys. Rep.* **149** (1987), 1.

[121] COMPASS, M. Alekseev *et al.*, *Phys. Lett. B* **680** (2009), 217.

[122] M. Glueck, E. Reya, M. Stratmann and W. Vogelsang, *Phys. Rev. D* **63** (2001), 094005.

[123] E. Leader, A. V. Sidorov and D. B. Stamenov, *Phys. Rev. D* **82** (2010), 114018.

[124] M. Hirai *et al.*, *Phys. Rev. D* **69** (2004), 054021.

Acknowledgement

First of all I like to thank C. Quintans and B. Badełek for their support for this work and given suggestions. I am grateful to K. Klimaszewski and L. Silva for the work we did together on the gluon polarisation extraction from COMPASS data. I am indebted to K. Kurek who introduced me to the analysis of high p_{T} hadrons and also for plenty of interesting discussions about physics. I appreciate very much the help of R. Sulej who took his time to teach me about neural networks. I would like to thank LIP-Lisbon Institute where I did most of the presented work. Special thanks are due to my LIP COMPASS colleagues A. S. Nunes, M. Quaresma, and C. Franco. I would like to thank to Y. Bedfer, E. Kabuss, and J. Pretz for many useful discussions about physics and analysis methods. Finally, I would like to thank the COMPASS Collaboration, as only the common effort of all the members make this and other COMPASS works possible.